National Library
of Canada

Bibliothèque nationale
du Canada

Canadian Theses Service

Service des thèses canadiennes

Ottawa, Canada
K1A 0N4

NOTICE

The quality of this microform is heavily dependent upon the quality of the original thesis submitted for microfilming. Every effort has been made to ensure the highest quality of reproduction possible.

If pages are missing, contact the university which granted the degree.

Some pages may have indistinct print especially if the original pages were typed with a poor typewriter ribbon or if the university sent us an inferior photocopy.

Previously copyrighted materials (journal articles, published tests, etc.) are not filmed.

Reproduction in full or in part of this microform is governed by the Canadian Copyright Act, R.S.C. 1970, c. C-30.

AVIS

La qualité de cette microforme dépend grandement de la qualité de la thèse soumise au microfilmage. Nous avons tout fait pour assurer une qualité supérieure de reproduction.

S'il manque des pages, veuillez communiquer avec l'université qui a conféré le grade.

La qualité d'impression de certaines pages peut laisser à désirer, surtout si les pages originales ont été dactylographiées à l'aide d'un ruban usé ou si l'université nous a fait parvenir une photocopie de qualité inférieure.

Les documents qui font déjà l'objet d'un droit d'auteur (articles de revue, tests publiés, etc.) ne sont pas microfilmés.

La reproduction, même partielle, de cette microforme est soumise à la Loi canadienne sur le droit d'auteur, SRC 1970, c. C-30.

NL-339 (r. 88/04)

Canada

THE UNIVERSITY OF ALBERTA

SPONGY ICE FORMATION

by

©

R.Z. BLACKMORE

A THESIS
SUBMITTED TO THE FACULTY OF GRADUATE STUDIES AND RESEARCH
IN PARTIAL FULFILMENT OF THE REQUIREMENTS FOR THE DEGREE
OF MASTER OF SCIENCE
IN
METEOROLOGY

DEPARTMENT OF GEOGRAPHY

EDMONTON, ALBERTA
FALL 1988

Permission has been granted to the National Library of Canada to microfilm this thesis and to lend or sell copies of the film.

The author (copyright owner) has reserved other publication rights, and neither the thesis nor extensive extracts from it may be printed or otherwise reproduced without his/her written permission.

L'autorisation a été accordée à la Bibliothèque nationale du Canada de microfilmer cette thèse et de prêter ou de vendre des exemplaires du film.

L'auteur (titulaire du droit d'auteur) se réserve les autres droits de publication; ni la thèse ni de longs extraits de celle-ci ne doivent être imprimés ou autrement reproduits sans son autorisation écrite.

ISBN 0-315-45630-2

THE UNIVERSITY OF ALBERTA

RELEASE FORM

NAME OF AUTHOR	R.Z. BLACKMORE
TITLE OF THESIS	SPONGY ICE FORMATION
DEGREE FOR WHICH THESIS WAS PRESENTED	MASTER OF SCIENCE
YEAR THIS DEGREE GRANTED	FALL 1988

Permission is hereby granted to THE UNIVERSITY OF ALBERTA LIBRARY to reproduce single copies of this thesis and to lend or sell such copies for private, scholarly or scientific research purposes only.

The author reserves other publication rights, and neither the thesis nor extensive extracts from it may be printed or otherwise reproduced without the author's written permission.

(SIGNED) ..Ryan Blackmore..........

PERMANENT ADDRESS:

#109, 5730 Riverbend Rd.
Edmonton, Alberta
T6H 4T4

DATED ...August 26.........1988

THE UNIVERSITY OF ALBERTA

FACULTY OF GRADUATE STUDIES AND RESEARCH

The undersigned certify that they have read, and recommend to the Faculty of Graduate Studies and Research, for acceptance, a thesis entitled SPONGY ICE FORMATION submitted by R.Z. BLACKMORE in partial fulfilment of the requirements for the degree of MASTER OF SCIENCE in METEOROLOGY.

Edward Lozowski
....
Supervisor

J D Wilson
....

....

Date.........................August 26, 1988

Abstract

The complexity of the spray ice growth process makes ice growth modelling difficult. A review of the fundamentals of solidification, including ice crystal growth, helps to explain why liquid water is entrapped in spray ice accretions. Sponginess, a measure of the degree of liquid entrapment, may have a pronounced influence on the accuracy of spray ice accretion mass modelling. Spongy spray ice accretion is examined and an empirical freshwater spongy spray ice formation model is presented for a rotating cylinder. The model assumes (1) known atmospheric icing conditions, (2) collection of freshwater spray droplets, supercooled to the temperature of the atmosphere, (3) a surface heat energy balance on the basis of a non-rotating smooth cylinder in perpendicular crossflow with a surface liquid film temperature of 0 °C, (4) no droplet bouncing or splashing from the surface, (5) complete thermal mixing through the thickness of the surface liquid film before shedding or accretion, (6) a hypothetical liquid entrapment mechanism for the growing surface of the accretion, and (7) equitable accretion distribution around the cylinder.

The modelling approach to overall mass conservation in the spray icing process shows that the collected ice and water mass flux components are either accreted or shed. The accreted and shed fluxs are also each characterized by ice and water components. A heat energy balance is used to develop an equation for the maximum potential ice accretion

flux. A radial surface growth velocity based on this maximum potential ice accretion flux is used as part of the empiricism to describe sponginess. A surface growth mechanism is postulated which allows for two separate equations of ice mass conservation: one for the entire mechanically and thermodynamically active surface layer, and one for the surface liquid film. Finally, dendritic ice crystal growth, breakage and transport from the icing surface is postulated and described according to an empirical formulation. This empiricism is composed of four dimensionless groups that are related to the breakage and transport process by a power law formulation in which the empirical constants are evaluated according to five specific conditions extracted from four data sets.

The resulting empiricism appears able to describe sponginess variation with air temperature from 0°C to -14 °C, wind velocity from 0 ms^{-1} to 45 ms^{-1} and liquid water content from 0 gm^{-3} to 10 gm^{-3}. In adddition, the reader is cautioned that the present model predicts sponginess of the accretion, and not necessarily the mass accretion rate.

Recommendations for future work include (1) the development of better techniques for sponginess measurement, (2) better measurement techniques for examining the shed flux and the ice fraction of the shed water-substance, (3) examination of crystallographic evidence to verify mechanisms of surface growth.

Finally, the spongy spray icing process, even in the case of freshwater icing, is an extremely complicated process. Empiricism appears to be unavoidable, and future work in this area will probably depend upon identifying the component processes to be described empirically.

Acknowledgements

Warm thanks to my supervisor, Dr. E.P. Lozowski, for his steady encouragement and support.

Also, I would like to thank Dr. J.D. Wilson and Dr. T.W. Forrest, who served on my examination committee.

I am grateful to Dr. W.P. Zakrzewski for the opportunity to work on ship icing research, a portion of which is presented in this thesis, and to Mr. R. Narten for his considerable help with the FROST tunnel experimentation.

Finally, special thanks to my wife, Heide, for her patient editorial assistance.

List of Figures

Figure Page

1.1 Power transmission line and tower damage............. 3

1.2 Ice accumulation on a small Dutch Chemical Tanker.... 7

2.1 The crystal lattice structure of ice................ 11

2.2 Solidification of a pure substance 11

2.3 Initial evolution of an unstable or stable interface 13

2.4 A growing dendrite tip 16

2.5 Sketch showing the skeleton layer in sea ice........ 18

2.6 Steady-state distribution of solute in the liquid ahead of an advancing solid/liquid interface........ 20

3.1 Water and salt transport on the front face of the superstructure...................................... 34

3.2 Constitutionally supercooled zone of liquid ahead of an advancing interface........................... 42

4.1 Schematic diagrams of the hypothesized filtration (a) and surface (b) accretion/shedding............. 51

5.1 Ice fraction versus air temperature................. 84

5.2 Ice fraction versus air temperature................. 85

5.3 Ice fraction versus air temperature................. 87

5.4 Ice fraction versus air velocity.................... 88

5.5 Ice fraction versus liquid water content............ 90

5.6 Ice fraction versus rotation rate................... 91

Nomenclature

In this thesis, a number of sets of equations from different sources are reviewed; notation native to each source is used. In consequence, some of the variables listed below represent the same parameter, and some parameters are represented by more than one variable. The reader will find however, that all variables are defined at appropriate places in the main text.

a - empirical constant in the dendritic breakage/exit equation (dimensionless)

a - the linear radiation constant ($a=8.1\times10^{7}K^{3}$)

a - the linearized coefficient for the heat flux due to long-wave radiation ($a=4.4Wm^{-2}K^{-1}$)

A - the dendrite breakage/exit ratio (documented in section 4.6.2, dimensionless)

b - empirical constant in the dendritic breakage/exit equation (dimensionless)

c - empirical constant in the dendritic breakage/exit equation (dimensionless)

c_a, c_p - specific heat of air at constant pressure ($Jkg^{-1}K^{-1}$)

C - empirical constant in the dendritic breakage/exit equation (dimensionless)

C - solute concentration in a liquid (dimensionless)

Ci - solute concentration at the interface (dimensionless)

Ci - specific heat of pure ice ($Jkg^{-1}K^{-1}$)

C_1 - solute concentration in the fluid as $x \to \infty$ (dimensionless)

Cs - solute concentration in the solid (dimensionless)

Cw - the specific heat of water ($Jkg^{-1}K^{-1}$)

d - droplet median volumetric diameter (m)

d - empirical constant in the dendritic breakage/exit equation (dimensionless)

D - accretion diameter (m)

D - diffusion coefficient of the solute (m^2s^{-1})

e_a - actual vapor pressure in the airstream (Pa)

$e_{i,j}$ - the saturation vapor pressure at the temperature θ (Pa)

e_s' - equilibrium water vapor pressure over water at t_s (Pa)

e_s - saturation vapor pressures over water at the icing surface temperature (Pa)

E - collection efficiency (dimensionless)

f - growth velocity of the crystal (ms^{-1})

F - mass flux of saline water to a cylinder ($kgm^{-2}s^{-1}$)

g - gravitational acceleration (ms^{-2})

h - overall convective heat transfer coefficient for a flat plate ($Jm^{-2}s^{-1}K^{-1}$)

h - overall heat transfer coefficient for a cylinder ($Jm^{-2}s^{-1}K^{-1}$)

$H_{i,j}$ - the thickness growth rate of ice (mh^{-1})

I - rate of accretion including ice, salt and water ($kgm^{-2}s^{-1}$)

$I_{i,j}$ - the mass flux of ice formed and accreted in the ijth cell ($kgm^{-2}s^{-1}$)

$\bar{I}_{i,j}$ - the time averaged local icing rate ($kgm^{-2}h^{-1}$)

J_0 - the shed flux ice mass fraction (dimensionless)

J_1 - the liquid incorporation ratio (dimensionless)

k - effective distribution coefficient (dimensionless)

k_a - the thermal conductivity of air ($Jm^{-1}s^{-1}K$)

k_0 - equilibrium distribution coefficient (dimensionless)

k^* - interfacial distribution coefficient (dimensionless)

l_f - latent heat of fusion for pure water (Jkg^{-1})

lv - latent heat of vaporization (Jkg^{-1})

L - the latent heat of freezing for brine at t_s (Jkg^{-1})

L - the characteristic dimension for the front face of the superstructure (m)

Le - the latent heat of evaporation for water (Jkg^{-1})

L_f - the latent heat of freezing for pure water (Jkg^{-1})

$\hat{m}_{i,j}$ - the accretion loading rate for cell i,j (kgh^{-1})

Mi_1 - the mass flux of pure ice particles collected ($kgm^{-1}s^{-1}$)

Mw_1 - the mass flux of pure water collected ($kgm^{-1}s^{-1}$)

Mi_2 - the mass flux of ice accreted ($kgm^{-1}s^{-1}$)

Mw_2 - the mass flux of pure water accreted ($kgm^{-1}s^{-1}$)

Mi_3 - the mass flux of shed ice particles ($kgm^{-1}s^{-1}$)

Mw_3 - the mass flux of shed pure water ($kgm^{-1}s^{-1}$)

Mi_4 - the mass flux of ice formed on the surface of the cylinder ($kgm^{-1}s^{-1}$)

Mi_5 - the mass flux of ice that enters the liquid film and is shed from the icing surface ($kgm^{-1}s^{-1}$)

M_{pi}, M_s, M_{pw} - are the masses of pure ice, salt, and pure water in spongy saline ice (kg)

n - the accretion fraction (dimensionless)

$n_{i,j}$ - the freezing fraction of the ijth cell (dimensionless)

n_f - the freezing fraction of an ice accretion assumed to contain no liquid (dimensionless)

Nu - Nusselt number (dimensionless)

Pa, p - air pressure (Pa)

$P_{i,j}$ - the surface area of a grid cell (m^2)

Pr - Prandtl number (Pr=0.711, dimensionless)

r - radius of the accretion (m)

r - the overall recovery factor of a cylinder (r=0.79, dimensionless)

Re - Reynolds number (dimensionless)

$R_{i,j}$ - average spray flux for the ijth cell ($kgm^{-2}s^{-1}$)

$\hat{R}_{i,j}$ - the total mass accretion flux for the ijth cell ($kgm^{-2}s^{-1}$)

$\mathring{R}_{i,j}$ - the mass flux of brine entrapped in the ijth cell ($kgm^{-2}s^{-1}$)

$R^*_{i-1,j}$ - the mass flux of shed brine from the cell immediately above the ijth cell ($kgm^{-2}s^{-1}$)

$R^*_{i,j}$ - the mass flux of shed brine from the ijth cell ($kgm^{-2}s^{-1}$)

$s_{i,j}$ - the liquid mass fraction or sponginess of the ice in the ijth cell (dimensionless)

Sc - Schmidt number (Sc=0.595, dimensionless)

$\dot{S}_{i,j}$ - the salinity of the entrapped brine in the ijth cell (dimensionless)

$\hat{S}_{i,j}$ - the overall salinity of the accretion in the ijth cell (dimensionless)

$S^{*}_{i-1,j}$ - the salinity of the shed brine from the cell immediately above the ijth cell (dimensionless)

$S^{*}_{i,j}$ - the salinity of the shed brine from the ijth cell (dimensionless)

S_o - the salinity of the impinging spray (dimensionless)

Sw,Si,Sb - salinities of impinging brine, ice and the liquid film, respectively (dimensionless)

t - time (s)

t_a, t_d, t_s - temperature of the air, impinging droplets and icing surface (°C)

Ta - air temperature (°C)

Td - droplet temperature at impact on the icing surface (°C)

Te, T_f - equilibrium freezing temperature (°C)

Ts - equilibrium surface temperature (°C)

Ur - the wind speed relative to the moving ship (ms^{-1})

v - air velocity (ms^{-1})

V - the actual radial surface growth velocity (ms^{-1})

$\vec{V}$ - fluid velocity vector (ms^{-1})

Va - air velocity (ms^{-1})

Vmax - maximum possible radial surface growth velocity (ms^{-1})

Vmin - minimum surface growth velocity (ms^{-1})

V_s - the surface growth velocity assuming that the ice formed by heat loss will grow solidly (ie: without liquid inclusion, ms^{-1})

Vx - fluid velocity in the x-direction relative to the solid/liquid interface (ms^{-1})

w - fluid velocity normal to the interface (ms^{-1})

w - liquid water content (gm^{-3})

x - distance ahead of the solid/liquid interface (m)

$z_{i,j}$ - the height of the i,jth cell (m)

δ - concentration boundary layer (m)

ΔT - supercooling temperature increment (°C)

ϵ - ratio of the molecular weights of water and air (ϵ=0.622, dimensionless)

θ - freezing point of the shed brine (°C)

λ_s, λ_f - the liquid fraction of saline and freshwater ice, respectively (dimensionless)

ν_a - the kinematic viscosity of air (m^2s^{-1})

ρ - density of pure ice (kgm^{-3})

ρ_i - density of ice (kgm^{-3})

$\overset{\circ}{\rho}_{i,j}$ - density of brine entrapped in the ice deposit (kgm^{-3})

ρ_s - density of the salt in seawater (kgm^{-3})

ρ_w - density of water (kgm^{-3})

σ - the Stefan-Boltzmann constant ($Jm^{-2}s^{-1}K^{-4}$)

τ_1 - characteristic time scale for alteration of conditions in the liquid film (s)

τ_2 - rotational period of the cylinder (s)

Ω - the rotation ratio (rad/sec in the empirical equations)

Table of Contents

Chapter Page

1. INTRODUCTION 1

1.1 The Icing Problem 1

1.2 Modelling the Formation of Ice 3

1.3 Ice Sponginess 5

1.4 Objectives 8

2. ICE FORMATION 10

2.1 Ice Crystal Formation from Pure Water 10

2.1.1 Constrained growth 10

2.1.2 Unconstrained growth 14

2.2 Sea Ice Formation 17

2.2.1 The skeleton layer 18

2.2.2 The constitutional supercooling model 19

3. EXISTING SPONGY SPRAY ICING MODELS 24

3.1 The Makkonen (1987) sea spray icing model 24

3.2 The University of Alberta ship icing model 31

3.3 Discussion 41

3.3.1 Supercooling and dendritic growth 41

3.3.2 The interfacial distribution coefficient ..44

3.3.3 The two models 47

4. THE FRESHWATER SPONGY SPRAY ICING PROCESS 49

4.1 The Geometry of the Icing Surface 49

4.2 Accretion/Shedding Mechanism Hypotheses 50

4.3 The Influence of Rotation 54

4.4 Conservation of Mass 56

4.5 Conservation of Heat Energy 58

4.6 Conservation of Ice Mass 60

4.6.1 Overall ice mass conservation 60
4.6.2 Free ice particle mass conservation 61
5. A NEW FRESHWATER SPONGY SPRAY ICING MODEL 65
5.1 The Surface Growth Velocity 65
5.2 The Ice Crystal Breakage/Exit Ratio 68
5.2.1 The wet/dry icing transition 68
5.2.2 The icing threshold 70
5.2.3 Dimensionless parameterization 73
5.3 The Equations and Assumptions 76
5.4 The Experimental Method 79
5.5 The Data and Empirical Constants 82
5.6 Model Performance 92
6. CONCLUSIONS AND RECOMMENDATIONS 102
Bibliography 108
Appendix A 112
Appendix B 117
Appendix C 120
Appendix D 127
Appendix E 138

1. INTRODUCTION

Some icing events are of great value to mankind and some are dangerous and costly. When icing becomes a problem, modelling, from the point of view of preparedness, becomes a priority. Modelling the expected mass accumulation for a particular icing event may provide the most crucial information required for an effective response to the problem. When this is the case, the degree of water inclusion (sponginess) in the growing ice accretion becomes an important factor. This thesis will present a new empirical model of spongy ice growth, and will recommend directions for future investigation.

1.1 The Icing Problem

Even though there is a great variety of ways in which icing can become a menace, usually only three conditions are required for its formation. In each class of icing problem, the modelling of formation characteristics should lead to better engineering solutions and responses.

Icing may be characterized by three essential criteria: (1) an object must be present on which ice can accumulate, (2) liquid water must be delivered to the surface of the object and (3) there must be sufficient heat transfer from the surface to solidify and accumulate a portion of the collected liquid. Hail growth is an example of icing in which the hailstones collect water from the air, and ice is accumulated as a result of heat loss to the cooler airstream. These three criteria may be present in many other circumstances as well, and produce a variety of icing phenomena. Other examples include transmission line icing, aviation icing and icing of structures at sea (drilling platforms and vessels).

Icing events can be disastrous for a variety of industrial and economic concerns. For example, in marine storm conditions, ocean-going vessels may become unstable under large ice loads. Aksjutin (1979) estimates that about ten vessels are lost each year due to vessel icing. This implies a heavy financial loss in addition to the loss of human life.

On land, there is concern over the icing of power transmission lines and towers (Fig. 1.1), as well as over dangerous road and runway icing. Hail exacts a considerable toll on the agricultural industry. In Alberta alone there is, on average, 100 million dollars worth of crop damage each year. (Alberta Report, June 24 1985, pp. 29-30). The Gander tragedy of Dec. 12, 1985 in which 248 American servicemen lost their lives (Macleans, April 26 1986, p.18), exemplifies the dangers of aircraft icing. Continuing interest in aircraft icing is shown by conferences such as the International Workshop on Aircraft Icing Technology held at the NASA Lewis Research Center in Cleveland Ohio, Nov. 4-6, 1987.

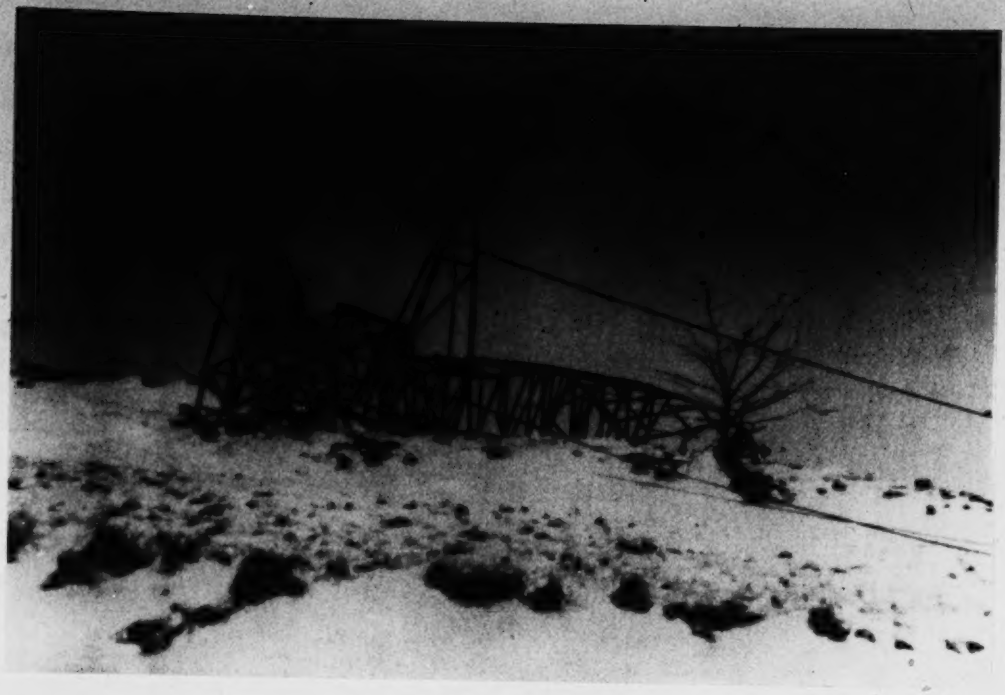

FIGURE 1.1 Power transmission line and tower damage after heavy wind and icing in East Serbia February 17, 1979 (after Plazinic and Miljkovic 1982).

For each case of icing, the ability to model the occurrence of icing and the physical characteristics of the accretion should lead to better engineering designs, and also to better forewarning and operational responses.

1.2 Modelling the Formation of Ice

There are a number of icing characteristics that can be modelled, depending on user needs. Ice accumulation rates are important in many applications. One aspect of ice mass accumulation modelling that is not well developed is spongy growth.

The diversity of ice accumulation characteristics is part of the difficulty of modelling the icing process. In the modelling of sea ice growth for instance, the mechanical strength of the ice could be of primary concern. When considering ice removal, models that predict mechanical and adhesive strength are valuable. The shape of an accretion may be the most influential characteristic when aircraft wings ice, and in aerodynamically induced galloping of transmission lines. Another characteristic of ice growth, which may be considered the most significant of the ones identified here, is the mass accretion rate. With time, large loads may result in damage such as that exemplified by Figure 1.1.

Sponginess adds to the mass accretion rate. Ludlam (1950), for instance, suggests that ice particles falling in cumulonimbus clouds may consist largely of liquid water. List (1963) indicates that the inclusion of liquid water in a growing ice formation may significantly increase the mass of a hailstone beyond that which would be expected on the basis of an assumed solid ice accumulation. If the spongy ice mechanisms at work in cases such as these were more clearly understood, the modelling of accretion growth, including entrapped water, could be done more effectively, since the liquid portion in the ice adds directly to the mass accumulation rate. Sponginess therefore, at present, must be considered a major problem in ice growth mass accumulation modelling.

1.3 Ice Sponginess

In this section, ice sponginess is defined, and the importance of sponginess is briefly reviewed in the light of early thermodynamic approaches to ice mass accretion models. Sponginess, which is observed in both freshwater icing and in sea water icing, may affect not only the mass accretion rates, but possibly also the structural strength of the ice.

Ice may form either as a dense solid, or as a porous structure which contains water and air. Ice with this second characteristic is termed spongy. List (1963) characterizes sponginess with the ice fraction, which is the solid ice mass fraction of an accretion. Sponginess is defined here as the liquid mass fraction of an accretion.

Sponginess may have a pronounced influence on the accuracy of spray ice accretion mass modelling. The early cylinder ice accretion model of Ludlam (1951) assumed solid ice growth on the basis of an assumed energy balance at the surface of the accretion; also any remnant surface water was assumed to be efficiently shed. List (1963) investigated the importance of sponginess in hailstones and found that the maximum mass accretion rate would occur under spongy growth conditions. Later, the possibility of liquid entrapment in hailstones was again inferred by Knight (1968) and List (1977) along with the need to understand the mechanisms involved. The problem remained, however, because a purely thermodynamic heat balance was thought to be incapable of accounting for what appeared to be, in part, a mechanically conditioned ice formation process. In other words, a heat balance can give an indication of the amount of solid ice material produced but may not determine how the solid portion of the accretion grows to entrap liquid water.

The phenomenon of sponginess is observed in both freshwater and saline ice formation. Freshwater sponginess had been observed in atmospheric ice particles, hailstones, icicles and in experimental cylinder icing. Saline or sea water spongy ice formations are observed in spray icing on board ships and in sea ice growth (Makkonen, 1987).

Saline spongy spray ice formation encountered by ocean-going vessels in cold seas under stormy conditions may show the importance of liquid inclusion in ice. Zakrzewski and Lozowski (1987) measured sponginess from 8% to 20% as a function of height on the front face of a ship superstructure. Savyel'ev (1971) states that up to 50% sponginess may be expected as a maximum value in saline ice formed on board ships. This maximum implies a mass loading approximately 100% larger than would otherwise be predicted on the basis of solid ice formation. A vessel's dynamic stability may thus be seriously affected, especially if the ice formations are well above the vessel's center of gravity. For example, the vessel shown in Fig. 1.2 which has run aground, shows heavy accretion high on the foremast. The considerable influence of spongy ice formation will not be taken into account if only solid ice growth, on the basis of heat transfer considerations, is assumed.

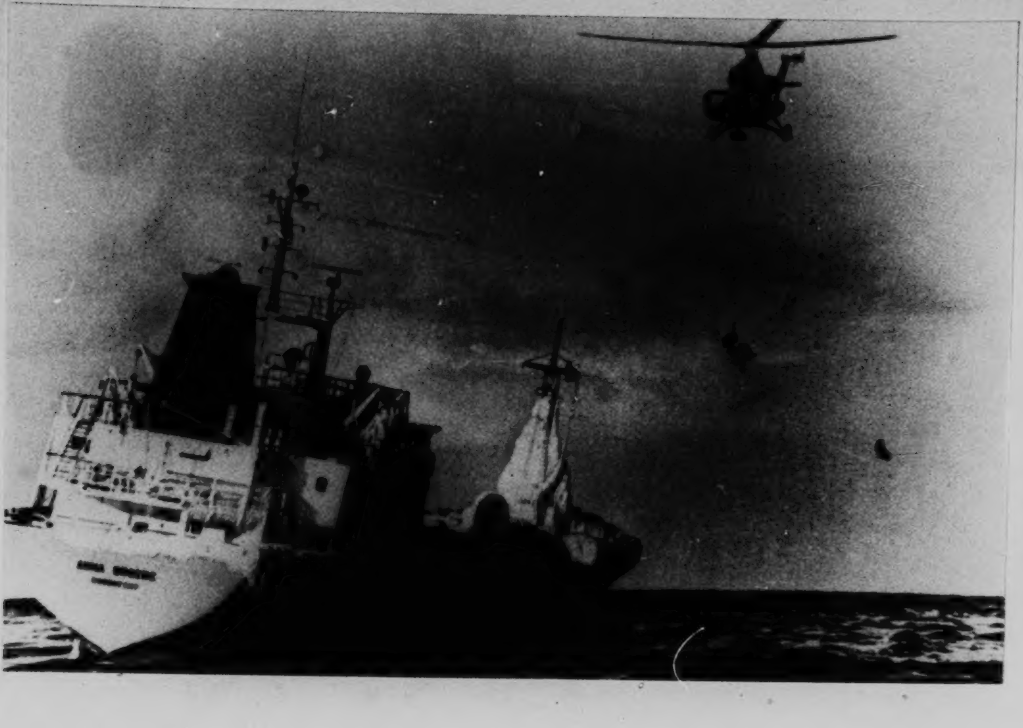

FIGURE 1.2 Ice accumulation on a small Dutch Chemical Tanker "Anna Broere" aground near Cape Rozewie, (Poland, Southern Baltic Sea), January 1, 1979. (Photo: W.P. Zakrzewski)

Weeks and Ackley (1982) show that ice sponginess influences the chemical, electrical, optical, mechanical and thermal properties of sea ice. Even though this evidence does not insure the same degree of influence for sponginess in cases of both fresh and sea water spray ice accretion, one could imagine that it is possible. The strength of sea ice, for example, (Weeks and Ackley, 1982) is known to vary as a function of the size and spacing of the entrapped brine pockets. Perhaps in a similar way the strength of spongy freshwater and seawater spray ice accretions could vary according to the concentration of the entrapped liquid in the cavities of the ice structure. This hypothesis appears to be corroborated by the observations of Knight (1980) who found that "a knife blade can be inserted easily a centimeter or more into the spongy parts" of icicles.

This thesis examines spongy spray ice formation and presents a freshwater spongy spray ice formation model for rotating cylinders which assumes: (1) atmospheric icing conditions are known; (2) collection of freshwater spray droplets supercooled to the temperature of the atmosphere; (3) surface heat transfer on the basis of a non-rotating smooth cylinder in perpendicular crossflow with a surface liquid film temperature of 0 °C; (4) no droplet bouncing or splashing from the surface; (5) complete thermal mixing through the thickness of the surface liquid film before shedding; (6) a hypothetical liquid entrapment mechanism for the growing surface of the accretion, and (7) equitable accretion distribution around the cylinder.

1.4 Objectives

The objectives of this thesis are: (1) to review some fundamentals of ice growth, including constitutional supercooling; (2) to review two current approaches to the problem of modelling spongy spray ice formation, one a sea spray icing model for a cylinder, and the other a sea spray icing model for a vertical flat surface; (3) to suggest the elements of a hypothetical framework which may provide the basis for a freshwater spongy spray icing model for a rotating cylinder; (4) to present a quasi-empirical freshwater spray icing model for a rotating cylinder based on dimensional analysis; (5) to briefly present an experimental methodology by which data was obtained to tune the proposed freshwater spongy spray icing model; (6) to demonstrate that this model has the potential for describing the dependence of sponginess on wind speed, air temperature, and liquid water content of the air, and (7) to make recommendations for future work in spongy spray ice growth modelling and experimentation.

2. ICE FORMATION

This chapter reviews the fundamental concepts of ice crystal growth which apply to solidification of pure water and seawater. Although the focus here is on spray ice formation, the basic mechanisms of sea ice growth are also considered in order to assist in understanding a recent sea spray ice growth model by Makkonen (1987), which is based on an analogy with sea ice growth.

2.1 Ice Crystal Formation from Pure Water

A distinctive feature of water is that the solid phase is less dense than the liquid phase. The molecular spatial structure of ice crystals is therefore on average less compact than that of liquid water. Naturally-occuring ice has two crystallographic axes of symmetry, one called the principal hexagonal or c-axis, and the other, the a-axis. Figure 2.1 shows the c-axis as well as the three a-axes, a_1, a_2 and a_3. Ice crystal growth may occur by the addition of water molecules in either the c-axis direction or the a-axis direction.

2.1.1 Constrained growth

In pure water, whether more molecules are added in either the a-axis direction or the c-axis direction depends significantly upon the imposed thermodynamic conditions. Consider Fig. 2.2 in which a surface perturbation is

PLEASE NOTE:

Figure 2.1 has been removed due to copyright restrictions. It was originally from Weeks and Ackley, 1982. (see bibliography). The figure shows the crystal lattice structure of ice.

Figure 2.2 has been removed due to copyright restrictions. It was originally from Kurz and Fisher, 1986. (see bibliography). The figure shows an initially perturbed solid/liquid interface.

FIGURE 2.1 The crystal lattice structure of ice. (Weeks and Ackley, 1982)

FIGURE 2.2 Solidification of a pure substance. In a pure substance, stability of the growing interface depends on the direction of heat flow. (Kurz and Fisher, 1986)

postulated for an initially planar interface (as shown by the straight line). If the solid (labelled s in Fig. 2.2) is refrigerated in order to produce crystal growth at the perturbed interface and also to produce a surface growth velocity V in the direction shown in Fig. 2.2, then heat flow will be constrained by conduction through the solid. This is called constrained or directional solidification. In constrained solidification, Fourier's law of heat conduction, in tandem with the assumption that the liquid/solid interface temperature is uniform, leads to the conjecture that the thermal gradients along cross sections A and B are different. Because the thermal gradient in the solid along cross section A is smaller in the vicinity of the perturbation than the thermal gradient along cross section B, the heat conduction from the "hollow" at cross section B will be larger than that at the perturbation at A. This implies that a larger quantity of water will solidify at section B than at A, resulting in an eventual elimination of the perturbed surface structure. The growth of lake ice may be an example of constrained solidification in which a planar interface will be maintained as solidification progresses. A schematic example of a stable constrained growth sequence for an initially perturbed surface is shown in Figure 2.3(b).

PLEASE NOTE:

Figure 2.3 has been removed due to copyright restrictions. It was originally from Kurz and Fisher, 1986. (see bibliography). The figure shows unstable and stable interface development during unconstrained solidification.

FIGURE 2.3 Initial evolution of an unstable (a) or stable (b) interface. The initially perturbed surfaces on the left are either amplified as in case (a) or damped out as in case (b). For pure substances the direction of heat transfer will determine the stability of the planar interface. In this case the instability shown in (a) results from an unconstrained heat transfer configuration and the stability exhibited in (b) results from constrained solidification. (Kurz and Fisher, 1986)

The planar stable constrained solidification of lake ice is an example of ice growth in which the ice crystals show a preferred orientation with the a-axis parallel to the advancing interface. Weeks and Ackley (1982) point out that ice crystal growth parallel to the c-axis is orders of magnitude slower than growth in the a-axis direction. Ice crystals whose a-axes are perpendicular to the growth direction will be suppressed by unfavorable constraining temperature gradients in the crystals (as described above).

However, ice crystals whose a-axes are parallel to the advancing ice interface will grow slowly in the c-axes direction (same as the ice growth direction), and more quickly in the a-axes direction (parallel to the ice surface). A geometric argument may be used to show that the ice crystals whose a-axes are perpendicular to the interface, are enclosed or covered by the more quickly growing crystals whose a-axes are parallel to the growth direction. In this way, the constrained growth of lake ice is associated with a crystal orientation in which the a-axis is perpendicular to the direction of growth.

2.1.2 Unconstrained growth

Unconstrained crystal growth occurs when the direction of heat flow is the same as the direction of crystal growth, ie: heat flow at the interface is directed into the liquid. Re-examination of Fig. 2.2 under different thermodynamic boundary conditions illustrates how the crystallographic a-axis may tend to account for most of the crystal growth.

If the direction of heat flow is reversed as a result of a liquid temperature that is lower than that of the growing solid, we may argue that a perturbed surface (as shown in Fig. 2.2), will become unstable. In this case, the liquid in contact with the surface must be at a temperature that is less than the equilibrium freezing temperature of water. This is because the equilibrium freezing temperature T_e is defined as the temperature at which the rate of addition of water molecules to the crystal lattice equals the rate of molecular loss. The amount ΔT by which the equilibrium freezing temperature exceeds the solid/liquid interface temperature is known as either the undercooling or the supercooling of the solid/liquid interface.

Due to the release of latent heat at the interface, the liquid will have a higher temperature near the interface than at some distance from the interface. Therefore, a given perturbation that protrudes out into the supercooled liquid will experience a higher temperature gradient, a greater heat loss, and consequently, a greater rate of mass accumulation. This greater mass accumulation causes the small surface perturbation to grow and advance, thereby producing an unstable solid/liquid interface and free dendritic growth. The evolution of a columnar dendritic structure which is the result of instability due to unconstrained growth of a pure substance is shown in Fig. 2.3(a). Free-growing dendritic structures will result for many substances and they may be similar to the morphology shown in Fig. 2.4. These tree-like structures grow in response to liquid supercooling, which is for the most part the result of imposed thermodynamic boundary conditions. The dendrites tend to grow radially until they encounter warmer liquid produced by neighboring dendrites. Therefore, this mode of growth will result in a network of dendrites growing in the same direction with a characteristic spacing λ_1, as shown in Fig. 2.4.

PLEASE NOTE:

Figure 2.4 has been removed due to copyright restrictions. It was originally from Kurz and Fisher, 1986. (see bibliography). The figure contains a schematic of a growing dendrite in supercooled liquid.

FIGURE 2.4 A growing dendrite tip in a supercooled liquid. The characteristic spacing of dendrites λ_1 tends to equal the characteristic dendrite size as their growth is heat limited by their nearest neighbours. (Kurz and Fisher, 1986)

The growth of the main dendrite trunk may not entirely eliminate the supercooling in the liquid, which may prompt secondary and even tertiary growth (shown in Fig. 2.4).

When unconstrained solidification of water begins at an interface, ice crystals may form with random orientations. As the growth continues, a preferred orientation may prevail. This is because crystals that are oriented favorably will grow more rapidly and with less interference from neighboring crystals. Interfacial instability will tend to stimulate growth of ice crystals whose a-axes are perpendicular to the advancing interface. These crystals tend, geometrically, to be extended further from the solid into the supercooled liquid, and as a consequence, encounter larger liquid temperature gradients than those crystals whose a-axes are parallel to the advancing interface. Therefore, the crystals with a-axes that are perpendicular to the interface will grow more quickly. Another aspect of this is that the latent heat of fusion from the advancing crystals will reduce the liquid supercooling for crystals growing parallel or closer to the interface. This means that the crystals with a-axes parallel to the interface will be limited by the lack of supercooling. In addition, because a-axis growth is orders of magnitude larger than c-axis growth, geometric selection may take place. This selection mechanism is apparent when a-axis growth occurs close to the perpendicular, and geometrically engulfs crystals whose a-axes are parallel to the interface, and which grow very slowly in the c-axis direction (perpendicular to the interface). The geometric selection mechanism is discussed further in Weeks and Ackley (1982).

2.2 Sea Ice Formation

Sea ice formation represents a case of constrained solidification which demonstrates spongy growth, in contrast to the solid constrained growth of pure substances. The presence of impurity in solution at the solid/liquid interface is believed to be primarily responsible and the constitutional supercooling model has been used to quantitatively and qualitatively describe spongy sea ice growth. Initial brine entrapment in a mature sea ice cross section occurs in the skeleton layer, the growing solid/liquid interface portion of the ice. Constitutional supercooling is used to analyze and model the entrapment of brine in this layer.

PLEASE NOTE:

Figure 2.5 has been removed due to copyright restrictions. It was originally from Weeks and Gow, 1978. (see bibliography). The figure shows the a-axis orientation in the skeleton layer of sea ice.

2.2.1 The skeleton layer

The skeleton layer in sea ice is the layer at the bottom of the ice sheet that is in direct contact with the sea water. The skeleton layer is often composed of ice platelets (as shown in Fig. 2.5). Typically there are no lateral structural bonds between the individual platelets. Cox and Weeks (1975) assumed a constant skeleton layer thickness of 3 cm and Weeks and Ackley (1982) report that the typical skeleton layer has "essentially no strength".

FIGURE 2.5 Sketch showing the skeleton layer with two possible c-axis orientations. The a-axis is perpendicular to the c-axis, in the growth direction of the platelets. (Weeks and Gow, 1978)

Skeletal platelets are cooled by conduction of heat through the sea ice slab to the cool environment above the ice. This heat transfer configuration is an example of constrained growth as defined in section 2.1.1. As the platelets advance downward, a layer of concentrated brine is formed ahead of the solid/liquid interface. This concentrated brine is accumulated in the grooves between the platelets and is eventually sealed off and incorporated into the ice as a result of the forward advance of the platelets and ice bridging between the platelets. In this way, initial platelet spacing strongly influences the entrapped brine pockets found in the more mature layers of the sea ice sheet.

Fig. 2.5 shows that the crystallographic c-axis is perpendicular to the growth direction of the platelets. This implies that these platelets are growing in the a-axis direction and are therefore dendritic in nature. However, they are not free dendritic, the result of unconstrained growth, as shown in Fig. 2.4. These platelet structures are a type of cellular dendrite and neither the constrained or unconstrained mechanisms as described in section 2.1.1 or 2.1.2 are able to explain these formations. The growth of the skeleton layer is commonly explained in terms of a model called constitutional supercooling (Weeks and Ackley, 1985).

2.2.2 The constitutional supercooling model

Burton et al. (1953a) proposed a model of solute incorporation into single crystals of germanium, which became known as the constitutional supercooling (CS) model. CS characterizes the steady-state transport of solute by diffusion and fluid motion into a growing crystal. Burton et al. (1953b) found that incorporation of solute into germanium crystals was critically dependent on fluid motion

PLEASE NOTE:

Figure 2.6 has been removed due to copyright restrictions. It was originally from Weeks and Ackley, 1982. (see bibliography). The figure shows the solute distribution at a freezing interface.

over the growing crystal. The CS model is used to explain the morphological development of the skeleton layer in growing sea ice (Figure 2.5). CS is caused in part by the extraction of water molecules from the brine at the advancing solid/liquid interface of a platelet. As pure water is extracted, a concentration boundary layer of thickness δ is formed, as shown in Fig. 2.6, which displays the variation of solute concentration with distance from the solid/liquid interface.

FIGURE 2.6 Steady-state distibution of solute in the liquid ahead of the advancing solid/liquid interface (Weeks and Ackley, 1982).

The steady state profile of salinity in this layer is a result of the balance between salt rejection into the liquid at the interface and salt transport by diffusion from the concentration boundary layer.

In a general development of CS, Burton et al. (1953a) represent the mass conservation of solute by the continuity equation:

$$\frac{\partial C}{\partial t} = -\nabla\cdot(C\vec{V}-D\nabla C) \qquad 2.1$$

where C is the concentration of the solute, t is time, $\vec{V}$ is the vector fluid velocity , and D is the diffusion coefficient of the solute. A one-dimensional steady-state assumption is made, along with fluid incompressibility, to yield:

$$D\frac{d^2C}{dx^2} - V_x\frac{dC}{dx} = 0 \qquad 2.2$$

Burton et al. (1953a) fix the coordinate system to the solid/liquid interface with the origin at the interface and positive x direction out into the liquid. The velocity V_x is taken to be the sum of the crystal growth velocity, f, and, w, the normal fluid velocity due to the density difference between solid and liquid.

Next, Burton et al. (1953a) propose that beyond the concentration boundary layer, the concentration of solute is uniform and equal to C_1. Therefore, the first boundary condition is:

$$C = C_1 \quad \text{at } x = \delta \qquad 2.3$$

In this way, complete mixing is assumed beyond the concentration boundary layer δ, and solute transport is assumed to be governed by diffusion within the boundary layer.

A second boundary condition is formulated on the steady-state assumption that the amount of solute entering the concentration boundary layer as a result of the forward movement of the solid/liquid interface, equals the amount of solute escaping by diffusion back into the well mixed layer from the concentration boundary layer. This second boundary condition is written:

$$(C_i - C_s)f + D\frac{dC}{dx} = 0 \quad \text{at } x = 0 \qquad 2.4$$

where C_s is the concentration of solute in the solid, and C_i is the concentration at the interface. The solution to equation 2.2 under the boundary conditions 2.3 and 2.4 is:

$$\frac{C_i - C_s}{C_l - C_s} = e^{\Delta} \qquad 2.5$$

where $\Delta = f\delta/D$.

Under equilibrium, the equilibrium distribution coefficient' $k_0 = C_s/C_i$ and the effective distribution coefficient $k = C_s/C_l$ were used along with equation 2.5 by Burton et al. (1953a) to produce:

$$k = \frac{k_0}{k_0 + (1-k_0)e^{-\Delta}} \qquad 2.6$$

'k_0 in this case applies only at the interface and not throughout the melt.

For equilibrium to be strictly in force, the liquid/solid interface will not be moving forward. Consequently, the effective distribution coefficient must be derived for the non-equilibrium case using the interfacial distribution coefficient $k^*=C_s/C_i$ to yield:

$$k = \frac{k^*}{k^* + (1-k^*)e^{-\Delta}} \qquad 2.7$$

Two experimental investigations of sea ice growth used this constitutional supercooling model as a basis from which to analyse their respective data. Cox and Weeks (1975) and Lofgren and Weeks (1969) obtained the same value for k_o=0.26. Since k_o is an equilibrium constant, this implies that the salinity for the ice will be 0.26 that of the salinity of sea water in the limit as no ice is being added to the structure.

3. EXISTING SPONGY SPRAY ICING MODELS

Two spongy spray icing models which have been recently proposed, are reviewed here. The first, presented by Makkonen (1987), involves an analogy between the entrapment of salt in sea ice growth and in spongy sea spray icing, and then incorporates the resulting assumptions into a cylinder icing model. The University of Alberta ship icing model (Zakrzewski and Lozowski, 1987) is also reviewed. It parameterizes the total and local icing rates over the front face of a trawler's superstructure. The models are compared, and the basic assumptions of each are discussed.

3.1 The Makkonen (1987) sea spray icing model

Makkonen (1987) presents a theoretical model for salt incorporation into spray ice that is founded upon an analogy with sea ice growth. Makkonen (1987) starts by assuming salt conservation for spongy spray ice growth. As essentially pure ice crystals form, the rejected salt will tend to increase the surface brine film salinity. A portion of the surface brine is trapped in the growing ice matrix to form brine pockets and the remaining portion is shed. The conservation of salt is expressed by:

$$FS_w = IS_i + (F - I)S_b \tag{3.1}$$

where F is the mass flux of saline water collected by the icing surface, I is the rate of mass accretion of ice and brine, and S_w, S_i and S_b are the salinities of spray water, ice and the surface brine film, respectively. These salinities are defined as the ratio of salt mass in solution to the total mass, and therefore salinity is a dimensionless parameter. All salinity ratios are in parts per unit, unless otherwise stated. The author is careful to define the "accretion fraction" as the ratio of the total accreted mass flux (salt and water substance that remains) to the collected mass flux (salt and water substance initially captured by the surface).

If equation 3.1 is divided by FS_b and the accretion fraction (n=I/F) incorporated, then:

$$\frac{S_w}{S_i}\,\frac{S_i}{S_b} = n\frac{S_i}{S_b} + (1-n) \qquad 3.2$$

The interfacial distribution coefficient is defined as:

$$k^* = \frac{S_i}{S_b} \qquad 3.3$$

and parameterizes the non-equilibrium capture of salt at the advancing solid/liquid interface. The effective distribution coefficient is defined as:

$$k = \frac{S_i}{S_w} \qquad 3.4$$

and describes the salt entrapment efficiency in the growing solid. Rearrangement of equation 3.2, along with substitution of the interfacial distribution coefficient and the effective distribution coefficient results in:

$$k = \frac{k^*}{1 - (1-k^*)n} \qquad 3.5$$

Equation 3.5 shows that the effective distribution of salt for the spray icing process depends upon k^*, the interfacial distribution coefficient and n, the accretion fraction. Therefore, for a given icing event, if k^* and n were known, the value of k could be calculated. The salinity of the surface brine, S_b, is also known in this case by solving equations 3.3 and 3.4.

Since no experimental data are available for k^* in spongy sea spray icing, Makkonen proposes an analogy with salt entrapment in sea ice growth. There is a considerable body of experimental work on the interfacial distribution coefficient, k^*, for initial entrapment of salt in sea ice growth. Weeks and Ackley (1982) document this body of work and the constitutional supercooling model that appears to provide a useful framework for evaluating salt distribution in the skeleton layer of sea ice. On the basis of the work of Weeks and Lofgren (1967), and Cox and Weeks (1975), a value of $k^* = 0.26$ is assumed to be reliable at low growth rates.

The flow of heat in sea ice growth is opposite in direction to that in sea spray icing. Makkonen therefore suggests that although the solute buildup at the solid/liquid interface is responsible for dendritic growth in sea ice, in accordance with CS, dendritic growth in spray icing is the result of imposed supercooling.

Makkonen suggests that sea spray icing may be analogous to sea ice growth at rates between the planar growth regime and the CS based dendritic growth regime. For sea ice growth, $k^* = 0.26$ in this range, and therefore he proposes that as a first working assumption, $k^* = 0.26$ for sea spray icing as well.

Next Makkonen shows that k^* for sea spray icing may be interpreted as the saline sponginess or liquid water fraction of the accretion. In the limit as the salt mass becomes negligible, the saline sponginess becomes equal to fresh water sponginess. This concept is expressed by:

$$k^* \cong \lambda_s \cong \lambda_f \cong 0.26 \qquad 3.6$$

where λ_s and λ_f are the liquid mass fractions for saline and fresh water accretions, respectively.

Assuming that $k^* = 0.26$, equations 3.3 and 3.5 may be used to solve for the ice accretion salinity:

$$S_i = \frac{0.26}{1 - 0.74n} S_w \qquad 3.7$$

With equation 3.4 the salinity of the brine film can be shown to be:

$$S_b = \frac{1}{1 - 0.74n} S_w \qquad 3.8$$

Equations 3.6 and 3.7 imply that the salinity of the surface brine and the salinity of ice accretion are known for a given spray salinity and accretion fraction, n. Makkonen (1987) then goes on to suggest that the factors that control n will control the ice salinity and surface brine salinity. The condition of the atmosphere and the dimensions of the icing surface will therefore influence these salinity distribution effects. These factors are explicitly described in a cylinder icing model (Makkonen,1984) that calculates n for fresh water icing. The accretion fraction is:

$$n = \frac{h}{FL} [t_s - t_a + \frac{\varepsilon Le}{c_p Pa} (e_s - e_a) - \frac{rv^2}{2c_p}] + \frac{C_w(t_s - t_d)}{L} + \frac{\sigma a(t_s - t_a)}{FL} \qquad 3.9$$

where Makkonen (1987) defines the variables as follows: h is the convective heat transfer coefficient, F is the flux of water to the surface, t_a the air temperature, t_s the temperature of the icing surface, t_d the spray droplet temperature, L the latent heat of freezing at t_s, ϵ=0.622, L_e the latent heat of evaporation, c_p the specific heat of air at constant pressure, P_a the air pressure, e_s and e_a are the saturation water vapour pressures over water at the surface temperature and dew-point temperature, respectively, r is the overall recovery factor (r=0.79) of a cylinder, as described by Lozowski et al. (1979), c_w the specific heat of water, σ the Stefan-Boltzmann constant, and $a = 8.1\times10^7\ K^3$, evaluated at $t_s = 0^\circ C$ and $t_a = -10^\circ C$ by Makkonen (1984).

The overall heat transfer coefficient h (in equation 3.9) incorporates the effect of a rough icing surface on heat transfer. This is accomplished by using a numerical boundary layer model of heat transfer (Makkonen, 1985) which requires an input estimate of the roughness of the cylindrical accretion surface.

Equation 3.9 was formulated for the freshwater case; consequently, Makkonen (1987) suggests that three effects of saline icing may be incorporated to model saline spongy spray icing more effectively. The first effect is that the salinity of the surface brine will determine an equilibrium freezing temperature t_s different from 0 °C according to the parameterization:

$$t_s = -54.0\ S_b - 600\ S_b^3 \qquad 3.10$$

In addition to altering the surface equilibrium temperature, the salinity of the surface will change the equilibrium water vapor pressure over the cylinder surface according to:

$$e_s = (1 - 0.537\ S_b)\ e'_s \qquad 3.11$$

This changes the mass transport of vapor and heat from the surface of the cylinder. The final effect to account for is the accretion of semi-solid spongy ice which will have a latent heat different from solid ice. The latent heat of spongy ice was assumed to be directly and linearly related to the fraction of solid ice mass in an accretion. As well, the sponginess can be shown to be equal to S_i/S_b, therefore the latent heat of accretion was defined according to

$$L = (1 - \frac{S_i}{S_b})\ L_f \qquad 3.12$$

where L_f is the latent heat of fusion for pure water at the temperature of the surface brine film.

An iterative procedure is suggested (Makkonen, 1987) to solve for accretion salinity and ice mass growth rate on a rotating cylinder under specified atmospheric conditions. Once the atmospheric conditions, the collected flux of water, the droplet temperature and the size of the cylinder are known, the accretion fraction n can be calculated from equation 3.9, assuming a freshwater accretion for the first iteration. This initial value of n is used in calculating S_i and S_b from equations 3.7 and 3.8, respectively. These values of S_i and S_b are then used in estimating the surface equilibrium temperature, t_s, the surface vapor pressure, e_s, and the latent heat of accretion L from equations 3.10, 3.11 and 3.12. Once these are estimated for the present iteration, a new value of n is produced which is used to infer new values of S_i and S_b. The iterative procedure is continued until the desired accuracy in n is achieved. Makkonen (1987) indicates that stability problems may occur when the value of n approaches one. The user should be aware of this when running a program based on these equations.

Makkonen found that the ratio of the mass accretion rate for freshwater spongy icing to the mass accretion rate for spongy saline spray icing was less than one for atmospheric conditions expected at typical marine structures. Further discussion of Makkonen's paper is in Section 3.3.

3.2 The University of Alberta ship icing model

The Zakrzewski and Lozowski (1987) model of sea spray spongy ice accretion (also described in Zakrzewski, Blackmore, Lozowski (1987)), is an integral part of the University of Alberta ship spraying/icing model. The model of sea spray transport to the front face of the superstructure of a ship as a result of ship/wave interaction has been documented by Zakrzewski, Blackmore, Lozowski and Muggeridge (1987). The total mass flux of sea water in the form of airborne spray to the front face of the vessel's superstructure is accounted for by summing the mass flux of sea spray to each of 91 grid cells. Each 0.5 meter square grid area in the 7 × 13 cell network receives a flux of sea spray dependent on a number of oceanographic, meteorological, vessel specific and operational parameters:

1. the locations of the grid cell centres with respect to the ship,
2. the spray trajectories with respect to the cell locations,
3. the spray droplet diameter,
4. the intensity of spray (a function of the source region),
5. the frequency of spraying events,
6. the fetch, and
7. the vessel speed and direction.

The ship splashing model averages the cyclical spraying flux associated with periodic ship/wave collisions, over time, to produce an average flux $R_{i,j}$ (in kgm^{-2} s^{-1}) for each grid cell (designated by the subscripts i,j). The ice accumulation is assumed to occur over a short time interval, during which the growth rate of ice and the properties of the accretion are assumed constant. The total mass accretion flux for a given grid cell is:

$$\hat{R}_{i,j} = \overset{o}{R}_{i,j} + I_{i,j} \qquad 3.13$$

where $\overset{o}{R}_{i,j}$ is the mass flux of brine entrapped within the ijth grid cell, $I_{i,j}$ is the icing flux of pure ice, and $\hat{R}_{i,j}$

is the total mass flux of the spongy deposit. $\overset{o}{R}_{i,j}$ can be defined in terms of ice sponginess, $s_{i,j}$:

$$\overset{o}{R}_{i,j} = \frac{I_{i,j}\,(1 - s_{i,j})}{s_{i,j}} \qquad 3.14$$

where the ice sponginess is equal to:

$$s_{i,j} = \frac{I_{i,j}}{I_{i,j} + \overset{o}{R}_{i,j}} \qquad 3.15$$

The salt balance equation for the ice deposit in the ijth grid cell is:

$$\overset{o}{R}_{i,j}\overset{o}{S}_{i,j} = \hat{S}_{i,j}(\overset{o}{R}_{i,j} + I_{i,j}) \qquad 3.16$$

where $\overset{o}{S}_{i,j}$ is the salinity of the entrapped brine, and $\hat{S}_{i,j}$ is the overall salinity of the accretion. Using equations 3.13, 3.15 and 3.16, $\overset{o}{S}_{i,j}$ can also be expressed in terms of the ice sponginess and the overall ice salinity:

$$\overset{o}{S}_{i,j} = \frac{\hat{S}_{i,j}}{1 - s_{i,j}} \qquad 3.17$$

For any grid cell the water mass balance equation is:

$$R_{i,j} + R^{*}_{i-1,j} = \overset{o}{R}_{i,j} + I_{i,j} + R^{*}_{i,j} \qquad 3.18$$

where $R_{i,j}$ is the direct spray flux, $R^{*}_{i-1,j}$ is the flux of shed water from the cell immediately above, $\overset{o}{R}_{i,j}$ is the mass flux of brine entrapped, $I_{i,j}$ is the pure ice growth flux, and $R^*_{i,j}$ is the flux of shed water from the cell (Figure 3.1). Here Zakrzewski, Blackmore and Lozowski (1987) have made the implicit assumption that the surface water flux is not wind driven and hence flows straight down.

The salt balance equation for the cell is:

$$R_{i,j}\, S_o + R^*_{i-1,j} S^*_{i-1,j} = \overset{o}{R}_{i,j}\, \overset{o}{S}_{i,j} + R^*_{i,j}\, S^*_{i,j} \qquad 3.19$$

where S_o is the spray salinity (assumed to be equal to the salinity of the seawater at the sea surface), $S^*_{i-1,j}$ is the salinity of the shed water flowing from the cell immediately above, $\overset{o}{S}_{i,j}$ is the salinity of the entrapped brine,

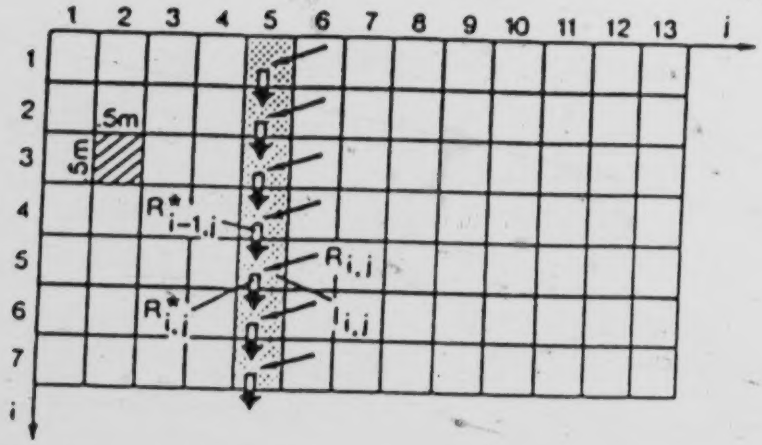

FIGURE 3.1 Water and salt transport on the front face of the superstructure (Zakrzewski et al. 1987).

and $S^*_{i,j}$ is the salinity of the shed water leaving the cell.

Panov (1976) has presented a figure giving the distribution of the overall salinity of the accretion on the vertical front face of a Soviet trawler. The Soviet data fairly well fit the regression line (Zakrzewski and Lozowski, 1987):

$$\hat{S}_{i,j} = -3.85 z_{i,j} + 25.8 \qquad 3.20$$

where $z_{i,j}$ is the height above the ship's deck, and $\hat{S}_{i,j}$ is in parts per thousand.

The sponginess of the ice deposit on the front face of the superstructure of the RFT "Wilfred Templeman" was measured during a research cruise in waters east and south of Newfoundland during January 1987 by Zakrzewski. It shows a tendency to decrease down the wall. The University of Alberta data fit the regression line:

$$s_{i,j} = 0.047 z_{i,j} + 0.79 \qquad 3.21$$

where $z_{i,j}$ is the same as in equation 3.20. At present there are no other data on ice sponginess which are appropriate for ships.

Rearrangement of equations 3.18 and 3.19 with the aid of equations 3.15 - 3.17 and 3.20 - 3.21 leads to an equation for calculating the rate of rundown to the cell immediately below (Zakrzewski and Lozowski, 1987):

$$R_{i,j} = (1 - \frac{n_{i,j}}{s_{i,j}}) (R_{i,j} + R^{*}_{i-1,j}) \qquad 3.22$$

and the overall salinity of the moving water film:

$$S^*_{i,j} = \frac{R_{i,j}S_o + R^*_{i-1,j}\ S^*_{i-1,j} - n_{i,j}\hat{S}_{i,j}(R_{i,j} + R^*_{i-1,j})/s_{i,j}}{(1 - n_{i,j}/s_{i,j})(R_{i,j} + R^*_{i-1,j})} \qquad 3.23$$

where all terms are the same as in equations 3.18 and 3.19, and $n_{i,j}$, the freezing fraction, is defined as:

$$n_{i,j} = \frac{I_{i,j}}{R_{i,j} + R^*_{i-1,j}} \qquad 3.24$$

To estimate the ice growth rate and freezing fraction, equations 3.22 and 3.23 are incorporated into the heat balance equation for the icing surface. Spray droplets of temperature T_d, (which varies over the grid due to different cooling flight times), impact on the superstructure. The temperature of the moving film of brine is assumed to be equal to the equilibrium surface temperature, T_s, and to be homogeneous over a grid cell, and throughout the thickness of the water film. If icing progresses, T_s is equal to the freezing temperature, T_f, of the shed water of salinity $S^*_{i,j}$. The freezing point of this water may be approximated from (Makkonen, private communication):

$$S_b = \frac{-T_f}{0.054} \qquad 3.25$$

where S_b is the salinity (in parts per thousand) of the seawater, and 0.054 has the dimensions of temperature (°C). Equation 3.25 may be derived from equation 3.10 by (1) assuming that 600 S_b' is negligible; (2) changing the units of S_b from parts per thousand to parts per unit; (3) solving for S_b instead of for t_s, and, (4) assuming $T_f = t_s$ (a notation difference).

If the heat flux through the ice deposit, and the heat fluxes due to the kinetic energy of the impinging spray and aerodynamic heating are neglected, the solution of the heat balance equation for the icing surface leads to the following formula for the pure ice growth rate (Zakrzewski and Lozowski, 1987):

$$\begin{aligned} I_{i,j} = {} & h l_f^{-1} \left[\left(\frac{Pr}{Sc}\right)^{0.63} \left(\frac{\varepsilon l_v}{c_a p}\right) (e_{i,j} - e_a) - (Ta - \theta_{i,j}) \right] \\ & + R_{i,j}\, l_f^{-1}\, c_w\, (\theta_{i,j} - (T_d)_{i,j}) \\ & - a\, l_f^{-1}\, (Ta - \theta_{i,j}) - R^*_{i-1,j}\, c_w\, l_f^{-1}\, (\theta_{i-1,j} - \theta_{i,j}) \end{aligned} \qquad 3.26$$

where Pr = 0.711 and Sc = 0.595 are the Prandtl and Schmidt numbers for air, l_v is the latent heat of vaporization, c_a and c_w are the specific heat capacities at constant pressure of air and seawater, l_f is the latent heat of fusion of pure water, p is the air pressure, θ is the freezing point of shed brine, $R^*_{i-1,j}$ is the shed water flux from the cell immediately above, $R_{i,j}$ is the direct spray flux to the cell, $R^*_{i,j}$ is the flux of shed water leaving the cell, T_a is the air temperature, T_d is the spray impact temperature, $e_{i,j}$ is the saturation vapour pressure at the temperature θ, and e_a is the actual vapour pressure in the airstream. The effect of salt on the saturation vapour pressure is neglected. ϵ is the ratio of the molecular weights of water vapour and dry air (ϵ=0.622), a is the linearization coefficient for the heat flux due to long-wave radiation (a=4.4 $Wm^{-2}K^{-1}$, evaluated at an ice surface temperature of 0 °C and an environmental temperature of -10 °C), h is the convective heat transfer coefficient, which is related to the Nusselt number, Nu, by:

$$h = \frac{k_a Nu}{L} \qquad 3.27$$

where L is the characteristic length of the object (here, L = 4.47 m denotes the geometric mean dimension of a surface whose height is 3.5 m and breadth 5.72 m), and k_a is the thermal conductivity of the air. Since at present there is a lack of experimental data giving the Nusselt number for such large objects as a ship superstructure, the formula of Kreith (1969) for a flat plate in a parallel airstream has been used:

$$Nu = 0.036\ Pr^{0.33} Re^{0.8} \qquad 3.28$$

where Re is the Reynolds number:

$$Re = \frac{L\ Ur}{\nu_a} \qquad 3.29$$

where ν_a is the kinematic viscosity of the air, and Ur is the wind speed relative to the ship.

An iterative procedure is required to solve for $I_{i,j}$. On the first iteration, the rundown flux, $R^*_{i,j}$, is assumed to be equal to $R_{i,j}$, the water supply flux, and the rundown salinity, $S^*_{i,j}$, is assumed equal to the spray salinity S_o. These assumptions, plus equation 3.25 and a known rundown flux from the grid cell immediately above, $R^*_{i-1,j}$, allow the solution of equation 3.26 for $I_{i,j}$. This first value of $I_{i,j}$ can be used with equation 3.24 to solve for the first value $n_{i,j}$. This value of $n_{i,j}$ is used in equations 3.22 and 3.23 along with the other required parameters, to calculate $R^*_{i,j}$, a new value of the rundown flux and $S^*_{i,j}$, a new value of the rundown salinity. This completes the first iteration. $R^*_{i,j}$ and $S^*_{i,j}$ are then used again to calculate another value for $I_{i,j}$. This iterative procedure is terminated when a sufficiently small change in $n_{i,j}$ occurs. Because $\hat{S}_{i,j}$ the salinity of the accretion, and $s_{i,j}$ the sponginess, are empirical functions of height, their values remain unchanged throughout the iterative process. This implies that the procedure searches out a mass and heat balance that will produce these empirically defined ice properties.

Equation 3.26 can be used to calculate the time-averaged local rate (in $\text{kgm}^{-2}\text{s}^{-1}$) of the growth of pure ice for a given cell, if the air-sea and ship motion parameters involved in the ice growth are constant. The thickness growth rate of spongy saline ice is:

$$H_{i,j} = \bar{I}_{i,j} \left(\frac{1}{\rho} + \frac{1}{\overset{o}{\rho}_{i,j}} \frac{1 - s_{i,j}}{s_{i,j}} \right) \qquad 3.30$$

where $\bar{I}_{i,j}$ is the time averaged local icing rate ($\text{kgm}^{-2}\text{h}^{-1}$) $s_{i,j}$ is the ice sponginess, ρ is the density of pure ice, and $\overset{o}{\rho}_{i,j}$ is the density of the brine entrapped in the ice deposit. $\overset{o}{\rho}_{i,j}$ can be estimated by:

$$\overset{o}{\rho}_{i,j} = \frac{\rho_s}{\overset{o}{S}_{i,j} + (\rho s/\rho w)(1 - \overset{o}{S}_{i,j})} \qquad 3.31$$

where $\overset{o}{S}_{i,j}$ is the salinity of brine (in parts per unit), ρ_s is the density of the salt in seawater, equal to approximately 3291 kgm^{-3} and ρ_w is the density of pure water.

The spongy ice accretion rate under steady state conditions is:

$$\hat{m}_{i,j} = \frac{P_{i,j}\,\bar{I}_{i,j}}{S_{i,j}} \qquad 3.32$$

where $P_{i,j}$ is the surface area of the grid cell (in m^2). Once $\hat{m}_{i,j}$ is determined for all the grid cells on the front face, the total mass loading rate for the front face of the superstructure will result from a summation of all $\hat{m}_{i,j}$ values.

3.3 Discussion

Supercooling from solute buildup at the solid/liquid interface (constitutional supercooling), and supercooling as a result of imposed heat transfer, may combine to enhance dendritic growth. This hypothesis supports Makkonen's (1987) supposition that saline spray icing assumes a dendritic substructure. The factors that control k^* in saline spray icing may have to be determined experimentally in the future. The two models under discussion in this chapter will now be compared.

3.3.1 Supercooling and dendritic growth

Makkonen concludes that "the ice-liquid interface during spray icing assumes a dendritic substructure regardless of the growth conditions and salinity of the spray. Consequently some liquid is always trapped within the spray ice matrix." This hypothesis appears reasonable since both freshwater and saline spray icing are examples of unconstrained accretion. In unconstrained growth the imposed supercooling at the growing ice surface will usually motivate dendritic ice crystal growth in the a-axis direction. The resulting network of dendritic ice would form a matrix capable of containing water. Knight (1980) suggests that "the preferred orientation in spongy hail growth has

PLEASE NOTE:

Figure 3.2 has been removed due to copyright restrictions. It was originally from Weeks and Ackley, 1982. (see bibliography). The figure shows the saline equilibrium freezing temperature and liquid temperature profiles in the freezing of solute at the interface.

the c-axis parallel to the growing surface." This supports the present supposition, as it implies a-axis dendritic growth perpendicular to the growing surface.

Figure 3.2 shows the thermal gradients which picture the criteria for constrained solidification from an impure solute (known as constitutional supercooling). In conventional CS (Chalmers, 1964) the direction of the heat flow is from the warm liquid to the cool solid. Lines G_1, G_2 and G_3 (Fig. 3.2) demonstrate how the liquid temperature varies in the vicinity of the solid/liquid interface. The curve T_e represents the variation of solute equilibrium freezing temperature as a function of displacement from the solid/liquid interface. The solute equilibrium freezing temperature varies in response to the variation of solute concentration (Fig. 2.6).

FIGURE 3.2 Constitutionally supercooled zone of liquid ahead of an advancing interface (Weeks and Ackley, 1982).

Curve G_1 represents a strong positive gradient of liquid temperature at the interface and a condition in which CS will not occur. Curve G_2 represents a smaller thermal gradient at the interface and the initiation of CS as a potential solidification mechanism. Curve G_3 represents a case of CS by virtue of the zone of CS shown in the figure. The points along line G_3 which are in the zone of CS represent locations at which the actual liquid temperature is lower than the equilibrium temperature, implying a discrete amount of liquid supercooling. Since the amount of supercooling increases with displacement from the liquid interface, CS will be initiated.

Consider a reversal of the heat flow in Figure 3.2, as might be expected in a case of saline spray icing. Such a reversal would demonstrate a case of unconstrained solidification as defined in Chap. 2, as well as liquid temperatures that decrease with displacement from the solid/liquid interface. In these conditions, the thermal profile line G_3 would appear rotated to the left. The profile of solute equilibrium temperature as shown by the curve labelled T_e may be hypothesized to remain unchanged, as an advancing solid/liquid interface may produce a solute buildup similar to solute accumulation in CS. If this is the case, then the primary difference, when compared to CS, will be that the zone of "spray" constitutional supercooling will be much larger. This may be especially true for spray icing in which the liquid temperature profile is marked by a rapid decrease in liquid temperature as the distance from the solid/liquid interface increases. Unconstrained solidification with a solute may thus lead to larger supercooling of the liquid and possibly more aggressive dendritic growth than would be expected for solidification of pure liquid. On the basis of these theoretical arguments, the present author supports Makkonen's contention that a dendritic substructure is to be expected in saline spray icing, and further suggests that more aggressive dendritic growth than in freshwater spray icing may result due to the possibility of enhanced liquid supercooling in spray constitutional supercooling. However, spray constitutional supercooling has not been studied experimentally, and, as such, remains hypothetical.

3.3.2 The interfacial distribution coefficient

Makkonen (1987) defines the interfacial distribution coefficient, k^*, for saline spongy ice growth in such a way that it can be interpreted as the saline sponginess, λ_s. The interfacial distribution coefficient may be defined in a slightly different manner, with the resulting relationship showing the dependence of k^* on saline sponginess λ_s as well as on the shed flux ice mass fraction J_0. This opens the question of what processes in saline spongy ice growth may influence k^*.

In the Makkonen (1987) approach, ice accretion salinity S_i is defined by:

$$S_i = \frac{M_s}{M_{pi} + M_s + M_{pw}} \qquad 3.33$$

where M_{pi}, M_s and M_{pw} are the masses of pure ice, salt and pure water, respectively, in a given saline spongy ice accretion. The salinity of entrapped brine S_b is defined as:

$$S_b = \frac{M_s}{M_s + M_{pw}} \qquad 3.34$$

Since $k^* = S_i / S_b$, the interfacial distribution coefficient can be expressed as:

$$k^* = \frac{M_s + M_{pw}}{M_{pi} + M_s + M_{pw}} \qquad 3.35$$

This derivation assumes that the salt masses, M_s, found in equations 3.33 and 3.34 are identical, and equal. One possible interpretation of equation 3.35 is, therefore, that k^* is the interfacial distribution coefficient at the solid/liquid interface of an enclosed brine pocket. However, a second interpretation of equation 3.35 is that the dendritic substructure of the saline spongy ice is open enough that the salinity of brine in the external brine film is equal to or unchanged from the salinity of brine held in the dendritic substructure. This second interpretation implies uniformity of the salt distribution throughout the spongy substructure, and in the external liquid layer. Makkonen's equation 3.35 rests upon this second interpretation.

If, however, the saline spongy ice growth process results in an internal brine salinity different from the surface film brine salinity for steady state growth, then another more general derivation may be of value. In Appendix A a derivation is presented in which (1) the interfacial distribution coefficient, k^*, is defined as the ratio of the accretion salinity and the surface shed flux salinity, (2) complete mixing occurs in the surface liquid film, and (3) breakage and shedding of surface ice dendrites may contribute to surface shed flux (List, 1977). The derivation given in Appendix A yields:

$$k^* = \frac{\lambda_s}{1 - J_o} \qquad 3.36$$

where J_0 is defined as the mass ice fraction of the shed flux. Since the assumption is made that the icing surface may provide the only source of broken ice dendrites or particles, this derivation shows that k^* may be dependent on physical conditions at the surface of the growing spongy formation. Since k^* may be a function of other processes at work on the growing spongy accretion surface (shown in Appendix A), as well as of dendrite crystal breakage and shedding, it seems important to develop experimental verification for any assumptions concerning k^*. However, until such experimental evidence is forthcoming, the approach of Makkonen (1977), or similar approaches, may yield valuable working models.

3.3.3 The two models

The Zakrzewski and Lozowski (1987) approach employs a heat and mass balance to achieve the modelling of sponginess and mass accretion on the front face of the superstructure of a fishing trawler. This approach makes the following assumptions, which may lead to errors in predicting icing rates: (1) the cyclical spray pattern generated by a vessel negotiating a field of waves is replaced by a time-averaged flux which may not model the non-steady-state saline spray ice growth very well; (2) the wind shear on the liquid brine layer on the saline spongy ice may alter the run-down pattern; (3) the empiricism inherent in using a profile of sponginess measured on a Canadian vessel. The problem arises because this vessel is much larger than the Soviet fishing trawler for which the model is meant to calculate icing rates; (4) the empiricism inherent in assuming that specific icing events on two different vessels can be generalized for all icing events, and, (5) heat transfer is assumed constant over the front face of the superstructure on the basis of a heat transfer correlation determined on a much smaller flat surface in a non-turbulent external flow.

Makkonen (1987) also employs a heat and mass balance approach for sponginess and accretion mass modelling on a cylinder. This approach makes the following assumptions which may lead to errors in predicting icing rates: (1) because the cylinder is considered as a whole with respect to rundown salinity, the increase in brine salinity is not modelled locally over the icing surface; and, (2) the choice of $k^*=0.26$ may prove to be a good first working assumption, but may need refinement on the basis of experimentation.

In the following chapter, hypothetical mechanisms and conservation principles which may be at work in freshwater spongy spray ice formation are presented as the basis for a quasi-empirical spongy spray icing model.

4. THE FRESHWATER SPONGY SPRAY ICING PROCESS

Freshwater spongy spray icing is a process that may be examined in order to demonstrate the influence of imposed conditions as well as the use of a number of conservation principles. In this chapter, these conservation principles and imposed conditions, along with a number of assumptions, are delineated. The geometry of the icing surface, two accretion/shedding mechanism hypotheses, the influence of rotation, the conservation of mass, the conservation of heat energy, and the conservation of ice are presented. Together they may form a theoretical foundation upon which a hypothetical spongy spray icing model for a rotating cylinder may be built.

4.1 The Geometry of the Icing Surface

The geometry of a growing ice formation may affect the sponginess of the ice. It may influence the thermodynamics and hydrodynamics of the surface liquid film observed under spongy freshwater growth conditions (Knight, 1980). The local heat transfer from an icing object is a function of the shape of the surface and the liquid film characteristics. In turn, the liquid surface flow pattern and depth may be directly affected by the object's shape. For example, Knight (1980) reported observing icicles with spongy portions associated with a "wrinkled" surface geometry. The hollows tended to show greater sponginess than the bulges; Knight (1980) surmised that flow rate and liquid film thickness, and local heat transfer might both be responsible for the observed sponginess variation.

The geometry of the accretion may also affect the local collection of spray droplets (List, 1977), and therefore the liquid film thickness. The local liquid film thickness will in turn influence the local heat transfer which may be partly responsible for variation in local sponginess.

4.2 Accretion/Shedding Mechanism Hypotheses

Two fundamentally different accretion/shedding regimes may be possible in growth of spongy spray ice. The first mechanism hypothesized is termed here surface accretion/shedding, (depicted in Fig. 4.1 (b)), in which only a discrete depth of the spongy ice accretion is thermodynamically and mechanically active (shown by the dashed line in Fig. 4.1 (b)). The essential feature of this hypothesized accretion/shedding mechanism is that the accreted substructure which is produced, surrounds the entrapped liquid completely, like a bubble in concrete, and allows no drainage. This implies that the structure which is formed, is dense enough to eliminate any possibility of liquid seepage or transport within the accretion, and also eliminates the possibility that entrapped liquid could be admitted to the surface accretion/shedding layer a second time. Therefore, liquid water in the surface accretion/shedding layer will be shed either directly from the surface or incorporated directly into the accretion.

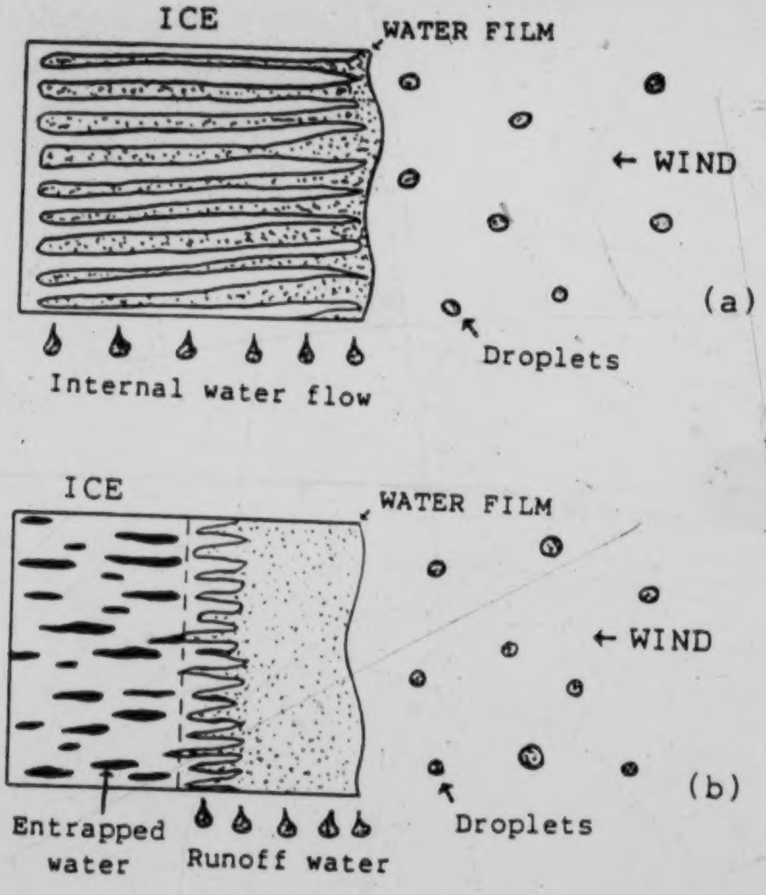
ICE
WATER FILM
← WIND
(a)
Droplets
Internal water flow
ICE
WATER FILM
← WIND
(b)
Entrapped water
Runoff water
Droplets

FIGURE 4.1. Schematic diagrams of the hypothesized filtration accretion/shedding (a), and surface accretion/shedding (b). In filtration accretion/shedding (a), the water film may be thin and internal water flow may occur in the dendritic substructure, represented here as columnar shapes in cross section. In surface accretion/shedding (b), the water film may flow through the surface dendrites but has no exchange with the entrapped water across the dashed line.

The structure of the postulated surface accretion/shedding layer might consist of free-dendrite ice crystal growth out into a liquid film (represented in Fig. 4.1 (b) by columnar cross sections). The excess free liquid (that which is not incorporated), is shed from the surface layer but is considered part of the surface accretion/shedding layer during its residence on the accretion. The surface liquid film is therefore a part of the surface accretion/shedding layer, while the free-dendritic ice crystal structure is assumed to account for the rest of the mass included in the surface accretion/shedding layer. Therefore, the surface liquid film, while not identical to the surface accretion/shedding layer, is considered part of it.

The second accretion/shedding mechanism hypothesized is termed filtration accretion/shedding (depicted in Fig. 4.1 (a)). The essential feature of this hypothesized mechanism is that a spongy, porous substructure is produced, which by its nature allows internal liquid flow, as for example a kitchen sponge might under a running tap. In this case, the accretion surface may advance by porous dendritic growth, (represented in Fig. 4.1 (a) by columnar cross sections), as a steady flow of liquid passes through the accretion under the influence of gravity or some other force. Water collected on the surface of such an accretion may be immediately "soaked" into the porous structure. The actual thickness of surface liquid may be very small as a result. One could picture the collected liquid being transported from the surface, following an internal seepage pattern, and subsequently being shed from another point on the accretion surface. If this hypothetical mechanism is at work, a further implication may be that the supercooled liquid transported from the surface may promote solidification within the accretion, which could produce a thermal gradient in the spongy ice.

Neither of these two hypotheses is discussed in the literature, to the best of the author's knowledge. However, they may relate to the interpretation of k^* given in Section 3.1. Makkonen's (1987) approach for instance, assumes first that the mass of salt, M_s, in equations 3.33 and 3.34 are identical, and so they must be, since the salinity of the entrapped brine and the salinity of the entire accretion depend upon captured salt mass, M_s. However, since the interfacial distribution coefficient, k^*, pertains to the processes at a particular solid/liquid interface, the assumptions about M_s, in equation 3.35 may carry implicit meaning.

If filtration accretion/shedding is assumed, then the interface for which k^* may be applicable is the total area of internal brine pocket surfaces, in addition to the external surface area of the accretion. In such a case, M_s, in the definition of k^*, is identical to M_s found in equations 3.33 and 3.34. Thus, the Makkonen (1987) derivation of k^* is directly applicable to the hypothesized filtration shedding icing regime.

If, on the other hand, surface accretion/shedding is assumed, as it is in this thesis, then M_s in the definition of k^* may apply only to salt mass in the surface liquid film, and not in the accretion as a whole or the entrapped liquid as a whole. The only exception occurs in the surface accretion/shedding case when the salinity of the entrapped brine equals the salinity of the surface liquid film. This is viewed as being a special case. In Appendix A, a general derivation, based on the possibility that the salinity of the entrapped brine may not equal the salinity of the surface brine, is presented.

The surface accretion/shedding mechanism is assumed in section 4.6 as the basis for the development of equations 4.3 and 4.5. The surface accretion/shedding layer is used in section 4.6.1 as a control volume for overall ice mass continuity on the surface of an accretion. The surface liquid film (which is part of the surface accretion/shedding layer) may also be defined as a control volume (as in section 4.6.2) for which an ice mass continuity of free ice particles may be postulated. Thus the surface accretion/shedding hypothesis forms the basis for development of equations 4.3 and 4.5.

Experimental work will be required to investigate these hypotheses and their influence, if any, on the freshwater spongy spray icing process.

4.3 The Influence of Rotation

Rotation is an imposed condition which may also influence the process of freshwater spongy spray icing. Lesins et al. (1980) have shown experimentally that the sponginess of a rotating cylinder under freshwater spray icing conditions may vary from 0% to 60% as a function of rotation rate. Rotation of a cylinder in a crossflow has been found to increase the heat transfer coefficient relative to its value for a non-rotating cylinder, but only after the cylinder's circumferential velocity exceeds twice the crossflow velocity (Kays and Bjorklund, 1956). This increase in heat transfer from the cylinder will increase the rate of ice growth, given a sufficient supply of surface water.

Rotation may also increase shedding, as liquid water may be forced off the icing surface under the influence of the centrifugal force. Increased shedding will reduce the surface film thickness. The surface wind shear will also increase with increased rotation rate. This too may alter conditions on the accretion surface.

Rotation is observed to minimize the effects responsible for asymmetric growth on non-rotating cylinders. This is the primary reason that the rotating cylinder was chosen for the present study. The growing surface is equitably although cyclically exposed to the different conditions at the front and back of the cylinder. The wind shear and droplet bombardment of the front face stand in sharp contrast to the relatively quiet rear face. If the liquid film, which may be of primary importance in spongy ice formation, alters its thermodynamic conditions with a characteristic time scale τ_1, then the above mentioned cyclical variation will or will not be important, according as $\tau_1 << \tau_2$, or $\tau_1 >> \tau_2$, where τ_2 is the rotation period.

4.4 Conservation of Mass

Conservation of mass plays a primary role in freshwater spongy spray icing. In the spray icing of a rotating cylinder, for instance, water droplets are collected or harvested from an air flow by collision with the cylinder. Once collected, the water substance may accumulate on the cylinder, or it may be shed back into the airstream. The flux of water substance mass harvested from the airstream is here termed the collected mass flux. The accreted mass flux is here defined as the portion of the collected mass flux of water substance that remains in the thermodynamically and mechanically inactive substructure according to the surface accretion/shedding hypothesis. The shed flux of water substance is defined here as the portion of the collected mass flux which is shed from the surface layer.

Assuming the surface accretion/shedding hypothesis, the thermodynamically and mechanically active surface layer responsible for the formation of the interior substructure contains water and ice that has been collected but not yet shed or incorporated into the final ice substructure. This layer may be described by a control volume which contains the water substance in the process of being distributed between the accretion and the shed mass. By definition, then, the surface liquid film is assumed to be part of the surface accretion/shedding layer.

Collection, accretion and shedding fluxes are characterized here on the basis of mass per unit time per unit length (in units of $kgm^{-1}s^{-1}$ over the cylinder). Therefore, the notation used here will differ from the notation used by Makkonen (1987) or by Zakrzewski and Lozowski (1987). The collected mass flux harvested from the air stream may include pure water as well as ice particles. These are represented as:

Mi_1 - the mass flux of pure ice particles collected
Mw_1 - the mass flux of pure water collected.

The accreted mass flux is represented as:

Mi_2 - the mass flux of ice accreted
Mw_2 - the mass flux of pure water accreted.

The shed flux is represented as:

Mi_3 - the mass flux of shed ice particles
Mw_3 - the mass flux of shed pure water.

The overall conservation of mass for the freshwater spongy icing process is:

$$(Mi_1 + Mw_1) = (Mi_2 + Mw_2) + (Mi_3 + Mw_3) \qquad 4.1$$

Spongy spray ice formation may be viewed as a mechanical and thermodynamical process which divides the collected mass into accreted and shed categories.

4.5 Conservation of Heat Energy

The freshwater spongy spray icing process demonstrates the principle of conservation of heat energy. Heat transfer from the rotating cylindrical icing surface may be primarily responsible for imposing the supercooling of the freshwater liquid film which subsequently motivates dendritic ice crystal growth in the surface growth layer. Another possible source of supercooling is the addition of supercooled droplets to the surface liquid film. A heat balance, applied to the surface, may model the maximum thermodynamically based formation flux of dendritic ice.

Heat transfer from the cylinder surface to the environmental air was modelled using a non-rotating cylinder formulation from Zukauskas (1972), in order to keep the present model simple. The purpose of the present study is not so much to produce an accurate and universal engineering model of freshwater spongy spray ice growth, as to suggest the lines along which such a model may eventually be developed. Since surface roughness is known to increase heat transfer from icing surfaces, an approach by Makkonen (1985) may help in developing a better evaluation of surface ice crystal growth in future spongy growth models. In addition, future rotating cylinder models may use the parameterization of Kays and Bjorklund (1956) to model heat transfer from rotating cylinders in crossflows.

In the present model, a heat balance is applied to the surface growth layer. The heat flux directed toward the surface is set equal to the flux of heat away from the surface. (This heat balance is derived and explained in Appendix B.) Heat is assumed to be lost from the surface by convective and evaporative cooling, sensible heating of the mass flux of impinging water and ice substance, and by radiation. Heat injection is assumed to result from the release of the latent heat of fusion as the ice grows. As shown in Appendix B, the resulting equation can be solved for the maximum potential growth flux of ice for given icing conditions Mi_*. The derived equation is repeated here:

$$Mi_* = \frac{\pi Dh}{L}\left[(t_s - t_a) + \left(\frac{Pr}{Sc}\right)^{0.63}\left(\frac{\epsilon L_e}{c_p Pa}\right)(e_s - e_a)\right] + L^{-1}\left[(Mi_1 c_i + Mw_1 c_w)(t_s - t_a)\right] + L^{-1}\pi D\sigma a(t_s - t_a) \qquad 4.2$$

Since many of the parameters in equation 4.2 are the same as those of equation 3.9, they will not be repeated here. Of the remainder, D is the accretion diameter, Pr is the Prandtl number, and Sc is the Schmidt number.

This equation may be applied under the restriction that the collected mass flux of liquid water is greater than Mi_*, the thermodynamic maximum ice growth flux. In the present approach, if Mi_* exceeds Mw_1 (the collected liquid flux), the accretion will be assumed to be a case of dry or rime icing, therefore , ineligible for spongy growth.

Now that the principle of heat conservation has yielded an equation for the maximum ice growth flux for the growth layer of a spongy cylindrical accretion, the conservation of ice for the growth layer may be considered as a principle which also affects the process of spongy spray ice formation.

4.6 Conservation of Ice Mass

Conservation of ice mass on the surface of a hypothetical spongy ice accretion may be modelled in terms of conservation of ice both in the surface accretion/shedding layer, and in the surface liquid film.

4.6.1 Overall ice mass conservation

In freshwater spray icing, the thermodynamically and mechanically active surface layer may be viewed as a control volume containing a constant mass of ice. The assumption of constant mass in the surface/accretion layer is arbitrary for lack of better knowledge. Whether or not this layer maintains the same mass, or maintains the same thickness, or varies with the radius of the cylinder is not known. However, in order for steady state conditions to prevail on the basis of a constant mass asumption in the surface layer, the flux of ice into the control volume must equal the flux out. The collected ice particle flux, Mi_1, and the ice converted from the liquid through freezing, Mi_4 represent sources of ice for the surface layer control volume. Mi_2, the accretion flux of ice, and Mi_3, the shed ice particle flux, represent ice flux sinks; conservation of mass in the surface layer is expressed as:

$$Mi_1 + Mi_4 = Mi_2 + Mi_3 \qquad 4.3$$

4.6.2 Free ice particle mass conservation

In freshwater spray icing, the liquid surface film (which is part of the surface layer), may be viewed as a control volume containing a constant mass of ice particles. The assumption of constant mass of ice particles in the surface liquid film is an arbitrary assumption for lack of better knowledge. However, as a first working assumption, it will suffice until studies of ice particles in the liquid film are availale. In order for steady state conditions to prevail in the liquid surface layer, the flux of ice particle mass into the control volume must equal the flux out.

Free ice particles are defined as discrete pieces of ice which are either airborne or immersed in water. Ice particles which are harvested by the cylinder from the air stream, for example, may arrive either as free airborne particles, or immersed in liquid droplets. Free ice particles that are collected from the air stream Mi_1, represent a mass flux into the surface liquid layer, and Mi_3, the shed ice flux, represents a mass flux of free ice particles out of the control volume. There is a third source of ice particles, dendritic breakage, which we assume to be important, and it is parameterized in the present approach.

List (1971) suggests that ice particles may form as a result of dendritic breakage from the ice surface, the result of aerodynamic shear and droplet bombardment. This appears possible. Single dendrites, as they grow out into the covering film of water on the surface of the ice, may have small and fragile cross sections. Garabedian and Strickland-Constable (1974) found that crystal breakage would normally occur in the c-axis direction for a 1.0 cm wide ice crystal rotating with a tip velocity of 1.5 m/s. In their study, the surrounding supercooled water was stationary, and the crystals grew in such a way that the thin cross section (in the c-axis direction) produced minimum fluid resistance. Although a controversial point, this evidence suggests that fluid shear alone may cause ice dendrite breakage in some circumstances. Verification of dendritic ice crystal breakage for freshwater spongy spray icing is yet to be established.

However, if dendrite breakage does commonly occur, then free ice particles may either be reincorporated or shed in the water which leaves the cylinder surface. The mass flux of dendritic particles that fracture and enter the surface liquid film is represented in the present study as Mi_s. Mi_s is the mass flux of free ice particles into the surface liquid and may be represented as a fraction A of the thermodynamically formed ice flux Mi_4. This relationship is:

$$Mi_5 = A\, Mi_4 \qquad 4.4$$

in which A describes the fraction of dendritic ice grown in the surface layer which fractures and ultimately exits in the shed flux. A is therefore called the ice crystal breakage/exit ratio.

The conservation of ice particle transport for the liquid film is expressed as:

$$Mi_1 + A\, Mi_4 = Mi_3 \qquad 4.5$$

Another possible mechanism for ice particle generation which will not be included in the present hypothetical framework for a freshwater spongy spray icing model, is nucleation as a result of friction, vibration or pressure pulses in the surface liquid. Chalmers (1964) states that these three agencies may cause nucleation in metastable supercooled melts. It is possible that supercooled droplets may produce ice particle nucleation on impact. If this process is found to be important in ice mass conservation in the liquid layer, it should be included in future models.

The two ice mass balances which are postulated in this chapter, and the two resulting equations, together with overall mass and heat balance, provide a partial framework for a freshwater spongy spray icing model. In Chapter Five, surface processes are hypothesized, added to the foundation laid in Chapter Four, and the details of an empirical model are considered.

5. A NEW FRESHWATER SPONGY SPRAY ICING MODEL

In this chapter, the arbitrary working assumptions which form the basis for describing the surface growth velocity and the ice crystal breakage/exit ratio, A, are presented. This is followed by a summary of the equations and their underlying assumptions, which together constitute a freshwater spongy spray icing model. This model is empirical in its description of the ice crystal breakage/exit ratio A, and is evaluated in light of a small data set. A brief descripton of the experimental methodology which produced the data precedes an evaluation of the empirical constants in the ice crystal breakage/exit ratio equation. Finally, the performance of the model is evaluated.

5.1 The Surface Growth Velocity

In crystal growth studies, the crystal growth speed is an important parameter. Since spongy spray ice formation is essentially a macroscopic demonstration of ice crystal growth, this parameter may be of interest in describing ice accretion. The present approach assumes that the spongy surface growth velocity is equal to the growth velocity of a solid ice formation under the same macroscopic heat energy and mass flux conditions. This assumption has neither theoretical nor experimental support, but is presented here to show how a knowledge of spongy spray icing surface growth velocity might be used in modelling sponginess in the future. The implications of this assumption are discussed at the end of this section, following the equation development.

The only rationale that can be provided here is that the assumed radial growth velocity lies between the maximum possible accretion velocity and the minimum possible accretion velocity. First, the maximum possible radial surface growth velocity for a cylinder, Vmax, occurs when all of the collected mass flux accretes as solid ice. Vmax may be expressed as:

$$Vmax = \left(\frac{1}{2\pi r}\right)\left(\frac{Mw_1}{\rho_i}\right) \qquad 5.1$$

where r is the radius of the accretion and ρ_i is the density of the solid ice.

If the actual ice accretion flux, Mi_2, is known for a given freshwater spongy icing event, then the minimum possible surface growth velocity, Vmin, is:

$$Vmin = \left(\frac{1}{2\pi r}\right)\left(\frac{Mi_2}{\rho_w}\right) \qquad 5.2$$

The actual surface growth velocity for an icing event is:

$$V = \left(\frac{1}{2\pi r}\right)\left[(Mi_2 / \rho_i) + (Mw_2 / \rho_w)\right] \qquad 5.3$$

The radial growth velocity of a solid ice formation (no sponginess) based on Mi_4 is:

$$V_s = \left(\frac{1}{2\pi r}\right)\left(\frac{Mi_4}{\rho_i}\right) \qquad 5.4$$

Mi_4 will lie between the values of Mw_1 and Mi_2. This is because Mi_4, the maximum potential ice accumulation flux, must be first of all less than Mw_1 for wet spongy icing to progress, and second, because Mi_2 must be less than Mi_4, the maximum potential ice accumulation flux. Therefore, for this reason, Vs will lie between Vmax and Vmin, and can provide a first working approximation to V, the actual radial growth velocity of the accretion. The proposition that the actual growth velocity, V, equals the solid heat balance based accretion velocity, Vs, can be expressed by combining equations 5.3 and 5.4 as:

$$\frac{Mi_4}{\rho_i} = \frac{Mi_2}{\rho_i} + \frac{Mw_2}{\rho_w} \qquad 5.5$$

An implication of the above equation development is that the present model should not be used to model the mass accretion rate directly. The reason for this is that once the radial growth velocity of the surface is arbitrarily determined, as it is in this case, (subject to the density difference between water and ice and the degree of sponginess predicted), the mass accretion rate is also largely determined. The reader is therefore warned that the present model is intended to empirically describe the sponginess of the accretion only, and not the mass accumulation rate. Furthermore, this assumption may be seen as a component of the model's empiricism and serves here only as a first working hypothesis. Experimental examination of spongy icing may yield better knowledge of the radial growth velocity of spray icing surfaces, which may lead to a profitable amendment to the present approach. Finally, the sponginess calculated by the present approach could be used in tandem with a mass accretion model of spray icing to help account for the effect of ice sponginess on mass accretion rates.

5.2 The Ice Crystal Breakage/Exit Ratio

In this section we look at three concepts: the wet/dry icing transition point, the icing threshold, and dimensionless parameterization. We conclude with an expression for A, the ice crystal breakage/shedding ratio.

5.2.1 The wet/dry icing transition

The wet/dry icing transition point (also known as the Ludlam limit), in freshwater spray icing will occur when the surface of the growing ice is at a temperature of 0 °C with no shedding or sponginess. Ludlam (1951) states that the surface of a hailstone in the wet growth regime may be hard and glassy, while at lower temperatures, it may become opaque and fragile. The hard and glassy hailstone ice is grown closer to the Ludlam limit, while the opaque and fragile rime ice is to be expected at lower temperatures, showing that the mechanical properties of the ice change in response to the imposed thermodynamics.

Druez, Laforte and Nguyen (1984) conclude that the compressive and adhesive strengths of ice formed by spray accretion show a maximum as a function of air temperature. It seems reasonable to postulate that the maximum ice strengths might correspond to the wet/dry ice growth transition; in this way one might expect ice strength to decrease with decreased density (the result of riming under lower air temperatures), and also with increased sponginess in the wet growth regions (associated with higher temperatures). If the compressive and adhesive strength of ice is found to be a maximum at the Ludlam limit, it may be reasonable to assume that ice crystal breakage and transport from the surface might show a minimum. The reason is that a stronger structure will not break and shed ice particles as easily as a weaker structure. This in turn holds implications for the ice crystal breakage/exit ratio, A.

Although the above suppositions are unsubstantiated, the present approach to spongy spray ice modelling assumes that the ice crystal breakage/exit ratio $A \rightarrow 0$ as $n_f \rightarrow 1$ (where n_f is the freezing fraction, defined as Mi_*/Mw_1). This may be supposed either because there are no dendrites forming and little rundown surface liquid to shed at $n_f = 1$, or because the growing structure may have sufficient strength to resist breakage, as proposed above.

5.2.2 The icing threshold

The icing threshold for freshwater spongy spray icing is defined here as the thermodynamic and mechanical condition that allows no ice formation to remain on the surface of the cylinder. This condition occurs when the accretion fraction n=0, and the surface liquid temperature approaches the equilibrium freezing temperature, Te, (0 °C for freshwater).

The cylinder icing experiment of Druez, Laforte and Nguyen (1984) shows that the adhesive strength of ice on an aluminium cylinder varies with the icing tunnel air temperature. In all cases examined, as the tunnel air temperature increased toward the freezing point, the adhesive strength of the ice dropped rapidly. This suggests the possibility that ice formed (as a result of supercooling) at the icing threshold may be sheared off the cylinder by forces such as aerodynamic drag. The author has observed ice forming on the surface of a plexiglass cylinder in the F.R.O.S.T. tunnel, in air temperatures one or two degrees below freezing temperature, only for the ice to be swept off the cylinder into the airstream. The icing threshold may thus represent a condition in which n=0 while the surface liquid film is supercooled enough to produce shedding ice particles.

Hillig (1959) showed that for ice crystals in stationary water with supercooling in excess of 0.2 °C, growth occured in the c-axis direction, and was heat limited (controlled by the lack of supercooled liquid). This suggests that ice crystals which are immersed in water with supercooling in excess of 0.2 °C will grow primarily in response to the imposed cooling. Ice crystals at supercooling of less than 0.02 °C grow in the basal plane with smaller growth velocities.

If the observations of Hillig (1959) remain valid for a possibly turbulent liquid water film on a cylinder close to the icing threshold condition, basal plane (a-axis) sheets may be expected to replace free dendritic growth below a supercooling of about 0.2 °C. As the air temperature increases toward the equilibrium freezing temperature, Te, of the freshwater surface liquid film, the supercooling, ΔT, should also decrease, causing an alteration of growth morphology from free dendritic to basal plane sheets. This hypothesis may have been partially substantiated by Knight (1980), who observed that icicle sponginess was characterized by parallel basal sheets of ice, separated by liquid water. It is therefore postulated here that near the threshold condition of icing, as the supercooling is decreased below 0.2 °C, freshwater spongy spray icing may tend toward no liquid entrapment. As the freezing fraction $n_f \to 0$, the surface accretion shedding mechanism breaks down. Thin laths of ice which have grown primarily in the basal plane may not adhere to the cylinder surface and may be "floated" off the cylinder, or these thin laths may drain efficiently under the influence of the surrounding air flow. Under such conditions, the sponginess may decrease and the crystal breakage/exit ratio, A, will be either 0 or 1, depending on whether the laths of ice are shed or not. If the laths of ice remain, the icing threshold, by definition, has not been passed.

The process of ice crystal fracture and transport in the liquid film is probably very complicated, likely involving thermodynamical as well as mechanical processes. Shearing of the dendrite tip, for instance, is mechanical in nature; it depends upon the aerodynamic skin friction, the form drag, the shear strength of the ice, and the resisting cross-sectional area. Thermodynamics also may govern the characteristic size of dendrites through imposed supercooling. Hallet (1964), for example, points out that large supercoolings lead to finer dendritic crystal growth, with a 3-D structure. Finer dendritic structures may be more prone to crystal breakage. Given this degree of complexity to the process, we have decided in the present approach to the modelling of freshwater spongy spray icing, to characterize the ice crystal breakage ratio, A, using dimensional analysis.

5.2.3 Dimensionless parameterization

The purpose of this section is to suggest freshwater spongy spray icing parameters that may influence the dendritic ice crystal breakage/exit ratio A, to organize those parameters into dimensionless groups within an equation for A, and to discuss the meaning of the dimensionless groups as far as A is concerned.

The velocity of the airstream, V, and the diameter of the ice cylinder, D, may be the most important variables in the mechanical shearing associated with aerodynamic skin friction and heat transfer. They may in part dictate the ice crystal morphology because they influence the heat transfer responsible for crystal growth. The air velocity, V, may also control the impulse force given to the surface by the colliding droplets, and consequently dendritic breakage/dislocation and surface liquid mixing. With respect to surface collision, the flux of collected liquid mass, Mw_1, will be important, as the amount of water mass in collision over the cylinder surface may be significant. The present approach does not include the effect of impacting ice particles on the dendritic ice crystal breakage/exit ratio A, even though this is probably a very significant factor (Gayet, Bain and Soulage, 1984). Instead, the airborne ice crystal content is assumed to be zero in the experimental tests. Therefore, the present approach assumes only supercooled water droplets, although Gayet, Bain and Soulage (1984) demonstrate a 50% reduction of accretion mass due to accretion surface bombardment by airborne ice crystals that result in surface breakage and exit for both wet and dry icing (a similar result is shown in Lozowski et al., 1979).

The gravitational acceleration, g, is included in the dimensional analysis, as it may influence surface liquid shedding. Gravitational acceleration in combination with centripetal acceleration and surface shearing may accentuate shedding at the bottom of the cylinder.

Macroscopic heat transfer is entrenched in the variable Mi_*, (the mass growth flux of ice) which represents the total possible accumulation of ice crystalline material. Mi_* tends to larger values for larger surface liquid undercoolings. This implies a tendency to greater dendritic morphology in the surface layer. Conversely, smaller values of Mi_* may imply smaller undercooling with a greater tendency to basal plane morphology (Hallet, 1964). Therefore, Mi_* may also influence the ice crystal breakage ratio A.

$(Mw_1 - Mi_*)$ represents the liquid mass shed flux for solid non-spongy ice growth where Mi_* is the solid accretion mass flux. If $(Mw_1 - Mi_*)$ is small, ice crystals that have broken may not be transported away from the surface and shed. If $(Mw_1 - Mi_*)$ is large, the surface liquid layer on a spongy accretion will tend to be either thick or flowing fast. Either result may facilitate more efficient ice particle shedding.

The cylinder rotation rate, Ω, will influence the thermodynamics of growth through heat transfer, as described in section 4.3. In addition, the peripheral velocity of the surface will affect the relative impact velocity between the droplets and the cylinder. Hence Ω the cylinder rotation rate in radians/second is included in the dimensionless group analysis.

Arrangement of the chosen variables ((Mw_1-Mi_4), Mw_1, Mi_4, V, Ω, D, g), into dimensionless groups results in a parameterization for A, the ice crystal breakage/shedding ratio. We have expressed this as:

$$A = C\left(\frac{Mw_1 - Mi_4}{Mi_4}\right)^a \left(\frac{Mw_1 - Mi_4}{Mw_1}\right)^b \left(\frac{V}{\pi\ D}\right)^c \left(\frac{g}{\pi^2 D}\right)^d \qquad 5.6$$

Equation 5.6 may be rewritten using the freezing fraction defined as $n_f=Mi_4/Mw_1$). The result is:

$$A = C\left(\frac{1}{n_f} - 1\right)^a (1 - n_f)^b \left(\frac{V}{\pi\ D}\right)^c \left(\frac{g}{\pi^2 D}\right)^d \qquad 5.7$$

where C, a, b, c and d are arbitary parameters which must be solved for as the basis for the empirical description of A. Equation 5.6 and 5.7 assumes a power law relationship between the dimensionless groups and A. The choice of simple power law relationships for the dimensionless groups is an arbitrary choice not in keeping with the general nature of dimensional analysis, which allows for a more general power series dependence on the variables involved.

The first two ratios contain the freezing fraction n_f which describes in a primitive way the effect of macroscopic heat transfer on ice surface growth morphology, as suggested above, for Mi_4. Neither the third nor fourth ratios have clearly interpretable influence on the ice crystal breakage/exit ratio. Given the above parameterization for the ice crystal breakage/exit ratio, the inherent equations and assumptions of the present approach to modelling freshwater spongy spray icing follow.

5.3 The Equations and Assumptions

Six equations, developed in Chapters 4 and 5, can be solved for freshwater spray icing sponginess on a rotating cylinder. The six variables that must be solved for are Mi_2, Mw_2, Mi_3, Mw_3, Mi_4 and A. The relevant equations that are sufficient for determining accretion sponginess are equations 4.1, 4.2, 4.3, 4.5, 5.5, and 5.7. These are repeated here:

$$(Mi_1 + Mw_1) = (Mi_2 + Mw_2) + (Mi_3 + Mw_3) \qquad 5.8$$

$$Mi_4 = f(Va, t_a, t_d, w, D, d) \qquad 5.9$$

$$Mi_1 + Mi_4 = Mi_2 + Mi_3 \qquad 5.10$$

$$Mi_1 + AMi_4 = Mi_3 \qquad 5.11$$

$$\frac{Mi_4}{\rho_i} = \frac{Mi_2}{\rho_i} + \frac{Mw_2}{\rho_w} \qquad 5.12$$

$$A = C \left(\frac{Mw_1 - Mi_4}{Mi_4}\right)^a \left(\frac{Mw_1 - Mi_4}{Mw_1}\right)^b \left(\frac{V}{\pi D}\right)^c \left(\frac{g}{\pi^2 D}\right)^d \qquad 5.13$$

where the mass flux of collected ice particles Mi_1, the mass flux of collected water Mw_1, the wind speed Va, the air temperature Ta, the droplet temperature t_d, the droplet diameter d, the cylinder diameter D and the liquid water content w, are required as input parameters in order to determine sponginess.

For the purpose of the present thesis, Mi_1 is assumed to be zero for lack of better information. Since Mw_1 includes the influence of the collection efficiency E, according to:

$$Mw_1 = EwD \qquad 5.14$$

the value of E must be known or estimated. For the present purpose, a parameterization of the Langmuir and Blodgett (1946) data is used on the basis of the median volume droplet diameter, d.

The present model depends on the following requirements and assumptions in modelling sponginess in freshwater spray icing on a rotating cylinder: (1) all the requisite input parameters are known, including Mi_1, Va, t_a, t_d, d, D, w and either Mw_1 or E; (2) heat transfer from the surface on the basis of a non-rotating smooth cylinder with a surface liquid film at 0 °C; (3) no droplet bouncing or splashing from the surface; (4) complete liquid film mixing before shedding; (5) equitable distribution of accretion on the cylinder; (6) the radial growth velocity for the spongy ice accretion is identical to that for a solid ice accretion given the same heat transfer; (7) the volumetric flux of shed ice particles that escape in the shed liquid flow is replaced in the accreted ice by an equivalent volumetric entrapment flux of liquid in order to maintain condition 6; (8) the surface layer hypothesis is assumed to describe the accretion/shedding mechanism (as discussed in section 4.2), and (9) the empiricism inherent in equation 5.13 for determining the ice crystal breakage/exit fraction, A, is general enough to apply to all input conditions.

Conditions 6 and 7 are an interpretation of equations 5.11 and 5.12. Equation 5.11 describes the mass balance of ice particles in the surface liquid and equation 5.12 describes the volumetric accretion of the spongy growth in relation to a solid ice accretion with the same ice growth rate Mi_4.

Since the parameterizations of the ice crystal breakage/exit ratio, A, depends upon C, a, b, c, and d, these must be determined on the basis of experimental data. A brief description of the experimental approach used to obtain a small data set is presented in the next section. This will be followed by a section on the data and the derivation of the empirical constants.

5.4 The Experimental Method

The experiments were run to obtain freshwater ice sponginess as functions of air temperature and wind speed. The F.R.O.S.T. tunnel at the University of Alberta was used for the experimental runs. This is a closed loop refrigerated wind tunnel, capable of producing spray ice accretion under controlled conditions.

The air temperature was varied in three of the cases studied, while other important parameters (wind speed, droplet size, cylinder diameter, and liquid water content) remained constant. Changing the air temperature is an effective way to alter the thermodynamics of the spongy icing process (primarily the value of n_f in equation 5.7). Another set of data was produced by varying the wind speed while holding the other parameters constant.

The tunnel air temperature control was set at a particular value for each run, and the tunnel was allowed to come to thermal equilibrium. The F.R.O.S.T. tunnel typically experiences a cyclical temperature variation with a peak-to-peak amplitude close to 1.0 °C at temperatures close to the freezing point. Therefore the air temperature was averaged over the accretion time.

The liquid water content at the cylinder location was measured before each run using a C.S.I.R.O. KING liquid water content probe (Knollenberg, 1981). The waterflow to the upstream spray nozzles was turned off just prior to the insertion of the rotating plexiglass cylinder into the working section of the tunnel. This was done in order to allow the cylinder temperature to reach equilibrium with the air. At temperatures close to the freezing point, this technique would allow an immediate ice formation while a cylinder initially at room temperature might not produce an accretion. The 5.0 cm plexiglass cylinder was oriented horizontally across the tunnel cross section, and was rotated at 0.5 Hz by a small direct current electric motor. Then the water was turned on, with the assumption that the liquid water content remained unchanged from the presetting. This assumption was verified many times in the course of the experimentation, as pressure and flow rate were observed to control the liquid water content well for each presetting.

The rotation rate of the cylinder was maintained at 0.5 Hz throughout the accretion interval. The cylinder and its accretion were removed from the tunnel after 10 to 15 minutes, depending on the apparent size of the formation. Since the calorimetric method used for liquid fraction measurement required a sample of ice close to 50g, a longer growth time was necessary at higher temperatures.

The calorimeter consisted of a vacuum flask embedded in a styrofoam shell. The lid fits into the top of the vacuum flask and a glass thermometer is inserted through the lid in such a way as to locate the mercury bulb at the centre of the vaccuum flask chamber. The thermometer was accurate to ±0.05 °C.

Initially, the flask is filled with hot tap water (45 °C to 50 °C) and the lid replaced. Before the ice sample is available, the initial hot water charge mass and temperature are recorded. Then the ice sample is carefully lowered into the hot water with the lid removed. The lid is replaced, and the operator may observe the temperature change while gently swirling the calorimeter. When the temperature stabilizes, the final temperature of the mixture is recorded along with the total mass of the calorimeter and contents. From this mass measurement, the ice sample mass can be calculated, since the calorimeter mass and hot water charge mass are known from previous measurements.

Once these temperatures and masses are known, a simple heat balance can be applied on the assumption of negligible heat loss to the container. The heat balance equation is then used to determine the sponginess of the ice sample. In this way the liquid water fraction of the sample was determined calorimetrically with an estimated absolute error of ±10 %. This technique required careful operator attention, and had to be completed immediately after taking the cylinder and its accreted ice out of the tunnel. Speed and care were required because the accretion would begin to drain liquid and to melt.

Since the droplet size was not measured, it was inferred from data that was collected. The method used is documented, along with the assumptions, in Appendix D.

Figures 5.1 to 5.3 show the resulting data as solid circles. Figure 5.4 shows the sensitivity of freshwater sponginess to variation in wind velocity. Examination of Figures 5.1 to 5.4 shows that the error in determining ice sponginess as functions of air temperature and velocity may be largely systematic in nature.

5.5 The Data and Empirical Constants

In order to use equation 5.13 in the set of equations proposed in section 5.3 to model freshwater spongy spray ice formation on a rotating cylinder, the constants C, a, b, c, and d should be evaluated statistically over a large and accurate data set. However, as this is only a preliminary study of a complicated phenomenon with little available data, five points were selected from the six available data sets, and were used to solve for the five constants. This method cannot form a reliable basis for a universal model of freshwater spongy spray icing on rotating cylinders, but the performance of the model may give an indication of the potential for modelling with dimensional analysis in the future.

Four data sets produced at the University of Albera are shown in Figures 5.1 to 5.4. Two relevant data sets from Lesin et al. (1980) are also used.

Figure 5.1 shows the experimentally determined ice fraction as a function of the air temperature and summarizes the most comprehensive data set presented. This data (represented as solid circles), was produced according to the method described in section 5.4 for a cylinder 5.0 cm in diameter, with rotational frequency 0.5 Hz, in a 23 ms^{-1} air flow with freshwater spray, having a liquid water content of 1.7 gm^{-3}. The median volume diameter was calculated to be 16 μm according to the method described in Appendix D, and the droplet temperature was assumed to equal the air temperature. It was also assumed that there were no ice particles collected. On the basis of the data cluster, a single point (shown in Fig. 5.1 by the arrow) at an air temperature of -3.0 °C and ice fraction 84% (16% sponginess) was chosen as one of five conditions necessary for determining the set of empirical constants from equation 5.13. Also shown in Figure 5.1 are three curves that represent the performance of the model. These will be discussed in section 5.6.

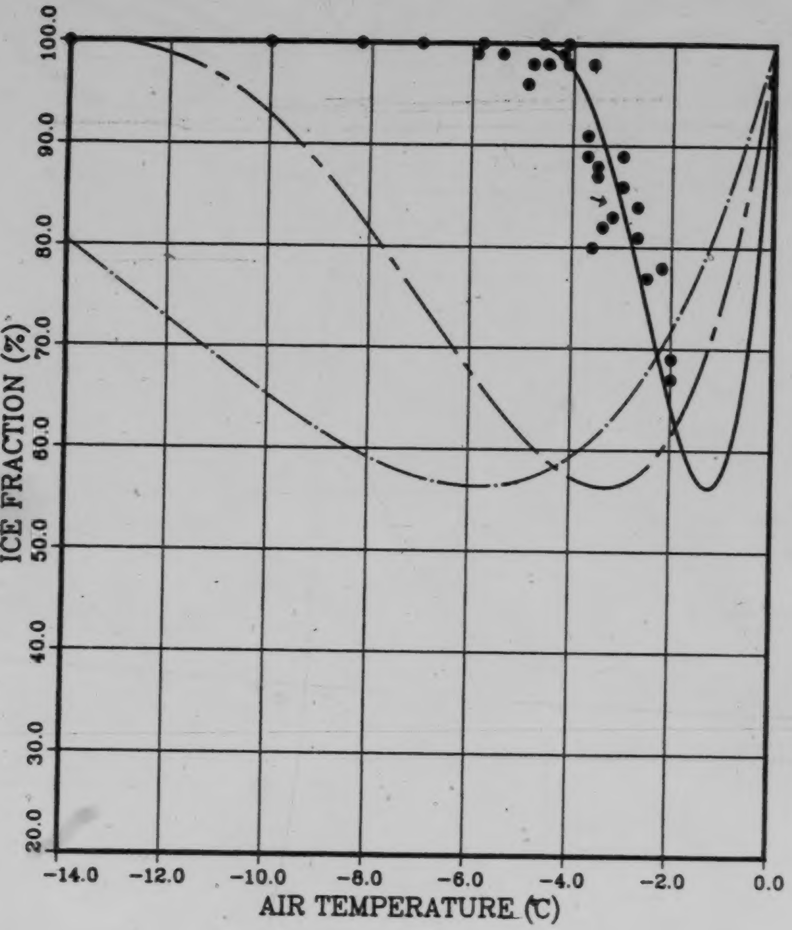

FIGURE 5.1 Ice fraction versus air temperature for spongy ice grown on a rotating cylinder over an air temperature range from 0.0 to -14.0 °C. The experimental data (shown as solid circles) was obtained with a plexiglass cylinder of a diameter D=5.0 cm, a median volume drop diameter d=16 μm, an air speed V=23 m/s, a liquid water content w=1.7 gm^{-3}, and a rotation rate Ω=0.5 s^{-1} The solid curve represents the fresh water icing model as described in section 5.3, with a liquid water content w=1.7 gm^{-3}. The chain-dashed curve is for the model with w=5.0 gm^{-3}, and the chain-dot curve, for the model with w=10.0 gm^{-3}. The arrow indicates the empirical anchor point taken from this data.

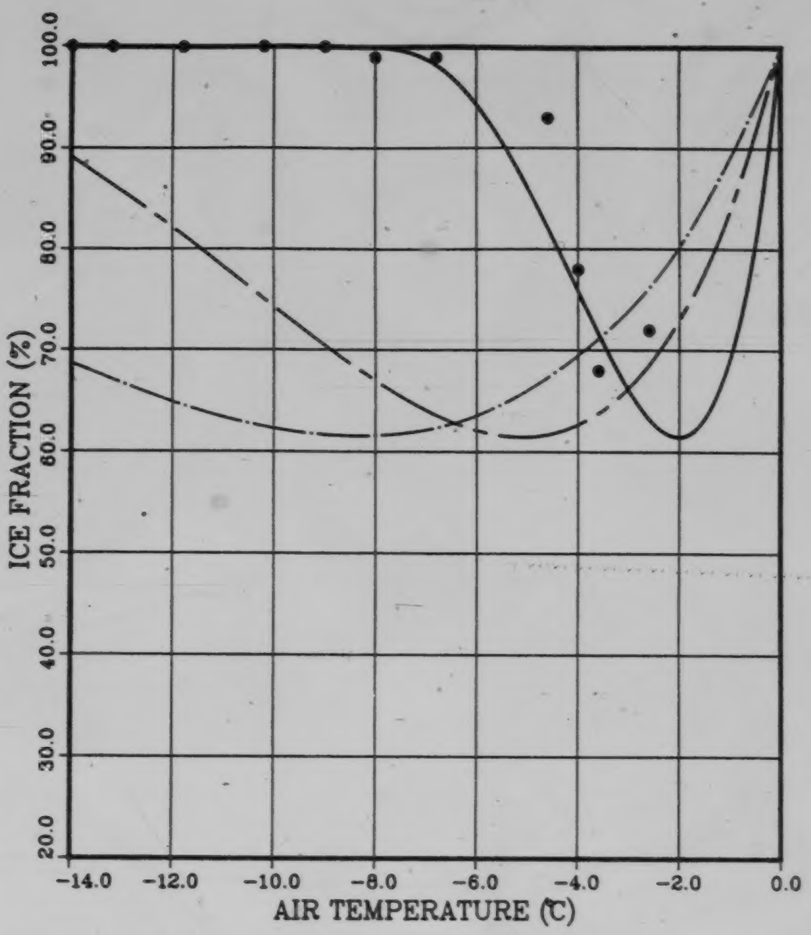

FIGURE 5.2 Ice fraction versus air temperature for spongy ice grown on a rotating cylinder over an air temperature range from 0.0 to -14.0 °C. The experimental data (shown as solid circles) was obtained with a plexiglass cylinder of diameter D=5.0 cm, a median volume drop diameter d=20 μm, an air speed V=28 m/s, a liquid water content w=1.7 gm^{-3} and a rotation rate Ω=0.5 s^{-1}. The solid curve represents the freshwater icing model as described in section 5.3 with a liquid water content w=1.7 gm^{-3}. The chain-dashed curve is for the model with w=5.0 gm^{-3}, and the chain-dot curve , for the model with w=10.0 gm^{-3}.

The data depicted in Figures 5.2 and 5.3 are the result of the same experimental procedures as the data shown in Figure 5.1 and described in section 5.4. The experimental conditions for each data set shown in Figures 5.2 and 5.3 were used to run the model. The model performance is shown. Figure 5.2 also includes two sets of model output at different liquid water contents. No data from Figure 5.2 was used in determining the empirical constants of equation 5.13. However, one condition from Figure 5.3 (shown by the arrow) was used: the point at an ice fraction of 57.4% (sponginess 42.6%), and an air temperature of -2.0 °C.

The data depicted in Figure 5.4, shows the dependence of ice sponginess on air velocity while the air temperature is kept at -5.0 °C. Two conditions were chosen from this data (as shown by the arrows) for determination of the constants in the empirical equation 5.13: an ice fraction of 52.7 % at an air velocity of 20.0 m/s, and an ice fraction of 63.5 % at an air velocity of 30.0 m/s.

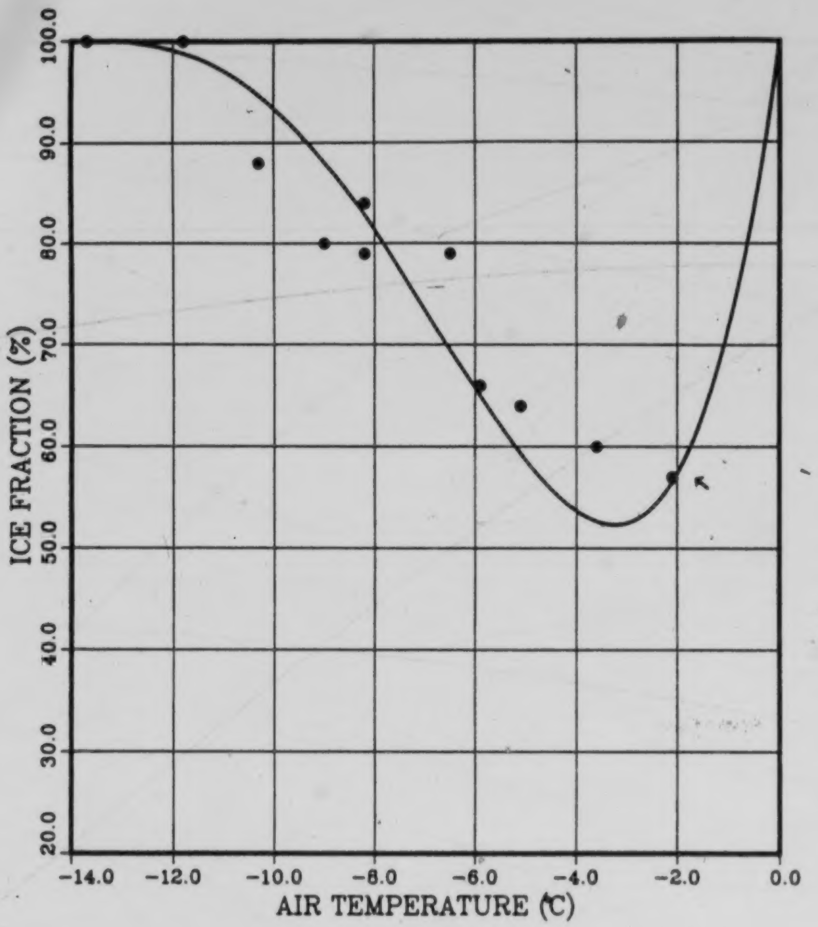

FIGURE 5.3 Ice fraction versus air temperature for spongy ice grown on a rotating cylinder over an air temperature range from 0.0 to -14.0 °C. The experimental data (shown as solid circles) was obtained with a plexiglass cylinder of diameter D=5.0 cm, a median volume drop diameter d=25 μm, an air speed V=20 m/s, a liquid water content $w=3.0$ gm^{-3}, and a rotation rate $\Omega=0.5$ s^{-1} The solid curve represents the fresh water icing model as described in section 5.3 with a liquid water content $w=3.0$ gm^{-3}. The arrow indicates the empirical anchor point taken from this data.

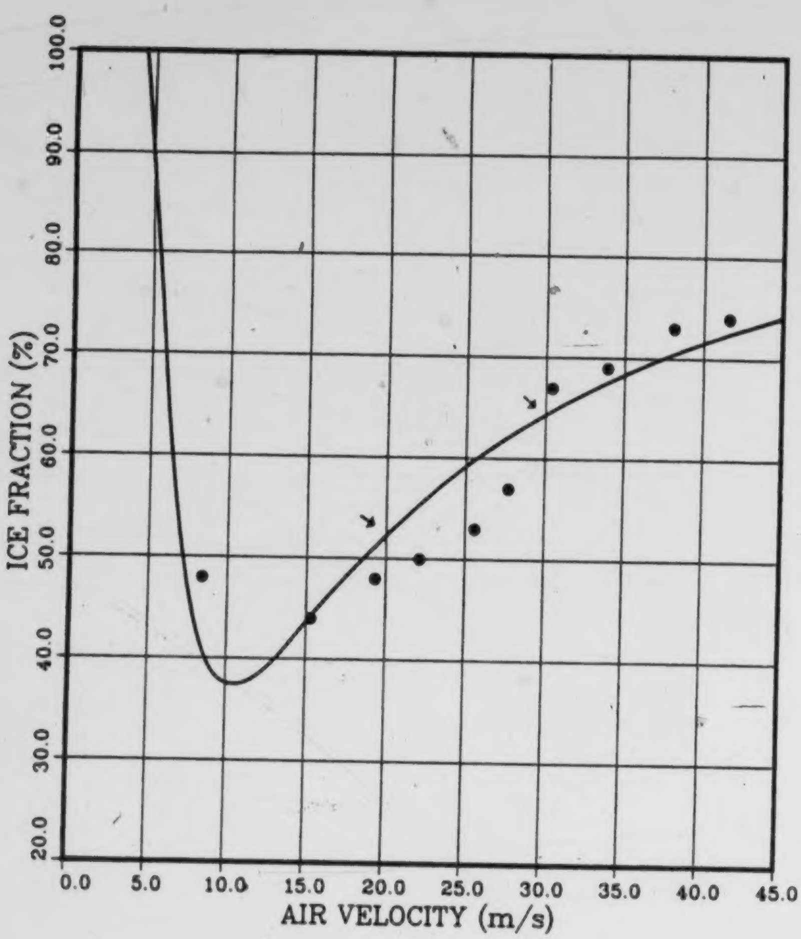

FIGURE 5.4 Ice fraction versus air speed for spongy ice grown on a rotating cylinder over an air velocity range from 0.0 to 45.0 m/s. The experimental data (shown as solid circles) was obtained with a plexiglass cylinder of diameter D=5.0 cm, a median volume drop diameter d = 25 μm, an air temperature t_a=-5.0 °C, a liquid water content w=4.4 gm^{-3}, and a rotation rate Ω=0.5 s^{-1}. The solid curve represents the freshwater icing model as described in section 5.3 as a function of air speed for a liquid water content of 4.4 gm^{-3}. The arrows indicate the empirical anchor points taken from this data.

Figures 5.5 and 5.6 show data taken from the experimental work of Lesins et al. (1980). This work was performed in a closed circuit wind tunnel at the University of Toronto, with a rotating cylinder under freshwater spray icing conditions. The sponginess of freshwater accretion was measured using a centrifuge and examined as a function of liquid water content and rotation rate. The primary finding of the investigation was the dependence of sponginess on the rotation rate.

Figure 5.5 shows the experimental results of Lesins et al. (1980) for the variation of ice fraction as a function of liquid water content. The experimental conditions for the data set are documented in the caption. The solid line represents the data which was taken over a range of air temperatures ($-4^{\circ}C \geq t_a \geq -16^{\circ}C$) and is therefore an average curve produced to show the variation of ice fraction with liquid water content. This was done by Lesins et al. (1980) because ice sponginess was assumed to be essentially constant over the temperature range from -4 to -16 °C. One condition used to determine the empirical constants of equation 5.13 was extracted on the basis of Figure 5.5: an ice fraction of 53% at a liquid water content of 10 gm^{-3}. For calculation purposes, the air temperature was assumed to be -10 °C. Figure 5.5 also shows the performance of the model for three different air temperatures, (-4°C, -10°C, -16°C), covering the specified temperature range given by Lesins et al. (1980).

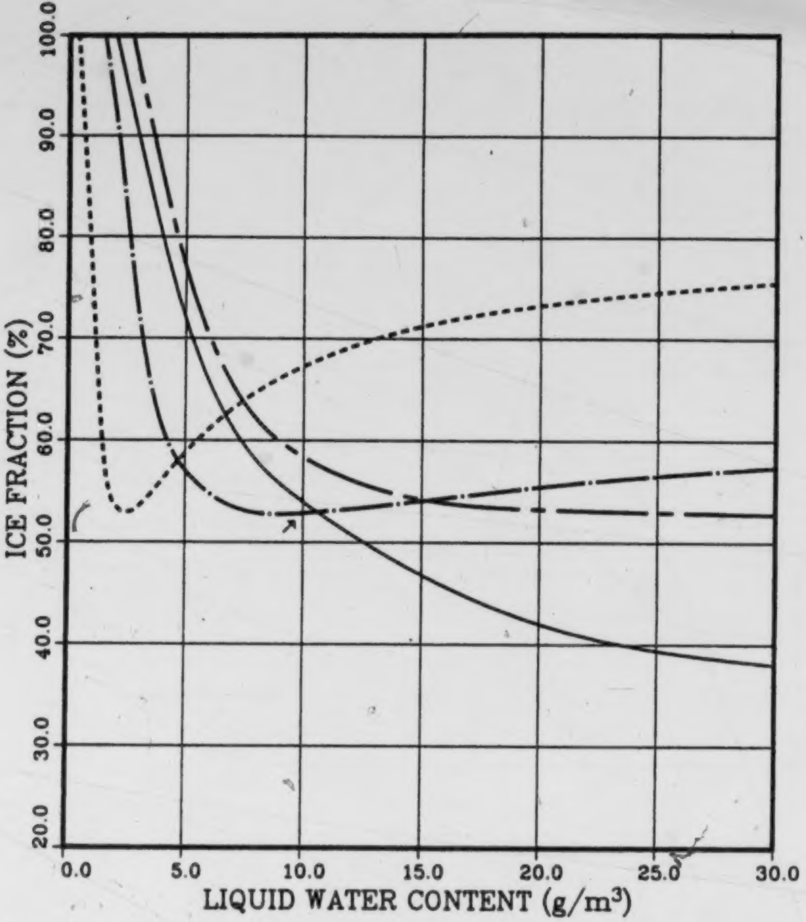

FIGURE 5.5 Ice fraction versus liquid water content for spongy ice grown on a rotating cylinder over an air temperature range from -4 to -16 °C. The experimental data (represented as a solid line) of Lesins et al. (1980) was obtained with a cylinder diameter D=1.9 cm, a drop diameter d=90 μm, an air speed V=18 m/s, and the rotation rate Ω=0.5 s^{-1}. The solid curve represents the experimental data averaged for a range of air temperatures from -4 to -16 °C. The chain-dashed curve is the model (as described in section 5.3) output for -16 °C. The chain-dot curve represents the model output for -10 °C, and the dashed line shows model output for -4 °C air temperature. The arrow indicates the empirical anchor point taken from this data.

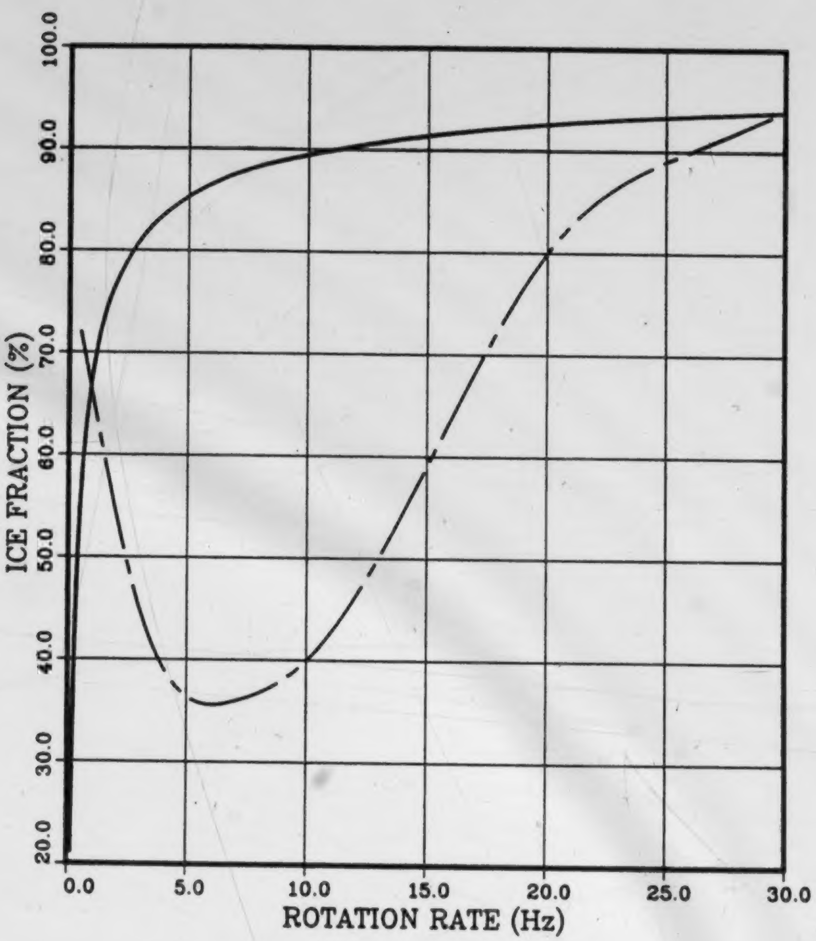

FIGURE 5.6 Ice fraction versus rotation rate for spongy ice grown on a rotating cylinder. The experimental data of Lesins et al. (1980) (shown as the chain-linked curve) was obtained with a cylinder diameter D=1.9 cm, a median volume drop diameter d=90 μm, an air speed V=18 m/s, a liquid water content w=5.0 gm⁻³, and an air temperature t_a=-5.0 °C. The solid curve shows the model (described in section 5.3) as a function of the rotation rate for the above conditions.

Figure 5.6 shows the experimental results of Lesins et al. (1980) for the variation of ice fraction as a function of rotation rate. The experimental conditions for this data set are documented in the caption. The chain-dashed line represents the data collected as a best fit curve. Figure 5.6 also shows the performance of the model under the conditions as specified by Lesins et al. (1980).

The five conditions chosen from Figures 5.1, 5.3, 5.4, and 5.5 (as indicated by the arrows) were used to solve for the five constants C, a,b,c,d found in equation 5.13. The resulting values for these empirical constants are:

$C = 17.5$

$a = -0.99$

$b = 3.8$

$c = -0.66$

$d = 0.58$

With the determination of these constants, the freshwater spongy icing model for rotating cylinders is capable of calculating empirically based values of sponginess. The model performance results appear along with the experimental data in Figures 5.1 to 5.6. A discussion of these results follows, in Section 5.6.

5.6 Model Performance

Figure 5.1 shows the model performance (as the solid curve) with the conditions responsible for the experimental data as input. The curve seems to model the data effectively; this is to be expected, as the model is empirically dependent on a condition extracted from Figure 5.1. However, it should be kept in mind that this condition was based on only a single data point from the Figure. The main point here is not that the model is proven correct, but that the inherent empiricism appears capable of describing the available data.

Examination of Figure 5.1 also shows an interesting functional relationship between ice fraction and air temperature. As temperature changes from -5 to 0 °C, the ice fraction varies from 100% to a minimum of approximately 56% and back to 100% at the freezing temperature. In the case of freshwater accretion, the ice fraction may be expected to approach one at the dry icing condition. This will not be strictly true as even quickly freezing droplets in rime icing may exist in the liquid phase over a small time period. Therefore, the model demonstrates the reasonable expectation of predicting an ice fraction equal to one at low temperatures. The model performance has been included (in Figure 5.1) for liquid water contents of 5.0 gm^{-3} and 10 gm^{-3} in order to show that an increase in collected water will force the Ludlam limit (dry/wet icing transition point) toward lower temperature.

An interesting feature of Figure 5.1 is that the ice fraction dramatically increases to a value of one close to the freezing point. Close to the freezing point, the ice fraction (or sponginess) of an accretion may only be of theoretical interest as (1) low adhesion strength of ice may preclude any actual ice attachment to the rotating cylindrical surface, (2) the definition of what an ice accretion is may become uncertain when the cylinder has far more liquid water on it than ice (as the author has observed in the F.R.O.S.T. tunnel at close to freezing, many times), and (3) the mass accretion rates will be very small and for such practical purposes as ice loading design, essentially negligible. However, these points aside, it is suggested that as the air temperature approaches 0 °C, the supercooling in the surface liquid film must also approach a small value. As the supercooling becomes small, free dendritic growth is suppressed in favor of basal plane growth, which is more solid by nature than is dendritic structure. These accretions grown under air temperatures close to 0 °C will be small with respect to mass accumulation, but will be solid according to the present sponginess model. This characteristic of the model may be partially substantiated by icicle studies done by Knight (1980) and Laudise and Barns (1979). Icicles are very comparable to cylinder icing, and may be thought of as vertically oriented, non-rotating cylinders with a liquid film moving axially under air temperatures often very close to the freezing point. Laudise and Barns (1979) report that in all cases they studied, the c-axis was not oriented in the direction of the axis of the icicle, and no sponginess was found. This implies that the ice growing under the descending liquid film was primarily growing solid in the a-axis direction (implying growth parallel to basal plane). This agrees with the present model at air temperatures close to the freezing point.

In their third concluding point, Lesins et al. (1980) briefly discuss an apparent inconsistency in their measurements of ice sponginess for a rotating cylinder in freshwater spray icing conditions. They expected great sponginess (a small ice fraction) at warm air temperatures (close to 0 °C) but instead, observed hard ice (ice fraction close to one). Examination of Figures 5.1, 5.2 and 5.3 shows that the present model of sponginess predicts ice fractions approaching one for air temperatures approaching the freezing point. Therefore, these observations of Lesins et al. (1980) also corroborate the present model, at least in this respect.

The data shown in Figure 5.2 appear to fall along the model's prediction curve (solid line). Model performance for liquid water contents of 5 gm^{-3} and 10 gm^{-3} have been included to once again show that the dry/wet transition is moved to lower air temperatures as the liquid water content is increased. The model predicts the same minimum ice fraction value for each of the liquid water contents shown. This is because air temperature will affect only the first two terms in equation 5.13, causing the same minimum values in A and λ_f to be computed.

Figure 5.3 shows a data set not independent of the present model's empiricism. One condition was derived from this figure, as stated in section 5.5. The model prediction curve (solid) as in Figure 5.1 appears to follow the data quite well with the largest datum to predicted error being 9% (absolute error). The empiricism inherent in the sponginess model appears capable of describing the available data.

Figure 5.4 shows a data set on which the spongy spray icing model is strongly dependent. Two conditions were extracted from this figure, and they are recorded in section 5.5. The model shows that as the wind speed drops, the heat transfer drops. In this case, an air velocity of 4 m/s results in solid ice growth (ice fraction of unity). As the air velocity increases above 4 m/s, dendritic surface crystal growth may be stimulated by an increased surface liquid supercooling with an increase in sponginess as a possible consequence . However, such increasing sponginess may begin to be suppressed at an air velocity of 10 m/s as a result of dendritic ice breakage and compaction by the wind. Compaction is defined here as the process by which the density of ice is increased by either rearrangement of free ice particles or by crushing of the structure. For the present, this supposition, along with those of Chapter 5 concerning dendritic breakage and shedding, will remain unsubstantiated. The model does, however, appear capable of modelling variations in sponginess for the conditions inherent in the data set represented in Figure 5.4.

Figure 5.5 shows the results of Lesins et al. (1980) for ice fraction versus liquid water content for freshwater spongy spray icing on a rotating cylinder, as specified in the caption. Lesins averages his spongy results for air temperatures from -4 °C to -16 °C on the basis of the assumption that ice sponginess is independent of air temperature in that range of temperatures. The presently proposed model was run for air temperatures of -4 °C, -10 °C and -16 °C, in order to facilitate comparison with the Lesins et al. (1980) averaged data. These three model curves are included in the figure and are specified in the figure caption.

The model performance shows the same general tendencies as the experimental data; however, this is to be expected as one empirical condition was extracted from Figure 5.5. The model could be considered to predict sponginess well, up to the 10 gm^{-3} point, and after that the ice fraction predicted is too large, depending on which of the model curves is compared.

In a way that is similar to Figure 5.4, each of the curves in Figure 5.5 reaches 100% ice fraction. In addition, they do so before intercepting the ice fraction axis. This implies solid ice growth over a small range of liquid water contents in Figure 5.5 and from the three model curves it is apparent that the solid ice growth range increases with decreasing air temperature. This is reasonable as the rate of heat transfer from the surface increases with lower air temperature and consequently the amount of liquid that may potentially freeze also increases. This region of Figure 5.5 for spray icing on a slowly rotating cylinder may be assumed to be similar to icicle growth.

For a given set of conditions (including air temperature) a number of icing regimes may be postulated on the basis of variation of liquid water content beginning at 0 gm^{-3}. Of course at 0 gm^{-3} there is no accretion but at the first increment of airborne liquid, the ice fraction is one, assuming an air temperature below the freezing point. The dry icing regime prevails until the Ludlam limit is reached. With a further increase in liquid water content, a surface liquid film develops in direct response. At lower liquid water contents the liquid film is thin with a small thermal mass, well mixed by droplet bombardment that eliminates large thermal gradients in the film. This condition produces a strong supercooling with dense and rapid growth. As the liquid water content is allowed to increase, the thickness and thermal mass of the film increases while the macroscopic heat flux to the airstream and ice accumulation remain unchanged. It is postulated that at some point the condition of the liquid film allows a-axis dendritic growth to become much less densely packed with resulting water inclusion. This point may be termed the sponginess limit and corresponds to the intersections of the ice fraction curves with the 100% ice fraction level in Figure 5.5. With a

7

further increase in liquid water content, the sponginess in the model and the spray icing data of Lesins et al. (1980) show a sharp decrease in ice fraction, possibly corresponding to a sharp increase in dendritic ice growth in the liquid film. Knight (1980) gives evidence that could be used to support this explanation, as he reports that sponginess was often found associated with surface hollows that showed characteristically thick liquid films. A glaze ice growth regime between the Ludlam limit and the sponginess limit may help explain the data in Figure 5.1. The cluster of data points between -6 and -4 °C gives the impression of an ice fraction that is slowly converging to one with decreasing air temperature. The apparent decrease in sponginess may not be a result of decreasing liquid inclusion but a decrease in surface liquid film mass, thus supporting the present hypothesis. Therefore, as a general tendency, sponginess may increase in response to thick liquid films that may result from higher liquid water contents in freshwater spray icing conditions as shown in Figure 5.5.

Figure 5.6 shows the results of Lesins et al. (1980) for the dependence of ice fraction on rotation rate of a cylinder undergoing freshwater spray accretion. Figure 5.6 demonstrates no agreement whatever (except at high rotation rates) between the Lesins et al. (1980) experimental data, and the present model of freshwater spongy spray ice formation. The Lesins et al. (1980) data show a sharp decrease in ice fraction with increase in rotation rate at low rotation rates (0 to 5 Hz), and an apparently asymptotic approach to an ice fraction of unity at high rotation rates. The present model simply starts at the origin and asymptotically approaches an ice fraction of one. The fact that the model will predict no ice formation at $\Omega=0$, implies that the present model is incapable of reliably modelling the influence of rotation on sponginess. This feature of the model performance is the result of assuming that the dimensionless groups are related to the crystal breakage/exit ratio, A, by power law relationships. Therefore, it is to be expected that as $\Omega \to 0$, Ω, taken to a particular power, will either be undefined or 0. In this case, as $\Omega \to 0$, $A \to \infty$ and because all of the ice is assumed to be shed, $\lambda \to 1$, which implies that there is no ice accretion at all. On the other hand, the approach of ice fraction to one as a result of increased rotation rates may be expected as water is forced from the ice accretion by centrifugal force. In fact, rotation has been used to determine sponginess by measuring weight before and after centrifuging.

The reason for the large discrepancy between the curves in Figure 5.6 is probably due to the arbitrary choice of power law relationships in the dimensional analysis. However, it may also have to do with the formation of the surface lobes and knobs as observed by Lesins. The growth of surface roughness would alter the heat transfer significantly from the smooth cylinder assumed in the model. It would give the surface liquid film protection from wind shear, producing thicker liquid films behind and around knobs and ridges than on the exposed tops. These variations in heat transfer and liquid film thicknesses are not taken into account in the model. Therefore, it may be difficult to amend the model in such a way as to improve the prediction of sponginess as a function of rotation rate, until these complexities can be taken into account with a more general form of dimensional analysis.

6. CONCLUSIONS AND RECOMMENDATIONS

The ability to model sponginess in spray icing may help in responding to some types of icing problems, and the fundamentals of solidification are valuable in understanding sponginess, especially the growth of dendritic structures capable of containing water.

The Makkonen (1987) sea spray icing model and the University of Alberta ship icing model apply conservation of heat energy and mass to the spongy spray ice growth process. These two principles were also applied in this thesis to produce a new model which includes a set of hypotheses concerning the spongy growth process at the accretion surface. An empirical description of this mechanism is proposed, and examined in the light of six data sets.

In freshwater spongy spray icing the heat transfer direction may result in unconstrained solidification. Where supercooling is sufficient, the resulting growth may be dendritic with subsequent entrappment of water in the structure. In contrast, growth of sea ice demonstrates the fundamentally different process of constrained solidification in which solute build-up at the interface may be mostly responsible for a growing structure that entraps brine. The growth of sea ice typically appears as a platelet structure, whereas freshwater spongy spray ice may show a fine dendritic substructure.

Makkonen (1987) starts the development of a spongy spray icing model for a cylinder by assuming a salt balance for collected, accreted and shed brine. As a result, the effective distribution coefficient ($k=S_i/S_w$) is found to be a function of the interfacial distribution coefficient ($k^*=S_i/S_b$) and n, the accretion fraction of a spongy saline spray ice accretion. K^* is shown to be equivalent to sponginess in sea spray icing, and a first working hypothesis is presented that assumes $k^*=0.26$. This hypothesis is based on the results from a number of sea ice growth investigations and an analogy between salt entrappment in sea ice growth and sponginess in spray icing. The cylinder icing model of Makkonen (1984) is used to evaluate the accretion fraction, n, and the resulting model predicts accretion rates and sponginess with an iterative procedure. The details of this approach are examined in section 3.1.

Makkonen (1987) has given an interpretation for k^* which implies that the surface liquid salinity in sea spray spongy ice accretion is the same as the salinity of the entrapped brine. One physical interpretation of this result is that surface liquid may flow more or less freely through the internal ice structure; this has been termed filtration accretion/shedding. Another interpretation of k^* is advanced which depends upon the possibility of the surface liquid having a different salinity than the permanently entrapped brine. A characteristic implied by this interpretation is that the growing surface layer is distinct from and sealed off from the deeper substructure. This has been termed surface accretion/shedding. If surface accretion/shedding is assumed, then two ice mass balances are possible--one for the liquid film and one for the whole surface accretion/shedding layer. Adoption of these two mass balances result in two equations that along with the overall mass and heat balance, result in a partial framework for a freshwater spongy spray icing model.

A surface growth assumption is made in such a way that the radial growth velocity of an assumed solid ice accretion equals the velocity of the progress of the spongy icing surface. (This assumption is part of the model's empiricism; it must be emphasized that the model predicts sponginess of accretions only, and not mass accretion rates.) In addition, it is assumed that the rate of volumetric inclusion of liquid into the structure of the spongy ice equals the shed ice particle volumetric flux. Thus the volumetric flux of ice particles controls the sponginess, λ_f, and is modelled empirically.

The empiricism chosen shows the feature that as the solid ice freezing fraction $n_f \to 1$ or $n_f \to 0$ the ice crystal breakage/exit ratio $A \to 0$. Thus a freshwater spongy spray icing model has been described for rotating cylinders that was tuned to five conditions from four data sets. The model in this way has shown that it is capable of describing accretion sponginess on rotating cylinders under variations of air temperature, air velocity and liquid water content. The model was found to be very poor in describing variations in sponginess with the rate of cylinder rotation, probably due to the assumption that Ω is related to sponginess through a simple power law relationship.

Because power law relationships are monatonic, a more complex form of relationship may be needed to model the variation of sponginess with rotation rate. The present study represents preliminary work and future approaches will likely benefit from a more rigorous use of dimensional analysis.

The understanding of surface growth processes is essential to modelling sponginess. The present thesis presents a model in which hypothetical surface processes were modelled empirically. The development of a better knowledge of these and other processes may depend largely on effective experimental work in the future.

Recommendations for future investigations include:
(1) To develop techniques to better measure the parameters in spongy spray ice growth. For instance, speedy and efficient measurement of sponginess and mass loads are needed. The drainage of liquid from a sample that is being weighed for total mass will distort a subsequent sponginess test on that sample. Possibly the best would be a technique that would accomplish both measurements at once, for example a calorimetric procedure which measures the sample mass produced by an effective and reliable sampling technique. Another possibility would be to use photographic or video records of the accretion dimensions and once the average

accretion sponginess is known, a total accretion mass may be calculated.

Since the shed flux may relate directly to processes on or in the accretion that could influence sponginess, the shed flux should be examined. While the amount of water substance shed as well as the relative amounts of ice and liquid are important characteristics to measure, the obstacles to such measurements appear considerable. For example, identifying droplets that have formed as a result of shedding may be difficult because they may be indistinguishable from droplets in the carrier air stream. Furthermore, once identified, it may be difficult to capture only the shed droplets, a process further complicated by the need to meausure the fraction of ice in the shed droplets. Determining the ice fraction of the shed flux may require a technique that does not promote either droplet heat loss or nucleation that could alter the ice fraction artificially. However, one approach to the measurement of the shedding flux might be to design a technique that gives a reliable determination of the collected flux, which, with an accurate measurement of the accretion rate, could be used to determine the shedding flux.

(2) To investigate the ice fraction of accretions grown in spray conditions near the freezing point. This may help to substantiate the hypothesis presented here, that the ice fraction of spongy spray ice accretion tends towards unity

as the air temperature approaches the freezing point.

(3) To investigate the sponginess structure of accretions in order to determine if shedding is primarily a surface phenomenon or whether liquid may flow through the ice substructure before shedding. An investigation like this might reveal two distinctly different shedding mechanisms, as postulated in this thesis, which might be responsible for distinct and identifiable icing regimes for spongy spray icing.

(4) To investigate the crystallographic orientations of ice crystals in spongy spray ice accretions in order to relate surface ice crystal growth to the sponginess of the accretion. The accretion substructure may show evidence that ice dendrites have grown and broken off, with subsequent distribution and compaction onto the accretion surface. In contrast, it may be found that ice dendrites grow without breakage and that the nature of their growth determines the nature of the resulting sponginess. A greater knowledge of the micro-processes of growth on the surfaces of spongy spray ice formations will be of importance if better physical models of sponginess are to be developed.

Bibliography

Aksjutin, I.L., 1979: Icing of ships (in Russian). Sudostroyenye Publishing House, Leningrad, 126 pp.

Bain, M. and Gayet, J.F., 1983: Contribution to the modelling of the ice accretion process: ice density variation with the impacted surface angle. Proceedings, First International Workshop on Atmospheric Icing of Structures, U.S. Army Cold Regions Research and Engineering Laboratory Special Report 83-17, 13-20.

Burton, J.A., Prim, R.C. and Slichter, W.P., 1953a: The distribution of solute in crystals grown from melt. Part I: Theoretical. J. Chem. Phys., 21, 1987-1991.

Burton, J.A., Kolb, E.D., Slichter, W.P., and Struthers, J.D., 1953b: Distribution of solute in crystals grown from the melt. Part II: Experimental. J. Chem. Phys., 21, 1991-1995.

Cansdale, J.T., and McNaughton, I.I., 1977: Calculation of surface temperature and ice accretion rate in a mixed water droplet/ice crystal cloud. Tech. Rep. 77090, Royal Aircraft Establishment, Farnborough, U.K., 29pp.

Chalmers, B., 1964: Principles of solidification. John Wiley and Sons, New York, 319pp.

Cox, G.F.N. and Weeks, W.F., 1975: Brine drainage and initial salt entrapment in sodium chloride ice. U.S.A. Cold Regions Research and Engineering Laboratory, Research Report 354, 85pp.

Druez, J., Laforte, J.L., and Nguyen, D.D., 1984: Mechanical properties of atmospheric ice. Proceedings, 2nd International Workshop on Atmospheric Icing of Structures, Trondheim, Norway, June 19-21, 1984, 51-56.

Gayet, J.F., Bain, M., and Soulage, R.G., 1984: Role of ice crystals on ice accretion processes. Proceedings, 2nd International Workshop on Atmospheric Icing of Structures, Trondheim, Norway, June 19-21, 1984, 65-69.

Garabedian, H., and Strickland-Constable, R.F., 1974: Collision breeding of ice crystals. Journal of Crystal Growth, 22, 188-192.

Hallett, J., 1964: Experimental studies of the crystallization of supercooled water. Journal of the Atmospheric Sciences, 21, 671-682.

Harrison, J.D., and Tiller, W.A., 1963: Controlled freezing of water. In Ice and snow: processes, properties and applications (ed. by W.D. Kingery). M.I.T. Press, Cambridge, 215-225.

Hillig, W.B., 1958: Kinetics of freezing in ice in the direction perpendicular to the basal plane. In, Growth and perfection of crystals: Cooperstown Conference Proceedings, Wiley, New York, 350-359.

Hillig, W.B. and Turnbull, D., 1956: Theory of crystal growth in undercooled pure liquids. Journal of Chemical Physics, 24, 914.

Hobbs, P., 1974: Ice Physics. Oxford University Press, 837pp.

Kachurin, L.G., 1962: The theory of aircraft icing. (in Russian) Bull. (Izv.) Acad. Sci. USSR, Geophys. Ser., 6, 823-832.

Knight, C.A., 1980: Icicles as crystallization phenomena. Journal of Crystal Growth, 49, 193-198.

Knight, C.A., 1968: On the mechanisms of spongy hailstone growth. J. Atmos. Sci., 25, 440-457.

Knollenberg R.G., 1981: Techniques for probing cloud microstructure, In, Clouds: their formation, optical properties and effects (ed. by P.V. Hobbs and A. Deepak). Academic Press, New York, 15-91.

Kochtubajda, B. and Lozowski, E.P., 1985: The sublimation of dry pellets used for cloud seeding. Journal of Climate and Applied Meteorology, 24:6, 597-605.

Kreith, F., 1969: Principles of heat transfer. International Textbook Co., Scranton, Penn., 620pp.

Kurz, W., and Fisher, D.J., 1986: Fundamentals of Solidification. Trans Tech Publications, Switzerland, 241pp.

Langer, J.S. and Muller-Krumbhaar, H., 1977: Stability effects in dendritic crystal growth. Journal of Crystal Growth, 42, 11-14.

Langmuir, I. and Blodgett, K.M., 1946: A mathematical investigation of water droplet trajectories. In: Collected Works of I. Langmuir. Pergamon Press, 10, 348-393.

Laudise, R.A., and Barns, R.L., 1979: Are icicles single crystals? Journal of Crystal Growth, 46, 379-386.

Lesins, G.B., List, R. and Joe, P.I., 1980: Ice Accretions, Part I: Testing of new atmospheric icing concepts. J. Rech. Atmos., 14, 347-356.

List, R., 1963: General heat and mass exchange of spherical hailstones. Journal of the Atmospheric Sciences, 20, 189-197.

List, R., 1977: Ice accretions on structures. J. Glaciol., 81, 451-465.

Lozowski, E.P. and Gates, E.M., 1987: On the modelling of ice accretion. Invited paper in "Freezing and Melting Heat Transfer in Engineering", K.C. Cheng, editor, 84pp, (in press).

Lozowski, E.P., Stallabrass, J.R., and Hearty, P.F., 1979: The icing of an unheated non-rotating cylinder in liquid water droplet -- ice crystal clouds. National Research Council Canada Report LTR-LT-96.

Ludlam, F.H., 1950: The composition of coagulation elements in cumulonimbus. Quarterly J. R. Met. Soc., 76, 52-58.

Ludlam, F.H., 1951: The heat economy of a rimed cylinder. Quarterly J. R. Met. Soc., 77, 663-666.

Makkonen, L., 1985: Heat transfer and icing of a rough cylinder. Cold Regions Science and Technology, 10, 105-116.

Makkonen, L., 1984: Modelling ice accretion on wires. Journal of Climate and Applied Meteorology, 23, 929-939.

Makkonen, L., 1987: Salinity and growth rate of ice formed by sea spray. Cold Regions Science and Technology, 14, 162-171.

Panov, V.V., 1976: Icing of ships (in Russian). Arkticheskii i Antarkticheskii Nauchno-Issledovatiel'skii Institut, Leningrad, Trudy No. 336, 263pp.

Plazinic, S. and Miljkovic, N., 1982: Damages of structures due to ice and wind. Proceedings of First International Workshop Atmospheric Icing of Structures. Hanover, New Hampshire, USA, June 1-3, 1982, 225-237.

Savyel'ev, B.A., 1971: Structure, chemical content and strength of the accretions formed on materials (in Russian). "Zhizn'ziemli" ("Life of the Earth"), No. 7, 23-33.

Terwillegar, J.P. and Dizio, S.F., 1970: Salt rejection phenomena in the freezing of saline solutions. Chem. Eng. Sci., 25, 1331-1349.

Weeks, W.F. and Ackley, S.F., 1982: The growth structure and properties of sea ice. U.S.A. Cold Regions Research and Engineering Laboratory, CRREL Monograph 82-1.

Weeks, W.F. and Lofgren, G., 1967: The effective solute distribution coefficient during the freezing of NaCl solutions. In, Physics of Snow and Ice (ed by H. Oura), Institute of Low Temperature Science, Hokkaido Vol. I, No. 1, 579-597.

Weeks, W.F. and Gow, A.J., 1978: Preferred crystal orientations along the margins of the Arctic Ocean. J. Geophys. Res., 84, no. C10, 5105-5121.

Zakrzewski, W.P., Blackmore, R.Z., and Lozowski, E.P., 1987: Mapping the ice growth rates on sea-going ships in waters east of Canada. In, Proceedings of 2nd Canadian Workshop on Operational Meteorology, Halifax, N.S., October 14-16,1987, 77-99.

Zakrzewski, W.P., Blackmore, R.Z., Lozowski, E.P., and Muggeridge, D., 1987: An improved ship spraying model. Unpublished manuscript, The University of Alberta, Division of Meteorology. Also, Journal of Geophysical Research (in preparation).

Zakrzewski, W.P. and Lozowski, E.P., 1987: The application of a vessel spraying model for predicting ice growth rates and ice loads on a ship. In, Proceedings of the 9th International Conference on Port and Ocean Engineering under Arctic Conditions, Fairbanks, Alaska, August 16-22, 1987(in press).

Zukauskas, A., 1972: Heat transfer from tubes in cross flow. Advances in Heat Transfer, 8, 93-160.

Appendix A

An Examination of the Algebraic Meaning of the Interfacial Solute Distribution Coefficient k^*

The following derivation will show that the interfacial distribution coefficient k^* may be a function of λ_s the sponginess and J_0 the ice fraction of the shed flux.

First define the overall salinity for the accretion Si_2 and the overall salinity for the shed flux Si_3 as:

$$Si_2 = \frac{Ms_2}{Mi_2 + Ms_2 + Mw_2} \qquad \text{A.1}$$

$$Si_3 = \frac{Ms_3}{Mi_3 + Ms_3 + Mw_3} \qquad \text{A.2}$$

where the mass flux variables (in units of $kgm^{-1}s^{-1}$) are:

Mi_2 - the mass flux of ice accreted.

Ms_2 - the mass flux of salt accreted.

Mw_2 - the mass flux of pure water accreted.

Mi_3 - the mass flux of shed ice.

Ms_3 - the mass flux of shed salt mass.

Mw_3 - the mass flux of shed pure water.

The salinity of entrapped brine in the accretion Sb_2 and the salinity of the shed brine Sb_3 are defined as:

$$Sb_2 = \frac{Ms_2}{Ms_2 + Mw_2} \qquad \text{A.3}$$

$$Sb_3 = \frac{Ms_3}{Ms_3 + Mw_3} \qquad \text{A.4}$$

The interfacial solute distribution coefficient k^* may be defined as:

$$k^* = \frac{Si_2}{Si_3} \qquad \text{A.5}$$

Introducing Sb_2 into equation A.5 gives:

$$k^* = \left(\frac{Si_2}{Sb_2}\right)\left(\frac{Sb_2}{Si_3}\right) \qquad \text{A.6}$$

The ratio (Si_2/Sb_2) in equation A.6 is a parameter that we can term the saline sponginess of the accretion λ_s; it can be shown that:

$$\lambda_s = \frac{Ms_2 + Mw_2}{Mi_2 + Ms_2 + Mw_2} \qquad \text{A.7}$$

Equation A.6 can therefore be rewritten as:

$$k^* = \lambda_s\left(\frac{Sb_2}{Si_3}\right) \qquad \text{A.8}$$

Equation A.8 shows the general nature of the present derivation since Sb_2 does not necessarily equal Si_3. Sb_2, the salinity of the entrapped brine, may be different from the equilibrium salinity of the surface liquid Si_3, which is assumed to be the same as the salinity of the shed brine. Algebraic rearrangement of the ratio (Sb_2/Si_3) may be written:

$$\left(\frac{Sb_2}{Si_3}\right) = \left(\frac{Ms_2}{Ms_3}\right)\left(\frac{Mi_3 + Ms_3 + Mw_3}{Ms_2 + Mw_2}\right) \qquad \text{A.9}$$

The ratio of Ms_2 and Ms_3 describes the division of salt mass between shedding and deposition by the icing process. We have called this η, the salt mass distribution coefficient.

$$\eta = \left(\frac{Ms_2}{Ms_3}\right) \tag{A.10}$$

The right hand factor in equation A.9 can be rearranged in terms of J_1 and J_0. J_1 is called the liquid incorporation ratio. It describes the degree to which the available surface brine on a spongy deposit is incorporated into the growing structure. J_0 is the shed ice fraction. It is the mass fraction of ice in the shed flux. J_1 and J_0 are given by:

$$J_1 = \frac{Ms_2 + Mw_2}{Ms_2 + Mw_2 + Ms_3 + Mw_3} \tag{A.11}$$

$$J_0 = \frac{Mi_3}{Mi_3 + Ms_3 + Mw_3} \tag{A.12}$$

Algebraic manipulation of equation A.9 with the parameters defined in A.10, A.11 and A.12, results in:

$$\left(\frac{Sb_2}{Si_3}\right) = \eta\left(\frac{1 - J_1}{J_1}\right)\left(\frac{1}{1 - J_0}\right) \tag{A.13}$$

The substitution of equation A.13 into equation A.8 results in:

$$k^* = \lambda_s \eta\left(\frac{1 - J_1}{J_1}\right)\left(\frac{1}{1 - J_0}\right) \tag{A.14}$$

Thus, the interfacial distribution coefficient is dependent upon the accretion sponginess as well as three other process-describing parameters. k^* is dependent on the sponginess of the accretion λ_s and this Makkonen (1987) has also suggested. However, k^* also depends upon η a parameter that by its definition describes the distribution of salt for the spongy spray icing process. η is probably related to the degree of solute build-up at the growing interface and the effectiveness with which the solute is transported away from the interface or into the accretion. k^* is also related to J_1 which is a parameter that reflects the tendency for liquid to stay in the accretion and not exit from the surface. k^* is also a function of J_0 which is defined as the ice mass fraction of the shed flux. One source of shed ice particles that might be associated with conditions at the interface of the accretion is dendritic ice crystal breakage. Therefore, equation A.14 shows that k^* depends upon the salt, pure water and ice crystal distribution mechanisms at work on the surface of sea spray spongy ice formation.

However, it is of interest to examine the influence of complete film mixing on equation A.14. Complete mixing in the liquid film may mean that the salinity of the shed water equals the salinity of the initially incorporated brine (ie. no solute build-up at the interface). This is can be represented as:

$$Sb_3 = Sb_2 \qquad \text{A.15}$$

Rearrangement of equation A.15 with the parameters as defined in equations A.10 and A.11 yields:

$$\eta = \frac{J_1}{(1 - J_1)} \qquad \text{A.16}$$

Substitution of equation A.16 into A.14 results in a simplification of the k^* equation. In this case k^* depends only on the sponginess λ_s, and the shed ice fraction J_0, under the assumption of complete mixing.

$$k^* = \frac{\lambda_s}{(1 - J_0)} \qquad \text{A.17}$$

Appendix B

Derivation of the
Ice Growth Flux Equation

The mass of ice grown at the surface of the cylinder may be modelled by assuming a heat balance. The heat balance is:

$$Q_1 = Q_2 + Q_3 + Q_4 + Q_5 \qquad \text{B.1}$$

Q_1 is the latent heat of fusion which is released as pure ice crystals grow. Q_2 is the heat lost from the surface of the cylinder through convective heat transfer. Q_3 is the evaporative heat transfer component. Q_4 is the sensible heat flux associated with bringing the impinging mass of ice and water to the equilibrium temperature of the icing surface. Q_5 is the radiative heat flux component directed from the icing surface to the surrounding environment. All the heat components (Q_1 to Q_5) are in units of $Jm^{-1}s^{-1}$.

Given Q_1, the mass growth rate is determined according to:

$$Q_1 = Mi_4 L_f \qquad \text{B.2}$$

where Mi_4 is the mass of ice grown per second per meter of cylinder length and L_f is the latent heat of fusion for pure ice at 0 °C.

Q_2 is defined as:

$$Q_2 = \pi Dh(t_s - t_a) \qquad \text{B.3}$$

where D is the diameter of the cylinder, h is the overall heat transfer coefficient, t_s is the surface temperature of the cylinder and t_a the air temperature.

Q_3 is defined as:

$$Q_3 = \pi Dh(\frac{Pr}{Sc})^{0.63}(\frac{\varepsilon Le}{c_p P a})(e_s - e_a) \qquad \text{B.4}$$

where Pr is the Prandtl number, Sc is the Schmidt number, ϵ is 0.622, L_e is the latent heat of vaporization, c_p is the specific heat of air at constant pressure, P_a is the air pressure, e_s is the saturation vapor pressure at the icing surface and e_a is the actual vapor pressure in the air.

Q_4 is defined as:

$$Q_4 = (Mi_1 C_i + Mw_1 C_w)(t_s - t_d) \qquad \text{B.5}$$

where Mi_1 is the impinging mass flux of ice particles, C_i is the specific heat of ice, Mw_1 is the impinging mass of water, C_w is the specific heat of water, t_s is the surface temperature (assumed equal to 0 °C) and t_d is the droplet temperature.

Q_5 is defined as:

$$Q_5 = \pi D\sigma a(t_s - t_a) \qquad \text{B.6}$$

where σ is the Stefan-Boltzmann constant and 'a' is a linearizing factor, t_s is the surface temperature, and t_a, the air temperature, is taken to be the temperature of the surroundings.

Equations B.2 through B.6 may be substituted into equation B.1 and solved for Mi_4 to yield equation:

$$Mi_4 = \frac{\pi Dh}{L} [(t_s - t_a) + (\frac{Pr}{Sc})^{0.63} (\frac{\varepsilon L_e}{c_p Pa})(e_s - e_a)] \qquad \text{B.7}$$

$$+ L^{-1} [(Mi_1 c_i + Mw_1 c_w)(t_s - t_a)] + L^{-1} \pi D \sigma a(t_s - t_a)$$

Mi_4 represents a maximum potential growth flux of ice to the growing surface. If the flux of collected liquid Mw_1 is smaller than Mi_4 the icing is assumed to be dry and consequently not a spongy formation. Under these circumstances, the availability of liquid water would control the mass accretion rate. Equation B.7 is thus used to model the mass growth of pure ice at the surface of the spongy accretion.

Appendix C

The program described here is designed to calculate the liquid water content for a freshwater spongy spray icing model (on a rotating cylinder). The model equations are given in section 5.3. First a flow chart is presented, then a Fortran program is listed and finally an output example.

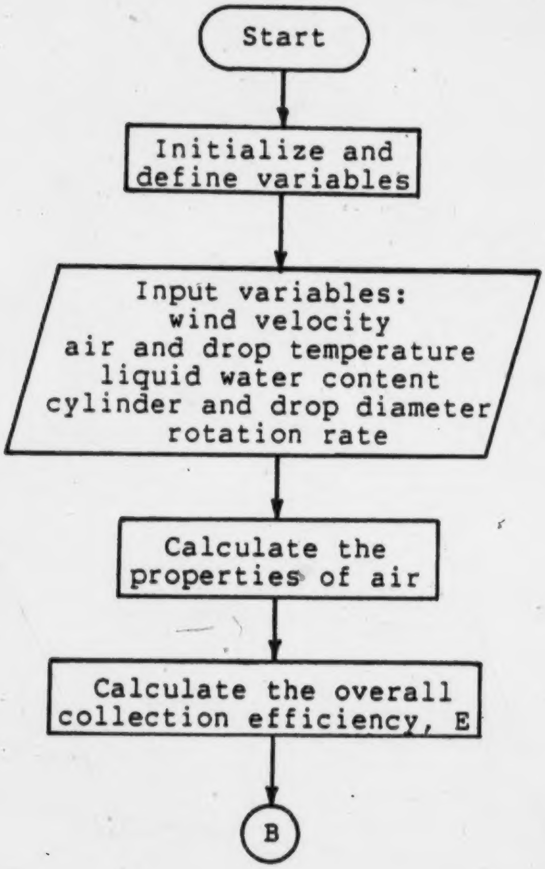
Start
Initialize and define variables
Input variables:
wind velocity
air and drop temperature
liquid water content
cylinder and drop diameter
rotation rate
Calculate the properties of air
Calculate the overall collection efficiency, E
B

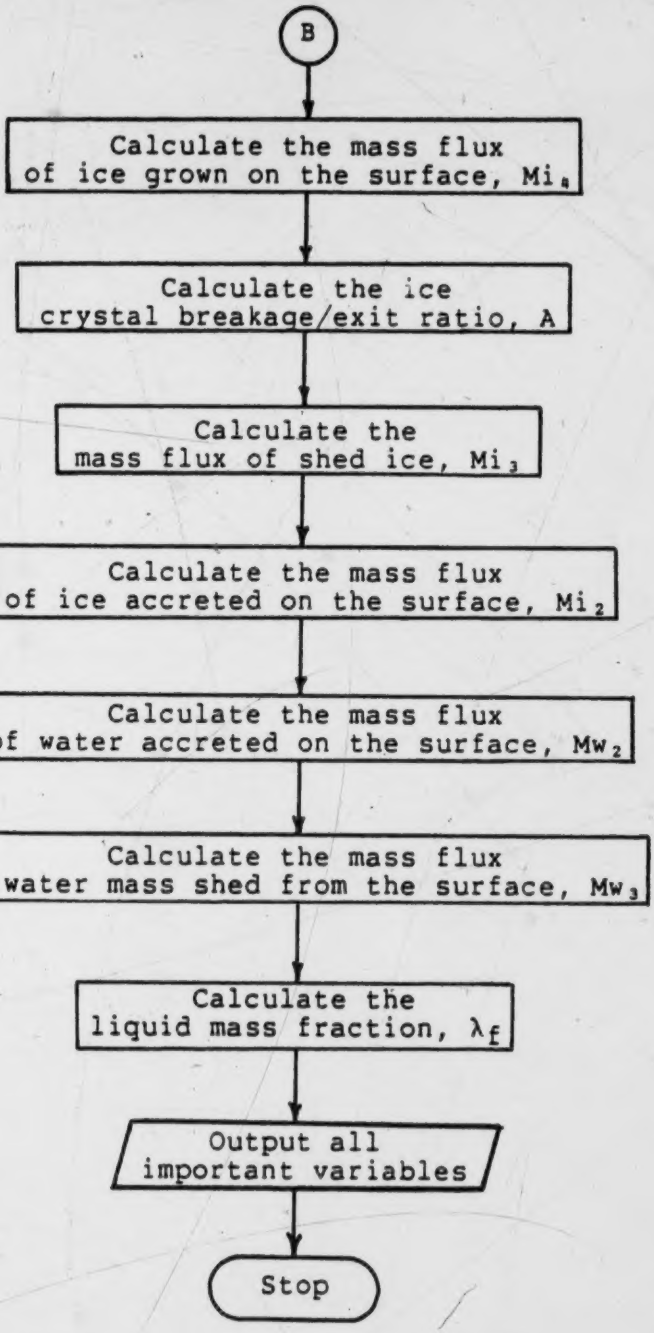
B
Calculate the mass flux of ice grown on the surface, Mi_4
Calculate the ice crystal breakage/exit ratio, A
Calculate the mass flux of shed ice, Mi_3
Calculate the mass flux of ice accreted on the surface, Mi_2
Calculate the mass flux of water accreted on the surface, Mw_2
Calculate the mass flux of water mass shed from the surface, Mw_3
Calculate the liquid mass fraction, λ_f
Output all important variables
Stop

A list of variables follows in the order that they first appear in the following program. The program variable is given first, followed by the variable name (in brackets) as given in the main text. This is followed by a brief description of the variable.

MPI1 (Mi_1) - the mass flux of pure ice particles collected
MPW1 (Mw_1) - the mass flux of pure water collected
MPI2 (Mi_2) - the mass flux of ice accreted
MPW2 (Mi_2) - the mass flux of pure water
MPI3 (Mi_3) - the mass flux of shed ice particles
MPW3 (Mw_3) - the mass flux of shed pure water
MPIT (Mi_4) - the maximum potential accretion flux of ice
LV (Le) - the latent heat of evaporation
LF (L) - the latent heat of fusion
NU (Nu) - the Nusselt number for the cylinder
MU (μ) - the dynamic viscosity of air
KA (k_a) - the thermal conductivity of air
L,LWC (w) - the liquid water content
K,KO - the inertial parameter and the modified inertial parameter (for collection efficiency calculation)
D0,D1,D2,D3,D4 - empirical constant for the saturation vapor pressure of air
TS (t_s) - the temperature of the icing surface
PR (Pr) - the Prandtl number
SC (Sc) - the Schmidt number
PRES (Pa) - air pressure
CP (c_p) - the specific heat of air at constant pressure
CW (Cw) - the specific heat of water
CI (Ci) - the specific heat of ice
EPS (ϵ) - the ratio of the molecular weight of water to that of air
RD (Rd) - the gas constant for dry air
SIGMA (σ) - the Stefan-Boltzmann constant
AS (a) - the linearized radiation constant
RHOW - the density of water
RHOI - the density of pure ice
PI (π) - π, the constant
VWIND (Va) - the air speed
TAIR (t_a) - the air temperature
TDROP (t_d) - the droplet temperature
DCYL (D) - the accretion diameter
OMEGA (Ω) - the rate of rotation (radians/second)
DDROP (d) - the median volume diameter of the droplets
RO - the density of gas
RED - droplet Reynolds number
EM - collection efficiency for a monodisperse droplet size
E (E) - collection efficiency for a median volume droplet size
RE (Re) - Reynolds number for the cylinder

H (h) - overall heat transfer coefficient for a cylinder
PART1,PART2,PART3 - heat transfer factors for the MPIT equation
EAIR,ETS (e_a,e_s) - the saturation water vapour pressures over water at the dew point and surface temperature, respectively
FRALIQ (λ_f) - the freshwater liquid mass fraction
FN (n_f) - the freezing fraction
R1,R2,R3 - the total collected, accreted and shed fluxes, respectively.

```
C
C     A FRESH WATER SPONGY ICING MODEL
C
      REAL MPI1,MPW1,MPI2,MPW2,MPI3,MPW3,MPIT,
     &LV,LF,NU,MU,KA,L,LWC,K,K0
      D0=6.107799961
      D1=4.436518521E-01
      D2=1.428945805E-02
      D3=2.650648471E-04
      D4=3.031240396E-06
C
C     DEFINE CONSTANTS
C
      MPI1=0.0
      TS=0.0
      PR=0.711
      SC=0.595
      PRES=1.0E+05
      LV=2.5E+06
      LF=3.34E+05
      CP=1005.0
      CW=4270.0
      CI=2070.0
      EPS=0.6221
      RD=287.04
      SIGMA=5.67E-08
      AS=8.1E+07
      RHOW=1000.0
      RHOI=917.0
      PI=3.1416
    4 CONTINUE
C
C     INPUT PROMPTS
C
      WRITE (6,5)
    5 FORMAT ( /,'WIND SPEED (M/S)?')
      CALL FREAD (5,'R:',VWIND)
      WRITE (6,10) VWIND
      WRITE (7,10) VWIND
   10 FORMAT (' ','WIND SPEED=',F6.1)
      WRITE (6,20)
   20 FORMAT ( /,'AIR AND DROP TEMPERATURE(DEGREES C)?')
      CALL FREAD (5,'2R:',TAIR,TDROP)
      WRITE (6,30) TAIR,TDROP
      WRITE (7,30) TAIR,TDROP
   30 FORMAT (' ','AIR TEMP=',F6.1,' DROP TEMP=',F6.1)
      WRITE (6,40)
   40 FORMAT ( /,'LIQUID WATER CONTENT-GMS/CUBIC METER?')
      CALL FREAD (5,'R:',L)
      LWC=L/1000.0
      WRITE (6,50) LWC
      WRITE (7,50) LWC
   50 FORMAT (' ','LIQUID WATER CONTENT=',F11.4,
     &'KG/CUBIC METER')
      WRITE (6,60)
   60 FORMAT ( /,'CYL.DIA. METERS AND ANGULAR VEL. Hz ')
      CALL FREAD (5,'2R:',DCYL,OMEGA)
      WRITE (6,70) DCYL,OMEGA
      WRITE (7,70) DCYL,OMEGA
   70 FORMAT (' ','CYLINDER DIAMETER=',F9.4,' OMEGA=',F6.3)
      OMEGA=OMEGA*2.0*PI
      WRITE (6,80)
   80 FORMAT ( /,'DROP DIAMETER-MICROMETERS?')
      CALL FREAD (5,'R:',DDROP)
      DDROP=DDROP/1.0E+06
      WRITE (6,90) DDROP
      WRITE (7,90) DDROP
   90 FORMAT (' ','DROP DIAMETER=',E11.4)
C
C     CALCULATE FUNCTIONS OF AIR TEMPERATURE:
C     AIR DENSITY,DYNAMIC VISCOSITY,CONDUCTIVITY
C
      RO=PRES/(RD*(TAIR+273.16))
      MU=1.718E-05+5.1E-08*TAIR
      KA=.0243+.000073*TAIR
C
C     CALCULATION OF SURFACE FLUX
C
C     CALCULATE THE OVERALL COLLECTION EFFICIENCY
C
      K=RHOW*VWIND*DDROP**2/(9.0*MU*DCYL)
      RED=VWIND*DDROP*RO/MU
      K0=K/(0.087*RED**(0.76*RED**(-1.0*0.027))+1.0)
      EM=0.0
      IF (K0.GT.0.125) EM=0.5*(ALOG10(8.0*K0))**1.6
      IF (K0.GT.0.8) EM=K0**1.1/((K0**1.1)+1.426)
      E=.69*EM**.67+.31*EM**1.67
      WRITE(6,150) K,RED,K0,EM,E
      WRITE(7,150) K,RED,K0,EM,E
  150 FORMAT(' ','K=',E11.4,' RED=',E11.4,' K0=',E11.4,
     &' EM=',E11.4,' E=',E11.4)
C
C     CALCULATE THE COLLECTED LIQUID MASS FLUX
C
      MPW1=E*VWIND*LWC*DCYL
```

```
C
C     CALCULATE THE HEAT TRANSFER COEFFICIENT
C
      RE=VWIND*DCYL*RO/MU
      NU=.24*RE**0.6
      H=KA*NU/DCYL
C     CALCULATE FACTORS FOR THE HEAT BALANCE
      PART1=PI*DCYL*H/LF
      PART2=(PR/SC)**0.63*EPS*LV/(CP*PRES)
      PART3=PI*DCYL*SIGMA*AS
      EAIR=D0+TAIR*(D1+TAIR*(D2+TAIR*(D3+TAIR*D4)))
      EAIR=EAIR*100.0
      ETS=D0+TS*(D1+TS*(D2+TS*(D3+TS*D4)))
      ETS=ETS*100.0
C     CALCULATE THE ICE ACCRETION MASS FLUX
      MPIT=PART1*((TS-TAIR)+PART2*(ETS-EAIR))
      MPIT=MPIT+(1.0/LF)*(MPI1*CI+MPW1*CW)*(TS-TAIR)
      MPIT=MPIT+(1.0/LF)*PART3*(TS-TAIR)
C     DRY ICING DECISION
      IF(MPIT.GE.MPW1) GO TO 800
C     OUTPUT COLLECTION AND THERMODYNAMIC COEFICIENTS
      WRITE(6,220)RO,MU,KA,RE,NU,H,
     &PART1,PART2,PART3,EAIR,ETS,MPIT
      WRITE(7,220)RO,MU,KA,RE,NU,H,
     &PART1,PART2,PART3,EAIR,ETS,MPIT
  220 FORMAT(' ','RO=',E10.4,' MU=',E10.4,' KA=',E10.4,/,
     &' RE=',E10.4,' NU=',E10.4,' H=',E10.4,/,
     &' PART1=',E10.4,' PART2=',E10.4,'PART3=',E10.4,/,
     &' EAIR=',E10.4,' ETS=',E10.4,' MPIT=',E10.4,/)
C     CALCULATE THE ICE CRYSTAL BREAKAGE/EXIT RATIO
      A=17.514*(MPIT/(MPW1-MPIT))**0.9879*
     &((MPW1-MPIT)/MPW1)**3.800*
     &(OMEGA*DCYL/VWIND)**0.6602*
     &(9.81/(OMEGA**2*DCYL))**0.5778
C     CALCULATE THE SHED ICE MASS FLUX
      MPI3=A*MPIT+MPI1
C     CALCULATE THE ICE ACCRETION MASS FLUX
      MPI2=MPI1+MPIT-MPI3
C     CALCULATE THE WATER ACCRETION MASS FLUX
      MPW2=(RHOW/RHOI)*(MPIT-MPI2)
C     CALCULATE THE SHED WATER MASS FLUX
      MPW3=(MPI1+MPW1)-(MPI2+MPW2)-MPI3
C     CALCULATE THE LIQUID FRACTION OF THE ACCRETION
      FRALIF=100.0*MPW2/(MPI2+MPW2)
      R1=MPI1+MPW1
      R2=MPI2+MPW2
      R3=MPI3+MPW3
      FN=MPIT/MPW1
      WRITE(6,720)A,FRALIF,MPIT,FN,MPI1,MPW1,
     &R1,MPI2,MPW2,R2,MPI3,MPW3,R3
      WRITE(7,720)A,FRALIF,MPIT,FN,MPI1,MPW1,
     &R1,MPI2,MPW2,R2,MPI3,MPW3,R3
  720 FORMAT(' A=',E10.4,' L.F.=',F7.3,'% MPIT=',E10.4,
     &' n=',F7.4,/,
     &' MPI1=',E10.4,' MPW1=',E10.4,' R1=',E10.4,/,
     &' MPI2=',E10.4,' MPW2=',E10.4,' R2=',E10.4,/,
     &' MPI3=',E10.4,' MPW3=',E10.4,' R3=',E10.4,//)
      GO TO 820
  800 CONTINUE
      WRITE(6,810)
      WRITE(7,810)
  810 FORMAT(' ',' DRY ICING: MPIT>MPW1',//)
  820 CONTINUE
      WRITE(6,830)
  830 FORMAT(' ','ENTER 1.0 TO RERUN')
      CALL FREAD(5,'R:',DECIS)
      IF(DECIS.EQ.1.0) GO TO 4
      STOP
      END
```

An Example of Output

```
WIND SPEED= 23.0
AIR TEMP= -3.0 DROP TEMP= -3.0
LIQUID WATER CONTENT= 0.0017KG/CUBIC METER
CYLINDER DIAMETER= 0.0500 OMEGA= 0.500
DROP DIAMETER= 0.1600E-04
K= 0.7685E+00 RED= 0.2787E+02 K0= 0.4092E+00 EM= 0.1729E+00
E= 0.2295E+00

RO=0.1290E+01 MU=0.1703E-04 KA=0.2408E-01
RE=0.8710E+05 NU=0.2209E+03 H=0.1064E+03
PART1=0.5004E-04 PART2=0.1731E-01 PART3=0.7214E+00
EAIR=0.4899E+03 ETS=0.6108E+03 MPIT=0.2785E-03

A=0.1496E+00 L.F.= 16.092% MPIT=0.2785E-03 n= 0.6209
MPI1=0.0 MPW1=0.4486E-03 R1=0.4486E-03
MPI2=0.2369E-03 MPW2=0.4543E-04 R2=0.2823E-03
MPI3=0.4166E-04 MPW3=0.1246E-03 R3=0.1663E-03
```

Appendix D

The experimental method described in section 5.4 did not allow for direct measurement of the droplet diameter. The method used to infer a median volumetric drop diameter is presented here along with the resulting droplet sizes for the data shown in Fig. 5.1, Fig. 5.2, and Fig. 5.3. The median volumetric diameter for the data in Fig. 5.4 could not be estimated in the same manner, so it was assumed to be 25 μm, the same as in Fig. 5.3. This represents an arbitrary, but perhaps not unreasonable choice, since the same spray nozzle was used in each case.

The reason that the data in Fig. 5.4 could not be used in the same way as that from Figures 5.1, 5.2 and 5.3, is that there was no data close to the Ludlam limit (wet/dry icing transition point). Figures 5.1, 5.2 and 5.3 show the variation of sponginess as a function of air temperature and consequently in each case, the transition from wet icing to dry icing is shown. It is at the Ludlam limit that all of the collected water mass flux $Mw_1=Mi_a$, the maximum potential ice growth flux.

The Ludlam limit offers a convenient thermodynamic condition for determining the median volumetric diameter, d. It is assumed that there is no liquid shed from the surface (ie: all collected water is solidified on the surface), and that the surface temperature is 0 °C for freshwater icing. Because there is no liquid shedding, the collected water mass flux may be modelled assuming no bouncing or splashing that may be present with shedding water films. Also, the heat transfer can be determined on the basis of an assumed 0 °C surface temperature with less concern for the possibility of incomplete surface water film mixing before shedding inherent in wet icing.

The present approach assumes heat transfer from a non-rotating smooth cylinder (Zukauskas, 1972), and collection mechanics based on the Langmuir and Blodgett (1949) data. The median volume drop diameter equation for overall collection efficiency of Bain and Gayet (1982) is used, along with the improved correlation for the overall median volume diameter droplet collection efficiency of Cansdale and McNaughton (1977).

The method assumes that there is a unique droplet size which will yield a collection efficiency such that the collected water mass flux will be completely solidified and stay on the cylinder. At the Ludlam limit, the cylinder cooling must just equal the latent heat released on the surface of the cylinder by solidifying water. The surface cooling depends on the temperature of the icing surface (assumed to be 0 °C) and the temperature of the surroundings (the air, droplets and surroundings are assumed to have the same temperature). For a given set of environmental conditions, the temperature of the surroundings at which all the collected water is just solidified, is here called the Ludlam limit temperature. The Ludlam limit temperature is assumed to be the temperature at which an accretion contains no liquid water ($\lambda_f=0$; not spongy), and the surface is still assumed (in freshwater spray icing), to be at the equilibrium freezing temperature, with no liquid film. Using these criterion, the Ludlam limit temperature for figures 5.1, 5.2 and 5.3 were chosen as -4.6 °C, -8.0 °C, and -13.5 °C. The environmental temperature at which the surface liquid film, inherent in wet icing, and the inclusion of liquid water, inherent in spongy icing, are no longer apparent is the temperature required to find the median volume droplet diameter.

The median volume diameter is solved with the algorithm shown in the following flow chart. Initially, the environmental conditions are input along with the Ludlam limit temperature and a first guess at d, the median volume diameter. The properties of the air, and the heat transfer parameters are calculated on the basis of the environmental conditions. Next, the first iterative value of the drop diameter is used to calculate the collection efficiency, E. Once E is known, both the collected water, Mw_1, and the solidification flux Mi_s are calculated. The solid growth freezing fraction is calculated as a result. If it is sufficiently close to one, the initial drop diameter guess is accepted. However, much more likely is that n_f will not be sufficiently close to 1.0 and a new value of drop diameter is subsequently assigned. The new value of drop diameter is assigned as a result of multiplying the old value by the freezing fraction, n_f, ($d_{new}= d_{old}n_f$). This new value of drop diameter is used to calculate a new collection efficiency, collection flux, solidification flux, and n_f. The iteration is terminated when n_f is sufficiently close to unity, and then the acceptable median volume diameter is output.

This method was found to converge in all the cases that had a Ludlam limit. However, the reader is warned that if the environmental conditions are specified in such a way that only dry icing is possible, then the search for a median volume droplet diameter will result in an unstable numerical solution.

This method of determining median volume drop diameter depends on the following assumptions: (1) availability of sufficient data around the Ludlam limit condition; (2) an accurate collection mechanics assumption; (3) accurately modelled heat transfer, and (4) that the spray system delivers droplet size independent of variations in the tunnel conditions, such as air temperature or air speed.

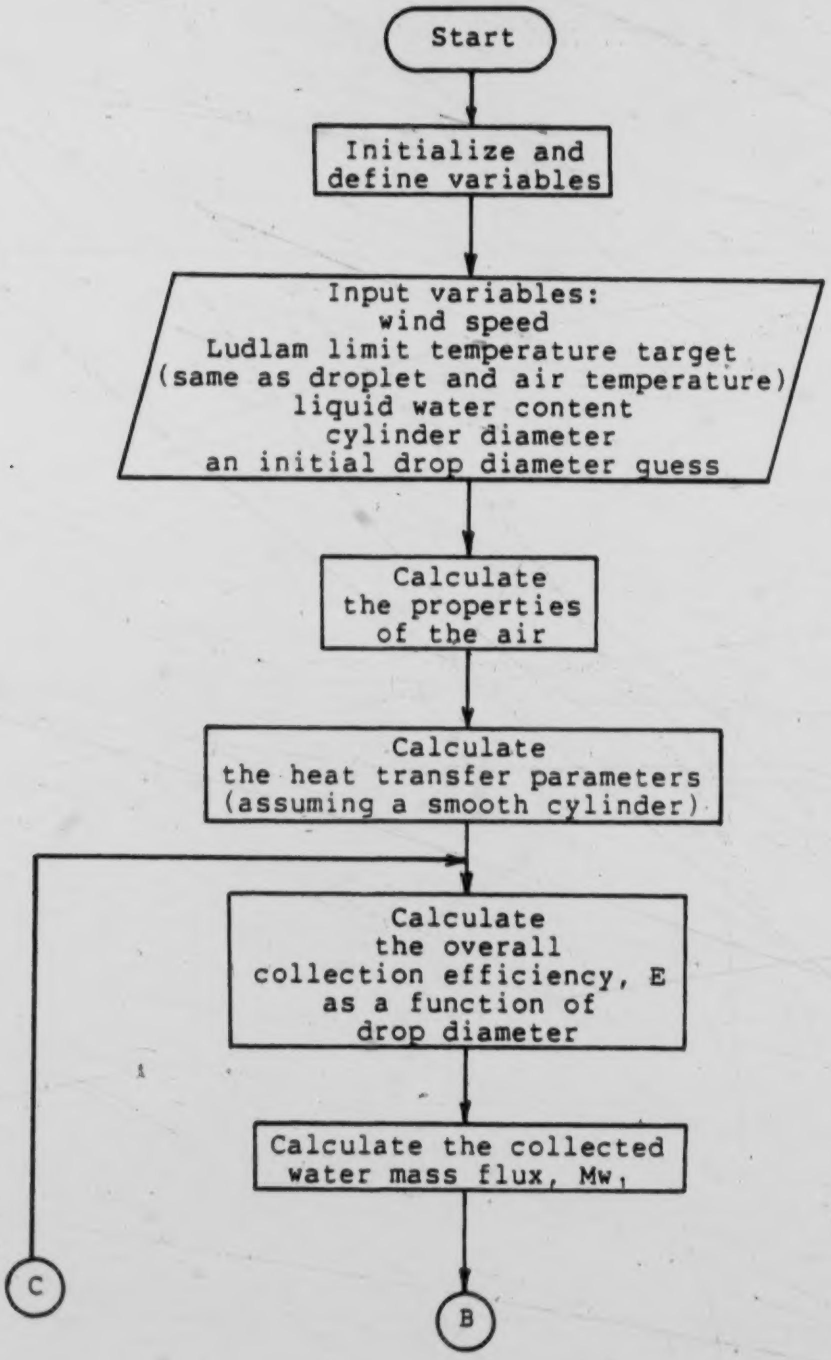
Start
Initialize and define variables
Input variables:
wind speed
Ludlam limit temperature target
(same as droplet and air temperature)
liquid water content
cylinder diameter
an initial drop diameter guess
Calculate the properties of the air
Calculate the heat transfer parameters (assuming a smooth cylinder)
Calculate the overall collection efficiency, E as a function of drop diameter
Calculate the collected water mass flux, Mw,
C
B

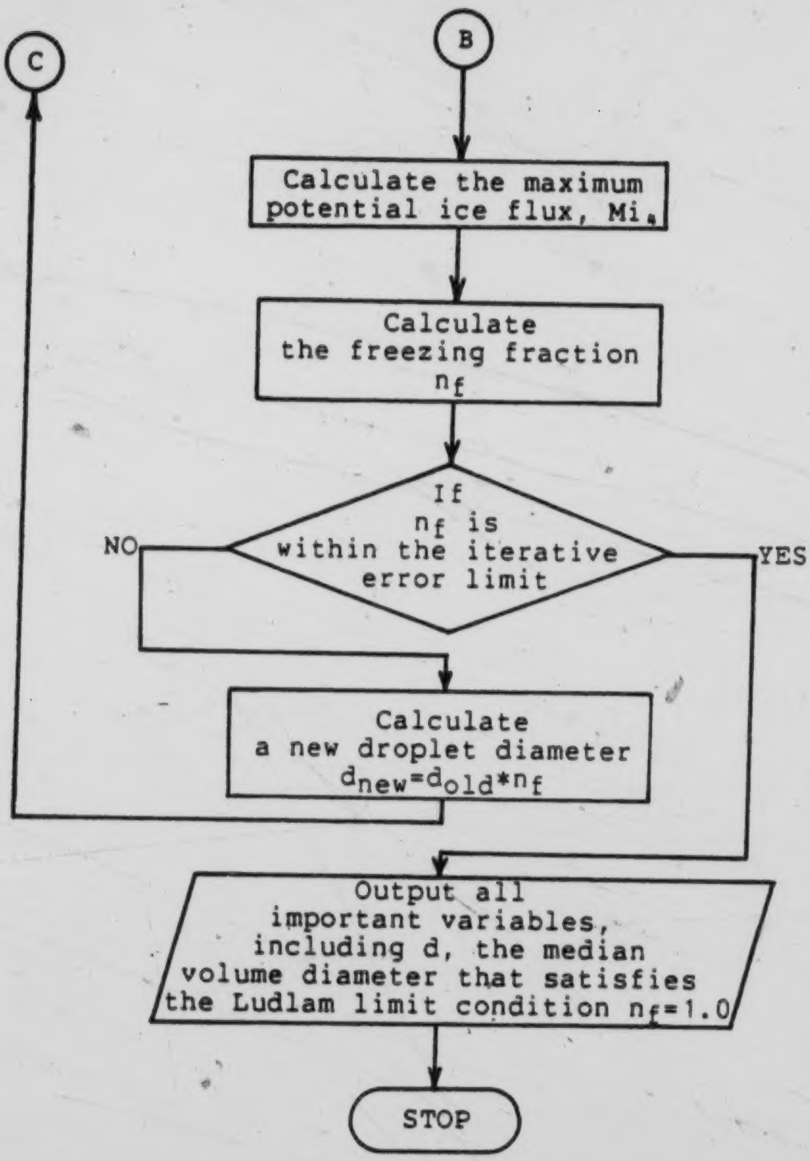
C
B
Calculate the maximum potential ice flux, Mi.
Calculate the freezing fraction n_f
If n_f is within the iterative error limit
NO
YES
Calculate a new droplet diameter $d_{new}=d_{old}*n_f$
Output all important variables, including d, the median volume diameter that satisfies the Ludlam limit condition $n_f=1.0$
STOP

Most of the variables in the following program are listed in the parameter list of Appendix C. Those that are in this program, but not in the above list, are noted below.

NF,NFNEW (n_f) - variables that contain iterative values of the freezing fraction
KOUNT - parameter used to report the number of iterations used before the error tolerance is satisfied
TDROP,TAIR - the Ludlam limit temperature is equal to both the droplet temperature and the air temperature (thermal equilibrium is assumed between the air and water droplets)

```
C
C     A PROGRAM TO FIND THE DROPLET DIAMETER
C     FOR A SPECIFIED LUDLAM LIMIT TEMPERATURE
C
      REAL MPW1,MPIT,NF,NFNEW,LV,LF,NU,MU,KA,L,LWC,K,K0
      D0=6.107799961
      D1=4.436518521E-01
      D2=1.428945805E-02
      D3=2.650648471E-04
      D4=3.031240396E-06
C     DEFINE CONSTANTS
      NF=1.0
      TS=0.0
      PR=0.711
      SC=0.595
      PRES=1.0E+05
      LV=2.5E+06
      LF=3.34E+05
      CP=1005.0
      CW=4270.0
      CI=2070.0
      EPS=0.6221
      RD=287.04
      SIGMA=5.67E-08
      AS=8.1E+07
      RHOW=1000.0
      RHOI=917.0
      PI=3.1416
      KOUNT=0
C     INPUT PROMPTS
      WRITE (6,5)
    5 FORMAT ( /,'WIND SPEED (M/S)?')
      CALL FREAD (5,'R:',VWIND)
      WRITE (6,10) VWIND
      WRITE (7,10) VWIND
   10 FORMAT (' ','WIND SPEED=',F6.1,' m/s')
      WRITE (6,20)
   20 FORMAT ( /,'ENTER THE LUDLAM LIMIT TEMPERATURE (deg
C)',/,
     &' (ASSUMED EQUAL TO BOTH THE AIR AND DROP
'TEMPERATURES)')
      CALL FREAD (5,'2R:',TAIR,TDROP)
      WRITE (6,30) TAIR,TDROP
      WRITE (7,30) TAIR,TDROP
   30 FORMAT (' ','AIR TEMP=',F6.1,' deg C',
     &' DROP TEMP=',F6.1,' deg C')
      WRITE (6,40)
   40 FORMAT ( /,'LIQUID WATER CONTENT-GMS/CUBIC METER?')
      CALL FREAD (5,'R:',L)
      LWC=L/1000.0
      WRITE (6,50) LWC
      WRITE (7,50) LWC
   50 FORMAT (' ','LIQUID WATER CONTENT=',F11.4,' Kg/m^3')
      WRITE (6,60)
   60 FORMAT ( /,'CYL.DIA. METERS')
      CALL FREAD (5,'R:',DCYL)
      WRITE (6,70) DCYL
      WRITE (7,70) DCYL
   70 FORMAT (' ','CYLINDER DIAMETER=',F9.4,' m')
      WRITE (6,80)
   80 FORMAT ( /,'INITIAL DROP DIAMETER GUESS-MICROMETERS?')
      CALL FREAD (5,'R:',DDROP)
      DDROP=DDROP/1.0E+06
      WRITE (6,90) DDROP
      WRITE (7,90) DDROP
   90 FORMAT (' ','DROP DIAMETER=',E11.4,' m')
C     CALCULATE FUNCTIONS OF AIR TEMPERATURE:
C     AIR DENSITY,DYNAMIC VISCOSITY,CONDUCTIVITY
      RO=PRES/(RD*(TAIR+273.16))
      MU=1.718E-05+5.1E-08*TAIR
      KA=.0243+.000073*TAIR
C     CALCULATE THE HEAT TRANSFER COEFFICIENT
      RE=VWIND*DCYL*RO/MU
      NU=.24*RE**0.6
      H=KA*NU/DCYL
C     CALCULATE FACTORS FOR THE HEAT BALANCE
      PART1=PI*DCYL*H/LF
      PART2=(PR/SC)**0.63*EPS*LV/(CP*PRES)
      PART3=PI*DCYL*SIGMA*AS
      EAIR=D0+TAIR*(D1+TAIR*(D2+TAIR*(D3+TAIR*D4)))
      EAIR=EAIR*100.0
      ETS=D0+TS*(D1+TS*(D2+TS*(D3+TS*D4)))
      ETS=ETS*100.0
C     OUTPUT COLLECTION AND THERMODYNAMIC COEFICIENTS
      WRITE(6,95)RO,MU,KA,RE,NU,H,PART1,PART2,PART3,EAIR,ETS
      WRITE(7,95)RO,MU,KA,RE,NU,H,PART1,PART2,PART3,EAIR,ETS
   95 FORMAT(' ','RO=',E10.4,' MU=',E10.4,' KA=',E10.4,/,
     &' RE=',E10.4,' NU=',E10.4,' H=',E10.4,/,
     &' PART1=',E10.4,' PART2=',E10.4,' PART3=',E10.4,/,
     &' EAIR=',E10.4,' ETS=',E10.4,/)
C     CALCULATE THE OVERALL COLLECTION EFFICIENCY
  100 CONTINUE
      K=RHOW*VWIND*DDROP**2/(9.0*MU*DCYL)
      RED=VWIND*DDROP*RO/MU
      K0=K/(0.087*RED**(0.76*RED**(-1.0*0.027))+1.0)
      EM=0.0
      IF (K0.GT.0.125) EM=0.5*(ALOG10(8.0*K0))**1.6
      IF (K0.GT.0.8) EM=K0**1.1/((K0**1.1)+1.426)
      E=.69*EM**.67+.31*EM**1.67
```

```
C     WRITE(6,150) K,RED,K0,EM,E
C     WRITE(7,150) K,RED,K0,EM,E
C 150 FORMAT(' ','K=',E11.4,' RED=',E11.4,' K0=',E11.4,
C    &' EM=',E11.4,' E=',E11.4)
C     CALCULATE THE COLLECTED LIQUID MASS FLUX
      MPW1=E*VWIND*LWC*DCYL
C     CALCULATE THE ICE ACCRETION MASS FLUX
      MPIT=PART1*((TS-TAIR)+PART2*(ETS-EAIR))
      MPIT=MPIT+(1.0/LF)*(MPW1*CW)*(TS-TAIR)
      MPIT=MPIT+(1.0/LF)*PART3*(TS-TAIR)
C     CALCULATE FREEZING FRACTION NF
      NFNEW=MPIT/MPW1
C     OUTPUT
C     WRITE(6,210)MPIT,MPW1,NFNEW,DDROP,E
C 210 FORMAT(' ',' MPIT=',E10.4,' MPW1=',E10.4,
C    &' NFNEW=',E10.4,/,' DROP DIA=',E10.4,' E=',E10.4)
C     ITERATIVE DECISION
      IF(ABS(1.0-NFNEW/NF).LT.0.0001) GO TO 500
      KOUNT=KOUNT+1
      DDROP=DDROP*NFNEW
      NF=NFNEW
      GO TO 100
  500 CONTINUE
C     FINAL OUTPUT
      WRITE(7,550)MPIT,MPW1,NF,NFNEW,E,DDROP,TAIR,KOUNT
 550 FORMAT(' ','MPIT=',E10.4,' MPW1=',E10.4,
     &' BOTH IN (Kg/ms)',/,
     &' NF=',E10.4,' NFNEW=',E10.4,' E=',E10.4,/,
     &' THE LUDLAM LIMIT DROP DIAMETER=',E10.4,' m',/,
     &' FOR A LUDLAM LIMIT TEMPERATURE=',F7.2,' deg C',/,
     &' ITERATIONS REQUIRED ',I4)
      STOP
      END
```

The following trials were run to establish the characteristic droplet diameter for each of the first three data sets. Upon the basis of these runs the median volumetric diameters were selected for Figures 5.1 to 5.3.

```
TRIAL 1 (FIGURE 5.1)

WIND SPEED= 23.0 m/s
AIR TEMP= -4.7 deg C DROP TEMP= -4.7 deg C
LIQUID WATER CONTENT= 0.0017 Kg/m^3
CYLINDER DIAMETER= 0.0500 m
DROP DIAMETER= 0.2000E-04 m
RO=0.1298E+01 MU=0.1694E-04 KA=0.2396E-01
RE=0.8810E+05 NU=0.2224E+03 H=0.1066E+03
PART1=0.5012E-04 PART2=0.1731E-01 PART3=0.7214E+00
EAIR=0.4312E+03 ETS=0.6108E+03

MPIT=0.4272E-03 MPW1=0.4272E-03 BOTH IN (Kg/ms)
NF=0.1000E+01 NFNEW=0.1000E+01 E=0.2185E+00
THE LUDLAM LIMIT DROP DIAMETER=0.1554E-04 m
FOR A LUDLAM LIMIT TEMPERATURE= -4.70 deg C
ITERATIONS REQUIRED 22

TRIAL 2 (FIGURE 5.2)

WIND SPEED= 28.0 m/s
AIR TEMP= -8.0 deg C DROP TEMP= -8.0 deg C
LIQUID WATER CONTENT= 0.0017 Kg/m^3
CYLINDER DIAMETER= 0.0500 m
DROP DIAMETER= 0.2500E-04 m
RO=0.1314E+01 MU=0.1677E-04 KA=0.2372E-01
RE=0.1097E+06 NU=0.2537E+03 H=0.1203E+03
PART1=0.5659E-04 PART2=0.1731E-01 PART3=0.7214E+00
EAIR=0.3350E+03 ETS=0.6108E+03

MPIT=0.8245E-03 MPW1=0.8245E-03 BOTH IN (Kg/ms)
NF=0.1000E+01 NFNEW=0.1000E+01 E=0.3464E+00
THE LUDLAM LIMIT DROP DIAMETER=0.1953E-04 m
FOR A LUDLAM LIMIT TEMPERATURE= -8.00 deg C
ITERATIONS REQUIRED 5

TRIAL 3 (FIGURE 5.3)

WIND SPEED= 20.0 m/s
AIR TEMP= -13.5 deg C DROP TEMP= -13.5 deg C
LIQUID WATER CONTENT= 0.0030 Kg/m^3
CYLINDER DIAMETER= 0.0500 m
DROP DIAMETER= 0.2000E-04 m
RO=0.1342E+01 MU=0.1649E-04 KA=0.2331E-01
RE=0.8136E+05 NU=0.2121E+03 H=0.9888E+02
PART1=0.4650E-04 PART2=0.1731E-01 PART3=0.7214E+00
```

```
EAIR=0.2171E+03 ETS=0.6108E+03

MPIT=0.1177E-02 MPW1=0.1177E-02 BOTH IN (Kg/ms)
NF=0.1000E+01 NFNEW=0.1000E+01 E=0.3923E+00
THE LUDLAM LIMIT DROP DIAMETER=0.2469E-04 m
FOR A LUDLAM LIMIT TEMPERATURE= -13.50 deg C
ITERATIONS REQUIRED 4
```

Appendix E

The experimental data which were presented in the graphs in Chapter 5 are documented here. Trial 1 through Trial 4 correspond to Figure 5.1 through Figure 5.4, respectively. All of these trials were carried out during the summer of 1986 in the F.R.O.S.T. facility at the University of Alberta.

TRIAL ONE
Wind speed: 23 m/s
Liquid water content: 1.7 gm^{-3}
Cylinder diameter: 5 cm
Rate of rotation: 0.5 Hz
Drop Diameter: 16 μm

Air Temperature (°C)	Ice Fraction
-14.0	100.0
-10.0	100.0
-8.2	100.0
-7.0	100.0
-5.8	100.0
-4.8	98.0
-3.4	82.0
-3.2	83.0
-2.2	78.0
-4.2	99.0
-3.6	98.0
-2.5	77.0
-2.0	69.0
-4.6	100.0
-3.0	89.0
-2.7	84.0
-4.1	98.0
-3.0	86.0
-2.7	81.0
-3.5	88.0
-3.6	80.0
-3.7	89.0
-5.9	99.0
-5.4	99.0
-4.9	96.0
-4.5	98.0
-4.1	100.0
-3.7	91.0
-3.5	87.0
-2.0	67.0

TRIAL TWO

Wind speed: 28 m/s
Liquid water content:1.7 gm$_{-3}$
Cylinder diameter: 5 cm
Rate of rotation: 0.5 Hz
Drop diameter: 20 μm

Air Temperature (°C)	Ice Fraction
-14.0	100.0
-13.2	100.0
-11.8	100.0
-10.2	100.0
-9.0	100.0
-8.0	99.0
-6.8	99.0
-4.6	93.0
-3.6	68.0
-2.6	72.0
-4.0	78.0

TRIAL THREE

Wind speed: 20 m/s
Liquid water content: 3.0 gm$_{-3}$
Cylinder diameter: 5 cm
Rate of rotation: 0.5 Hz
Drop diameter: 25 μm

Air Temperature (°C)	Ice Fraction
-5.9	66.0
-5.1	64.0
-3.6	60.0
-9.0	80.0
-8.2	79.0
-8.2	84.0
-6.5	79.0
-13.7	100.0
-11.8	100.0
-10.3	88.0
-2.1	57.0

TRIAL FOUR
Air temperature: -5.0°C
Liquid water content: 4.4 gm$_{-3}$
Cylinder diameter: 5 cm
Rate of rotation: 0.5 Hz
Drop diameter: 25 μm

Air Velocity (m/s)	Ice Fraction
41.6	74.0
38.1	73.0
33.9	69.0
30.4	67.0
27.7	57.0
25.6	53.0
22.1	50.0
19.3	48.0
15.3	44.0
8.4	48.0